BSC

Model Administrative Change Notice

Complete only applicable items.

1. Document Number:	ANL-WIS-PA-000001	2. Revision:	02	3. ACN:	01
4. Title:	EBS Radionuclide Transport Abstraction				
5. No. of Pages Attached	115				

6. Approvals:

Preparer:	Jeralyn Prouty Print name and sign	7/14/06 Date
Checker:	Ralph Rogers Print name and sign	7/14/06 Date
QER:	Darrell Svalstad Print name and sign	7/14/06 Date
Independent Technical Reviewer:	Bruce Kirstein Print name and sign	7/14/2006 Date
Responsible Manager:	Ernest Hardin Print name and sign	7/14/06 Date

7. Affected Pages	8. Description of Change:
v, vii, ix, x, xiv, 1-1, 1-2, 1-3, 3-1, 4-9, 4-11, 4-15, 4-18, 4-27, 5-1, 5-5, 6-1, 6-2, 6-3, 6-4, 6-5, 6-6, 6-8, 6-15, 6-17, 6-18, 6-21, 6-23, 6-25, 6-28, 6-35, 6-37, 6-39, 6-44, 6-45, 6-47, 6-49, 6-50, 6-52, 6-56, 6-63, 6-88, 6-89, 6-91, 6-95, 6-97, 6-102, 6-103, 6-123, 6-125, 6-127, 6-128, 6-143, 6-158, 6-163, 6-164, 6-165, 6-167, 6-168, 6-170, 6-178, 6-179, 6-180, 6-187, 6-188, 6-192, 6-193, 6-199, 6-203, 6-204, 6-205, 6-210, 6-214, 6-226, 6-228, 6-231, 6-238, 6-239, 6-243, 6-245, 6-267, 7-1, 7-6, 7-23, 7-28, 7-31, 7-34, 7-48, 7-50, 7-51, 7-52, 7-53, 7-54, 8-1, 8-4, 8-7, 8-11, 8-34, B-13, B-18, I-1, I-2, I-3, I-4, Appendix J cover sheet, J-1, and J-2	"TSPA-LA" changed to "TSPA" throughout document except when part of proper name. This ACN is being processed in preparation for submission of the report to the NRC in association with AINs for the following KTIs: ENFE 4.03, ENFE 4.06, TSPAI 2.02 Comment J-8, TSPAI 3.17, and GEN 1.01 Comment 37. Before NRC submission, the report must pass through a public release review, a process that in part involves examining how the document refers to the TSPA. As a result, the above change was needed to reflect the fact that the version of the EBS radionuclide transport abstraction model documented in this report will not be the version used for TSPA-LA.

1. Document Number:	ANL-WIS-PA-000001	**2. Revision**:	02	**3. ACN**:	01
4. Title:	EBS Radionuclide Transport Abstraction				

1-1	1st paragraph on page, last sentence: Change made to support change (discussed above) from "TSPA-LA" to "TSPA". Original REV 02 Text: The EBS radionuclide transport abstraction (or *EBS RT Abstraction*) is the conceptual model used in the total system performance assessment for the license application (TSPA-LA) to determine the rate of radionuclide releases from the EBS to the unsaturated zone (UZ). Changed to: The EBS radionuclide transport abstraction (or *EBS RT Abstraction*) is the conceptual model used in the total system performance assessment (TSPA) to determine the rate of radionuclide releases from the EBS to the unsaturated zone (UZ).
6-63	1st paragraph on page, 1st three sentences: Self-identified change. There are four—not three—incorrect data values in the DTN. Original REV 02 Text: Three data values in this DTN are incorrect. Changed to: Four data values in this DTN are incorrect.
8-34	Section 8.4, 2nd paragraph: Self-identified change. Language changed to reflect the roles of Appendices I and J more accurately. Original REV 02 Text: Differences between the preliminary and final DTNs are described in Appendix I. Changed to: Differences between the preliminary DTNs: SN0403T0507703.015 and SN0409T0507703.017 are described in Appendix I. This appendix also compares the second preliminary DTN: SN0409T0507703.017 with the corresponding final DTN: SN0410T0507703.018. Differences between the two related DTNs: SN0503T0503305.001 and SN0508T0503305.003 are described in Appendix J.
I-1	Appendix I, 1st paragraph: Self-identified change. This paragraph introduces five DTNs in all, but explains that this appendix only discusses three of the DTNs. For clarity, a sentence is needed to point the reader to Appendix J, which has the pertinent information on the other two DTNs. Sentence added to end of paragraph: Appendix J contains the comparison between DTNs: SN0503T0503305.001 and SN0508T0503305.003.

1. Document Number:	ANL-WIS-PA-000001	**2. Revision**:	02	**3. ACN**:	01
4. Title:	EBS Radionuclide Transport Abstraction				

J-1	Appendix J, 1st paragraph: This change supports the later use of "corrected" and "uncorrected" data sets (verbiage, discussed in rows below, meant to clarify captions, figure labels, and sources for Figures J-1 and J-2 and Tables J-1 and J-2). Original REV 02 Text: This appendix describes the erroneous data and the sorption parameter distributions that are used in TSPA-LA. Changed to: The erroneous data and the sorption parameter distributions that are used in TSPA are described in this appendix. In some instances, it refers to DTN: SN0503T0503305.001 as the "uncorrected data set" and to DTN: SN0508T0503305.003 as the "corrected data set" as a way of differentiating which data set has the correct values. As a result of this change, page J-1a was created.
J-2	3rd paragraph on page: Self-identified change. A grammatical error was fixed in last sentence of paragraph. Original REV 02 Text: The differences…is discussed here solely to provide full traceability of the data. Changed to: The differences…are discussed here solely to provide full traceability of the data.
J-2	Caption for Table J-1: This ACN is being processed in preparation for submission of the report to the NRC in association with AINs for the following KTIs: ENFE 4.03, ENFE 4.06, TSPAI 2.02 Comment J-8, TSPAI 3.17, and GEN 1.01 Comment 37. Before NRC submission, the report must pass through a public release review, a process that in part involves examining how the document refers to the TSPA. A preliminary review conducted by the Regulatory Compliance department within Licensing determined that Figures J-1 and J-2 and Tables J-1 and J-2 are potentially confusing because they may give the false impression that some of the results shown are generated by the TSPA model. The captions, figure labels, and sources have been changed as necessary to make it clear that the results are from two separate data sets, both of which were generated as product outputs of this report. Original REV 02 Text: Table J-1. Sample Ranges and Distributions Used for Irreversible Sorption on Stationary Corrosion Products in TSPA-La Changed to: Table J-1. Sample Ranges and Distributions Used for Irreversible Sorption on Stationary Corrosion Products from the Uncorrected Data Set

1. Document Number:	ANL-WIS-PA-000001	**2. Revision**:	02	**3. ACN**:	01
4. Title:	EBS Radionuclide Transport Abstraction				

J-3, J-4, J-5, and J-6	Continued caption for Table J-1: This ACN is being processed in preparation for submission of the report to the NRC in association with AINs for the following KTIs: ENFE 4.03, ENFE 4.06, TSPAI 2.02 Comment J-8, TSPAI 3.17, and GEN 1.01 Comment 37. Before NRC submission, the report must pass through a public release review, a process that in part involves examining how the document refers to the TSPA. A preliminary review conducted by the Regulatory Compliance department within Licensing determined that Figures J-1 and J-2 and Tables J-1 and J-2 are potentially confusing because they may give the false impression that some of the results shown are generated by the TSPA model. The captions, figure labels, and sources have been changed as necessary to make it clear that the results are from two separate data sets, both of which were generated as product outputs of this report. Original REV 02 Text: Table J-1. Sample Ranges and Distributions Used for Irreversible Sorption on Stationary Corrosion Products in TSPA-LA (Continued) Changed to: Table J-1. Sample Ranges and Distributions Used for Irreversible Sorption on Stationary Corrosion Products from the Uncorrected Data Set (Continued)
J-6	Labels in legend for Figure J-1: This ACN is being processed in preparation for submission of the report to the NRC in association with AINs for the following KTIs: ENFE 4.03, ENFE 4.06, TSPAI 2.02 Comment J-8, TSPAI 3.17, and GEN 1.01 Comment 37. Before NRC submission, the report must pass through a public release review, a process that in part involves examining how the document refers to the TSPA. A preliminary review conducted by the Regulatory Compliance department within Licensing determined that Figures J-1 and J-2 and Tables J-1 and J-2 are potentially confusing because they may give the false impression that some of the results shown are generated by the TSPA model. The captions, figure labels, and sources have been changed as necessary to make it clear that the results are from two separate data sets, both of which were generated as product outputs of this report. Figure J-1 replaced with new version having different labels in the legend. “TSPA-LA” has been changed to “Uncorrected Data Set”. “EBS RT Abstraction” has been changed to “Corrected Data Set”.
J-6	Sources for Figure J-1: This ACN is being processed in preparation for submission of the report to the NRC in association with AINs for the following KTIs: ENFE 4.03, ENFE 4.06, TSPAI 2.02 Comment J-8, TSPAI 3.17, and GEN 1.01 Comment 37. Before NRC submission, the report must pass through a public release review, a process that in part involves examining how the document refers to the TSPA. A preliminary review conducted by the Regulatory Compliance department within Licensing determined that Figures J-1 and J-2 and Tables J-1 and J-2 are potentially confusing because they may give the false impression that some of the results shown are generated by the TSPA model. The captions, figure labels, and sources have been changed as necessary to make it clear that the results are from two separate data sets, both of which were generated as product outputs of this report. Original REV 02 Text: Sources: TSPA-LA: Table J-2. EBS RT Abstraction: Output DTN: SN0508T0503305.003. Changed to: Sources: Uncorrected data set: Table J-2. Corrected data set: Output DTN: SN0508T0503305.003.

1. Document Number:	ANL-WIS-PA-000001	**2. Revision**:	02	**3. ACN**:	01
4. Title:	EBS Radionuclide Transport Abstraction				

J-6	Caption for Figure J-1: This ACN is being processed in preparation for submission of the report to the NRC in association with AINs for the following KTIs: ENFE 4.03, ENFE 4.06, TSPAI 2.02 Comment J-8, TSPAI 3.17, and GEN 1.01 Comment 37. Before NRC submission, the report must pass through a public release review, a process that in part involves examining how the document refers to the TSPA. A preliminary review conducted by the Regulatory Compliance department within Licensing determined that Figures J-1 and J-2 and Tables J-1 and J-2 are potentially confusing because they may give the false impression that some of the results shown are generated by the TSPA model. The captions, figure labels, and sources have been changed as necessary to make it clear that the results are from two separate data sets, both of which were generated as product outputs of this report. Original REV 02 Text: Figure J-1. Comparison of Cumulative Probabilities in Goethite Sorption Site Density Discrete Distributions Used in TSPA-LA and Developed in *EBS RT Abstraction* Changed to: Figure J-1. Comparison of Cumulative Probabilities in Goethite Sorption Site Density Discrete Distributions from the Uncorrected and Corrected Data Sets
J-7	Caption for Table J-2: This ACN is being processed in preparation for submission of the report to the NRC in association with AINs for the following KTIs: ENFE 4.03, ENFE 4.06, TSPAI 2.02 Comment J-8, TSPAI 3.17, and GEN 1.01 Comment 37. Before NRC submission, the report must pass through a public release review, a process that in part involves examining how the document refers to the TSPA. A preliminary review conducted by the Regulatory Compliance department within Licensing determined that Figures J-1 and J-2 and Tables J-1 and J-2 are potentially confusing because they may give the false impression that some of the results shown are generated by the TSPA model. The captions, figure labels, and sources have been changed as necessary to make it clear that the results are from two separate data sets, both of which were generated as product outputs of this report. Original REV 02 Text: Table J-2. Cumulative Probability Distributions for Goethite Site Density and Percentage of High-Affinity Goethite Sites Used in TSPA-La Changed to: Table J-2. Cumulative Probability Distributions for Goethite Site Density and Percentage of High-Affinity Goethite Sites from the Uncorrected Data Set

1. Document Number:	ANL-WIS-PA-000001	**2. Revision**:	02	**3. ACN**:	01
4. Title:	EBS Radionuclide Transport Abstraction				

J-8	Continued caption for Table J-2: This ACN is being processed in preparation for submission of the report to the NRC in association with AINs for the following KTIs: ENFE 4.03, ENFE 4.06, TSPAI 2.02 Comment J-8, TSPAI 3.17, and GEN 1.01 Comment 37. Before NRC submission, the report must pass through a public release review, a process that in part involves examining how the document refers to the TSPA. A preliminary review conducted by the Regulatory Compliance department within Licensing determined that Figures J-1 and J-2 and Tables J-1 and J-2 are potentially confusing because they may give the false impression that some of the results shown are generated by the TSPA model. The captions, figure labels, and sources have been changed as necessary to make it clear that the results are from two separate data sets, both of which were generated as product outputs of this report. Original REV 02 Text: Table J-2. Cumulative Probability Distributions for Goethite Site Density and Percentage of High-Affinity Goethite Sites Used in TSPA-LA (Continued) Changed to: Table J-2. Cumulative Probability Distributions for Goethite Site Density and Percentage of High-Affinity Goethite Sites from the Uncorrected Data Set (Continued)
J-9	Labels in legend for Figure J-2: This ACN is being processed in preparation for submission of the report to the NRC in association with AINs for the following KTIs: ENFE 4.03, ENFE 4.06, TSPAI 2.02 Comment J-8, TSPAI 3.17, and GEN 1.01 Comment 37. Before NRC submission, the report must pass through a public release review, a process that in part involves examining how the document refers to the TSPA. A preliminary review conducted by the Regulatory Compliance department within Licensing determined that Figures J-1 and J-2 and Tables J-1 and J-2 are potentially confusing because they may give the false impression that some of the results shown are generated by the TSPA model. The captions, figure labels, and sources have been changed as necessary to make it clear that the results are from two separate data sets, both of which were generated as product outputs of this report. Figure J-2 replaced with new version having different labels in the legend. “TSPA-LA” has been changed to “Uncorrected Data Set”. “EBS RT Abstraction” has been changed to “Corrected Data Set”.
J-9	Sources for Figure J-2: This ACN is being processed in preparation for submission of the report to the NRC in association with AINs for the following KTIs: ENFE 4.03, ENFE 4.06, TSPAI 2.02 Comment J-8, TSPAI 3.17, and GEN 1.01 Comment 37. Before NRC submission, the report must pass through a public release review, a process that in part involves examining how the document refers to the TSPA. A preliminary review conducted by the Regulatory Compliance department within Licensing determined that Figures J-1 and J-2 and Tables J-1 and J-2 are potentially confusing because they may give the false impression that some of the results shown are generated by the TSPA model. The captions, figure labels, and sources have been changed as necessary to make it clear that the results are from two separate data sets, both of which were generated as product outputs of this report. Original REV 02 Text: Sources: TSPA-LA: Table J-2. EBS RT Abstraction: Output DTN: SN0508T0503305.003. Changed to: Sources: Uncorrected data set: Table J-2. Corrected data set: Output DTN: SN0508T0503305.003.

1. Document Number:	ANL-WIS-PA-000001	**2. Revision**:	02	**3. ACN**:	01
4. Title:	EBS Radionuclide Transport Abstraction				

J-9	Caption for Figure J-2: This ACN is being processed in preparation for submission of the report to the NRC in association with AINs for the following KTIs: ENFE 4.03, ENFE 4.06, TSPAI 2.02 Comment J-8, TSPAI 3.17, and GEN 1.01 Comment 37. Before NRC submission, the report must pass through a public release review, a process that in part involves examining how the document refers to the TSPA. A preliminary review conducted by the Regulatory Compliance department within Licensing determined that Figures J-1 and J-2 and Tables J-1 and J-2 are potentially confusing because they may give the false impression that some of the results shown are generated by the TSPA model. The captions, figure labels, and sources have been changed as necessary to make it clear that the results are from two separate data sets, both of which were generated as product outputs of this report. Original REV 02 Text: Figure J-2. Comparison of Cumulative Probabilities in Goethite Percentage of High-Affinity Sites Discrete Distributions Used in TSPA-LA and Developed in *EBS RT Abstraction* Changed to: Figure J-2. Comparison of Cumulative Probabilities in Goethite Percentage of High-Affinity Sites Discrete Distributions from the Uncorrected and Corrected Data Sets

CONTENTS

Page

CONTENTS (Continued)

Page

CONTENTS (Continued)

Page

CONTENTS (Continued)

Page

TABLES (Continued)

Page

1. PURPOSE

The purpose of this report is to develop and analyze the engineered barrier system (EBS) radionuclide transport abstraction model, consistent with Level I and Level II model validation, as identified in *Technical Work Plan for: Near-Field Environment and Transport: Engineered Barrier System: Radionuclide Transport Abstraction Model Report Integration* (BSC 2005 [DIRS 173617]). The EBS radionuclide transport abstraction (or *EBS RT Abstraction*) is the conceptual model used in the total system performance assessment (TSPA) to determine the rate of radionuclide releases from the EBS to the unsaturated zone (UZ).

The *EBS RT Abstraction* conceptual model consists of two main components: a flow model and a transport model. Both models are developed mathematically from first principles in order to show explicitly what assumptions, simplifications, and approximations are incorporated into the models used in the TSPA.

The flow model defines the pathways for water flow in the EBS and specifies how the flow rate is computed in each pathway. Input to this model includes the seepage flux into a drift. The seepage flux is potentially split by the drip shield, with some (or all) of the flux being diverted by the drip shield and some passing through breaches in the drip shield that might result from corrosion or seismic damage. The flux through drip shield breaches is potentially split by the waste package, with some (or all) of the flux being diverted by the waste package and some passing through waste package breaches that might result from corrosion or seismic damage. Neither the drip shield nor the waste package survives an igneous intrusion, so the flux splitting submodel is not used in the igneous scenario class. The flow model is validated in an independent model validation technical review. The drip shield and waste package flux splitting algorithms are developed and validated using experimental data.

The transport model considers advective transport and diffusive transport from a breached waste package. Advective transport occurs when radionuclides that are dissolved or sorbed onto colloids (or both) are carried from the waste package by the portion of the seepage flux that passes through waste package breaches. Diffusive transport occurs as a result of a gradient in radionuclide concentration and may take place while advective transport is also occurring, as well as when no advective transport is occurring. Diffusive transport is addressed in detail because it is the sole means of transport when there is no flow through a waste package, which may dominate during the regulatory compliance period in the nominal and seismic scenarios. The advective transport rate, when it occurs, is generally greater than the diffusive transport rate. Colloid-facilitated advective and diffusive transport is also modeled and is presented in detail in Appendix B of this report.

Additional submodels and model parameters developed in this model report include:

- Diffusion inside a waste package. The time-dependent quantity of corrosion products inside a breached waste package is estimated; this enables the surface area available for adsorption of water to be approximated, which in turn gives the water volume through which diffusion of radionuclides may occur.
- Irreversible sorption onto stationary corrosion products in a breached waste package.

- Diffusion in the invert, accounting for the dependence of diffusion on porosity, saturation, and temperature.
- Sorption in the invert.
- EBS-UZ interface model. Implementation in the TSPA includes this model to provide a realistic concentration boundary condition.

Parameter uncertainty associated with each model and submodel is discussed. The transport model and the EBS-UZ interface model are validated using corroborative data and models as well as an independent model validation technical review.

Alternative conceptual models considered include:

- A "bathtub" flow model in which water must fill a breached waste package before any can flow out, as opposed to the flow-through model that is used
- Models that show the effect of limitations on diffusion of water vapor and oxygen into a breached waste package and consequential delays in releases of radionuclides
- A dual-continuum invert flow and transport submodel
- Alternative invert diffusion coefficient submodels
- Reversible sorption of radionuclides onto waste package corrosion products
- Pu sorption onto stationary corrosion products and colloids.

Output from the *EBS RT Abstraction* includes:

- The flow model—the algorithms for computing the flow in each flow path within the EBS, with parameter values or sources for those parameters used in the model
- The transport model—a model for advective and diffusive transport, specifying the computational procedure for both commercial spent nuclear fuel (CSNF) and codisposal waste packages in both the seep environment (where seepage into the drift and condensation on drift walls occur) and the no-seep environment (where no seepage into the drift or condensation on drift walls occurs), with parameter values or sources for those parameters used in the model
- Ranges and distributions for parameters that are uncertain and are sampled in the TSPA implementation of the *EBS RT Abstraction*.

Changes from the previous revision:

- The corrosion products formed in the waste package are assumed to be a mixed assemblage of iron (hydr)oxides, namely hydrous ferric oxide (HFO), goethite, and hematite. These are the solid phases most likely to form from the corrosion of all internal waste package components, except for fuel rods and spent nuclear fuel (SNF), under the anticipated moist and oxidizing repository conditions.

- The method of calculating sorption of radionuclides onto stationary corrosion products has been modified. First, reversible sorption of radionuclides onto stationary corrosion products has been eliminated from the calculation. Second, the number of sites available for irreversible sorption of Pu and Am onto stationary corrosion products has been reduced (to a range sampled in TSPA calculations). These modifications were made in response to calculations that resulted in the prediction of excessive amounts of radionuclide sorption under certain conditions of waste package chemistry. The changes to the calculational method now predict that greater quantities of radionuclides remain unretarded in solution.

- Corrosion product properties used in radionuclide sorption calculations have been modified to those of goethite and HFO. These phases will likely be present along with hematite in the corrosion product assemblage in the waste package. Using the aggregate surface properties of goethite and HFO in TSPA calculations of radionuclide sorption allows the implementation of a more realistic model for retardation.

- The implementation for codisposal (CDSP) waste packages in TSPA has been revised. Previously, DSNF was modeled in TSPA as part of the corrosion products domain, but now DSNF is modeled as a separate sub-domain as part of the waste form domain.

The scope of this abstraction and report is limited to flow and transport processes. Specifically, this report provides the algorithms that are implemented in TSPA for transporting radionuclides using the flow geometry and radionuclide concentrations determined by other elements of the TSPA model. The *EBS RT Abstraction* also identifies the important processes that are evaluated at the process level or component level using analytical or numerical solutions. Restrictions on the use of this abstraction are discussed in Section 8.4.

This report was prepared to comply with the U.S. Nuclear Regulatory Commission (NRC) rule for high-level radioactive waste (HLW), 10 CFR Part 63 [DIRS 173273], which requires the U.S. Department of Energy (DOE) to conduct a performance assessment to demonstrate compliance with postclosure performance objectives. The results from this conceptual model allow Bechtel SAIC Company, LLC (BSC) to address portions of the acceptance criteria presented in *Yucca Mountain Review Plan, Final Report* (NRC 2003 [DIRS 163274]).

The following reports provide input to the *EBS RT Abstraction*:

- *Multiscale Thermohydrologic Model*
- *Thermal Conductivity of the Potential Repository Horizon*
- *Calibrated Properties Model*
- *UZ Flow Models and Submodels*
- *Radionuclide Transport Models Under Ambient Conditions*
- *Analysis of Hydrologic Properties Data*

3. USE OF SOFTWARE

3.1 MICROSOFT EXCEL

Microsoft Excel 2002 "Add Trendline" capability was used to perform a statistical analysis of diffusion coefficient values reported in Section 6.3.4.1.1. Microsoft Excel 2002 was also used to analyze experimental data used to develop and validate the drip shield and waste package flux splitting submodels (Sections 6.5.1.1.2.4, 6.5.1.1.3, and 7.1.1). A calculation of the potential mass of corrosion products in fully degraded waste packages, summarized in Table 6.3-4, is described in Appendix A. A sample calculation to demonstrate the solution procedure used in the colloid transport model, described in Appendix B, was also carried out using Microsoft Excel 2002. A complete description of the formulas, inputs, and outputs used in the Microsoft Excel analysis of the drip shield experimental data is provided in Appendices C (the drip shield flux splitting submodel), D (the waste package flux splitting submodel), and E (validation of the flux splitting submodels). The formulas, inputs, and outputs used in Microsoft Excel to perform the sample colloid transport calculation are presented in Appendix F, and the invert diffusion properties model analysis is described in Appendix G.

3.2 GOLDSIM

GoldSim V8.01 Service Pack 1 (STN: 10344-8.01 SP1-00) (Golder Associates 2003 [DIRS 166572]) is run on Microsoft Windows 2000 on a Dell workstation with Intel Xeon processor and was developed to perform dynamic, probabilistic simulations. GoldSim V8.01 was used in accordance with LP-SI.11Q-BSC, *Software Management*. GoldSim calculations were done in support of validation of models developed in the *EBS RT Abstraction* (see Section 7.3.1). GoldSim calculations were also run to verify an alternative model implementation in Section 6.6.4.4. GoldSim V8.01 is used in these validation calculations because it is used in the TSPA model. This software was obtained from Configuration Management. The use of this software was consistent with the intended use and within the range of validation of the software. The range of validation is defined by the documented functionality (i.e., requirements) and the range of acceptable input. The requirements are located in the *Requirements Document for: GoldSim V8.02, Rev. No. 00,* Document ID: 10344-RD-8.02-00 (DOE 2004 [DIRS 169875]). The range of acceptable inputs is element-specific. The rules for the use of each type of element are discussed in *User's Guide, GoldSim Probabilistic Simulation Environment* (GoldSim Technology Group 2003 [DIRS 166226]).

Fuel rod dimensions—The fuel rod dimensions for assembly Westinghouse Electric (WE) 17 × 17 are given in *Characteristics of Potential Repository Wastes* (DOE 1992 [DIRS 102588]). This four-volume report is the definitive compilation of the characteristics of potential repository wastes. The concerns raised by *Deficiency Report VAMO-98-D-132* (DOE 1998 [DIRS 123628]) regarding inconsistencies between data reported in *Characteristics of Potential Repository Wastes* (DOE 1992 [DIRS 102588]) and its data sources do not impact the data used in this analysis with regard to the WE 17 × 17 fuel rods; thus, these data are considered reliable and are justified as suitable for intended use in this analysis. The WE 17 × 17 fuel assembly is used as the representative fuel assembly because (1) Westinghouse fuel assemblies comprise a large fraction (about 21 percent) of all fuel assemblies, (2) the 17 × 17 configuration comprises about 34 percent of discharged fuel assemblies (Faruque 1993 [DIRS 170706]), and (3) 21-pressurized water reactor (PWR) waste packages that will contain the WE 17 × 17 fuel assemblies are the most common type of waste package, nominally comprising 4,299 of the 11,184 waste packages planned for the repository (BSC 2005 [DIRS 173501], Table 13).

Initial Radionuclide Inventories (BSC 2004 [DIRS 170022], Section 5.1) uses a Babcock and Wilcox Mark B PWR assembly as representative of PWR systems instead of the WE 17 × 17 assembly used in this analysis. Because the number and dimensions of fuel rods used in the Babcock and Wilcox Mark B differ from those of the WE 17 × 17 assembly, the choice of a representative assembly could impact the initial waste package void volume calculation in Section 6.3.4.3.4. The calculation in that section is used to establish an approximate upper bound on the porosity of corrosion products and to validate the value of porosity used in TSPA calculations. Because the estimated bound is not used as output from this analysis, a variation of a few percentage points is of no consequence. The Babcock and Wilcox Mark B PWR assembly contains 208 fuel rods, with each rod having a length of 153.68 in. and an outside diameter of 0.430 in. (DOE 1992 [DIRS 102588], p. 2A-7). Thus, the total volume of fuel rods in 21 Babcock and Wilcox Mark B assemblies is 1.597 m^3, versus 1.513 m^3 in 21 WE 17 × 17 assemblies (see Table 6.3-9). The initial porosity of a 21-PWR waste package using Babcock and Wilcox Mark B assemblies will then be 0.58, which, to two significant digits, is identical to the estimated initial porosity using WE 17 × 17 assemblies obtained in Section 6.3.4.3.4. Therefore, the choice of representative assembly has no impact on this analysis.

The fuel rod length is reported in *Characteristics of Potential Repository Wastes* (DOE 1992 [DIRS 102588], Volume 1, p. 2A-30) as ranging from 151.560 in. to 151.635 in. Because no distribution for length is given in the reference (which would give some guidance on selecting a single representative value for length) and because the range is small (less than 0.05 percent variation from minimum to maximum), the minimum length is used as representative of the range.

Water molecule cross-sectional area—The cross-sectional area of the water molecule is taken from the paper "Adsorption of Water Vapour on α-Fe_2O_3" (McCafferty and Zettlemoyer 1970 [DIRS 154382]). The paper was published in *Discussions of the Faraday Society*, a publication started in 1947 and continuing to this day as the *Faraday Discussions* under the sponsorship of the Royal Society of Chemistry. The Royal Society of Chemistry is the largest organization in Europe for advancing the chemical sciences and is supported by a network of 45,000 members

Abstraction the specific surface area of hematite represents that of corrosion products, which will form under a wide range of conditions, this is a sampled parameter in TSPA. The values of specific surface area of hematite in Table 4.1-9 establish lower and upper bounds of the range to be sampled. The lower bound value, for natural hematite, is provided by Langmuir (1997 [DIRS 100051]), a widely used textbook on aqueous geochemistry by a reputable, extensively published author and environmental chemistry researcher. The upper bound value is provided by a study of catalytic behavior of metal oxides (Briand et al. 2001 [DIRS 161617]) published in the *Journal of Catalysis*, a reputable refereed journal. Further discussion and corroboration of the range of specific surface area of hematite is provided in Section 6.3.4.3.3.

Tuff matrix diffusion coefficient correlation—The diffusion coefficient correlation for tuff matrix, used as direct input in Section 6.6.5-2 (Equation 6.6.5.2-4), was developed by Reimus et al. (2002 [DIRS 163008]). The qualification of this report and the use of the equation are given here in accordance with item 5.2.1(k) of LP-SIII.10Q-BSC: Reliability of data source; and qualifications of personnel or organizations generating the data.

The diffusion equation was developed by Reimus et al. (2002 [DIRS 163008]) at Los Alamos National Laboratory (LANL), a nationally recognized scientific institution, supported by DOE, National Nuclear Security Administration, Nevada Operations Office, as part of the Underground Test Area Project. LANL is a DOE multidisciplinary science institution managed by the University of California and is highly regarded among the scientific community for both quality and the reliability of scientific work. Scientists at LANL are among the most highly respected in their scientific fields. Furthermore, the diffusion data used in the development of Equation 6.6.5.2-4 was collected under adequate QA procedures and protocol, comparable to the YMP QA program. Thus, the data source is considered reliable, and Equation 6.6.5.2-4 is justified for its intended use as direct input in this report.

Sorption site density and specific surface area of goethite and ferrihydrite—The sorption density and specific surface area data for goethite listed in Table 4.1-10 were compiled from many laboratory studies mainly addressing the single metal sorption from aqueous solutions. The data for ferrihydrite (designated as amorphous hydrous ferric oxide [HFO] in this report) were compiled from Dzombak and Morel (1990 [DIRS 105483]). The site densities for many ferric oxyhydroxide solids have been obtained mainly through the evaluation of sorption data using models such as the Surface Complexation Model (SCM) and other similar models. Given the difficulties in obtaining site density data, this parameter is usually constrained by either fitting the experimental sorption data or just using an accepted value for metal sorption models onto certain types of solids. Site density data have been obtained experimentally from acid-base surface titration measurements assuming complete surface saturation of ionic species that sorb to the oxyhydroxide surface (Villalobos et al. 2003 [DIRS 173017]). Other approaches include estimations of surface site densities on the basis of properties of the sorbent at distinct crystal planes (see Hiemstra and Van Riemsdijk 1996 [DIRS 173023]; Pivovarov 1997 [DIRS 173714]) and tritium exchange experiments.

Since most of the estimated site density values in these sources are obtained from single metal sorption and SCM studies, competitive effects are not taken into account. The assessment of competitive sorption in multi-component systems remains a subject of ongoing research and is restricted to a limited number of studies on few metal species. Therefore, it is reasonable to say

Table 4.1-10. Specific Surface Areas and Adsorption Site Densities for Goethite, Hematite, and HFO

Substrate	Site Density	Site Density Units	Specific Surface Area ($m^2\ g^{-1}$)	Source	Comments
Goethite	3.28×10^{-6}	mol m^{-2}	55	Rodda et al. 1996 [DIRS 173710], Table 1	Model fitting (2-site Langmuir adsorption model for Zn at 25°C). Tabulated site density denotes sum of low- and high-affinity sites: $2.90 \times 10^{-6} + 3.75 \times 10^{-7} = 3.28 \times 10^{-6}$ mol m^{-2}. Site density converted to sites nm^{-2} in Table 6.3-4a.
Goethite	1.43×10^{-5}	mol m^{-2}	55	Rodda et al. 1996 [DIRS 173710], Table 1	Model fitting (2-site Langmuir adsorption model for Zn at 25°C). Tabulated site density denotes sum of low- and high-affinity sites: $1.30 \times 10^{-5} + 1.26 \times 10^{-6} = 1.43 \times 10^{-5}$ mol m^{-2}. Site density converted to sites nm^{-2} in Table 6.3-4a.
Goethite	2.2×10^{-6}	mol m^{-2}	55	Rodda et al. 1996 [DIRS 173710], Table 5	Model fitting (BET adsorption model for Zn at 25°C). Site density converted to sites nm^{-2} in Table 6.3-4a.
Goethite	6.15	sites nm^{-2}	—	Hiemstra and Van Riemsdijk 1996 [DIRS 173023], p. 498	Total site density obtained from crystal plane structural relations for 021 and 110 goethite faces in corresponding proportions described by Hiemstra and Van Riemsdijk 1996 [DIRS 173023], p. 498. The listed value of 6.15 sites nm^{-2} is the total of low- and high-affinity sites given by the source: 3.45 + 2.7 = 6.15 sites nm^{-2}. A value of 5.92 sites nm^{-2} for site density is listed in preliminary output DTN: SN0503T0503305.001 and used in TSPA; see Appendix J.
Goethite	8.00	sites nm^{-2}	52	Villalobos et al. 2003 [DIRS 173017], Table 2	Calculated from maximum sorption data for Pb^{2+}
Goethite	4.90	sites nm^{-2}	45	Villalobos et al. 2003 [DIRS 173017], Table 2	Calculated from maximum sorption data for Pb^{2+}
Goethite	7.40	sites nm^{-2}	28.5	Villalobos et al. 2003 [DIRS 173017], Table 2	Calculated from maximum sorption data for F^- (assumed mononuclear complex)
Goethite	4.60	sites nm^{-2}	32	Villalobos et al. 2003 [DIRS 173017], Table 2	Calculated from maximum sorption data for F^- (assumed mononuclear complex)
Goethite	7.20	sites nm^{-2}	30.8	Villalobos et al. 2003 [DIRS 173017], Table 2	Calculated from maximum sorption data for F^- (assumed mononuclear complex)
Goethite	3.40	sites nm^{-2}	32	Villalobos et al. 2003 [DIRS 173017], Table 2	Calculated from maximum sorption data for phosphate (assumed binuclear)

Table 4.1-10. Specific Surface Areas and Adsorption Site Densities for Goethite, Hematite, and HFO (Continued)

Substrate	Site Density	Site Density Units	Specific Surface Area ($m^2 g^{-1}$)	Source	Comments
Goethite	6.31	sites nm^{-2}	85	Boily et al. 2001 [DIRS 173707], Table 3	Total site density estimated from crystallographic data at three different crystal planes
Goethite	1.8	sites nm^{-2}	27.7	Gao and Mucci 2001 [DIRS 173750], p. 2364	Acid-base surface titration
Goethite	2.31	sites nm^{-2}	49	Robertson and Leckie 1997 [DIRS 173763], Table 4	Range obtained from SCMs sensitivity analyses
Goethite	7.00	sites nm^{-2}	49	Robertson and Leckie 1997 [DIRS 173763], Table 4	Range obtained from SCMs sensitivity analyses
Goethite	8.38	sites nm^{-2}	49	Robertson and Leckie 1997 [DIRS 173763], Table 4	Range obtained from SCMs sensitivity analyses. A value of 8.83 sites nm^{-2} for site density is listed in preliminary output DTN: SN0503T0503305.001 and used in TSPA; see Appendix J.
Goethite	8.16	sites nm^{-2}	49	Robertson and Leckie 1997 [DIRS 173763], Table 4	Range obtained from SCMs sensitivity analyses
Goethite	1.68	sites nm^{-2}	39.9	Lövgren et al. 1990 [DIRS 173771], p. 1303	Acid-base surface titration
Goethite	3.12	sites nm^{-2}	81	Machesky et al. 1991 [DIRS 173758], p. 771	Estimated from maximum sorption data
Goethite	7.00	sites nm^{-2}	52	Hayes and Leckie 1987 [DIRS 173817], Table II	Pb sorption data
Goethite	2.3	sites nm^{-2}	45	van Geen et al. 1994 [DIRS 144702], Table 1	Adopted value is the same as that given by Davis and Kent (1990 [DIRS 143280]) and Dzombak and Morel (1990 [DIRS 105483])
Goethite	1.7	sites nm^{-2}	43	Persson et al. 1998 [DIRS 173762], p. 261	Acid-base surface titration
Goethite	5	sites nm^{-2}	110	Davis and Upadhyaya 1996 [DIRS 173743], p. 1895	Assumed value based on Stumm 1992 [DIRS 141778]
Goethite	4.84	sites nm^{-2}	64.3	Xue and Traina 1996 [DIRS 173713], p. 3163	Calculated value from the smallest average for constant capacitance model (CCM)

Table 4.1-17. Diffusion Coefficient for Granular Materials for Volumetric Moisture Content Between 1.5 Percent and 66.3 Percent (Continued)

Sample	Volumetric Moisture Content (%)	Diffusion Coefficient ($cm^2\ s^{-1}$)
122	42.5	3.22×10^{-6}
123*	43.4	1.02×10^{-5}
124	49.0	6.09×10^{-6}
125	66.3	1.83×10^{-5}

NOTE: All values are from Conca and Wright 1992 [DIRS 100436], Figure 2, except for those indicated by an asterisk, which are from Conca et al. 1993 [DIRS 170709], Figure 2.

4.1.3 Design Information

Some of the information necessary for the model presented in this document consists of parameters and other descriptions based on the license application (LA) conceptual design of the repository. Included are dimensions, material amounts and properties, and physical configuration of the drifts and their contents, listed in Tables 4.1-18 through 4.1-20. For TSPA analyses, this information was obtained from information exchange drawings (IEDs) and design drawings cited on IEDs.

In Table 4.1-20, the component materials in a 21-PWR waste package are obtained from *Design and Engineering, 21-PWR Waste Package Configuration* (BSC 2004 [DIRS 167394]), which is the design version preceding the current version (BSC 2004 [DIRS 170710]). In addition, the masses, thicknesses, and numbers of components in a 21-PWR waste package, listed in Tables 4.1-18 through 4.1-20, are obtained from Revision 00C of *D&E/PA/C IED Typical Waste Package Components Assembly* (BSC 2004 [DIRS 169472]), which has been superseded by *IED* [information exchange drawing] *Typical Waste Package Configuration* (BSC 2005 [DIRS 173501]). Justification for using the previous design data and the impact on TSPA calculations is provided in Section 6.3.4.2.3, where the impact is shown to be negligible.

In Table 4.1-20, the masses and numbers of components in a 5 DHLW/DOE - Short waste package are obtained from Revision 00B of *D&E/PA/C IED Typical Waste Package Components Assembly* (BSC 2004 [DIRS 167207]), which is the version of the IED preceding Revision 00C (BSC 2004 [DIRS 169472]), used for the 21-PWR waste packages, which in turn has been superseded by *IED Typical Waste Package Configuration* (BSC 2005 [DIRS 173501]). Minor changes in component masses were made in the 5 DHLW/DOE - Short waste package from Revision 00B (BSC 2004 [DIRS 167207]) to Revision 00C (BSC 2004 [DIRS 169472]) to BSC 2005 [DIRS 173501]. The impacts of the changes in component masses in the 5 DHLW/DOE - Short waste package are analyzed in Section 6.3.4.2.3 and are shown to be negligible.

5. ASSUMPTIONS

5.1 ALL SEEPAGE FALLS ONTO DRIP SHIELD/WASTE PACKAGE

Assumption: It is assumed that the locations of seeps in the emplacement drifts are random with respect to waste package locations, but that once a seep occurs, its location does not change over time. It is also assumed that fragments of the drip shield that may rest on the waste package, or fallen rock that may rest on the drip shield or waste package, do not divert any seepage flux. In addition, it is assumed that all seepage into the drift falls on the crown of the drip shield, and in the absence of a drip shield, all seepage falls on the crown of the waste package. In the event of a breach in the drip shield, all the seepage that penetrates the drip shield contacts the waste package.

Basis: Once seepage occurs during cooldown, the fracture characteristics that control the location of seepage are not expected to change. If such changes occur, they are likely to be limited in extent, or to occur in a random manner for many waste packages such that there is no overall, significant effect on the interaction of seepage water with waste forms. The mean seepage for the degraded drift is greater than for the non-degraded case, but the factors controlling seep locations are still likely to occur in a random manner for many waste packages.

Confirmation Status: This assumption does not require confirmation because it maximizes the duration of seepage contact with drip shields and waste packages as represented in TSPA. It also maximizes the flux of dripping water available to flow through breaches in the drip shield or waste package, once such flow is initiated as represented in the TSPA.

Use in the Model: This assumption is used throughout Sections 6 and 7.

5.2 EVAPORATION FROM A DRIP SHIELD DOES NOT OCCUR

Assumption: It is assumed that there is no evaporation of seepage water from the surface of the drip shield.

Basis: The heat output from the waste package will cause the drip shield generally to be hotter than the drift wall from which seepage water is dripping. Some seepage water that drips onto the drip shield may be evaporated, thereby reducing the flux of water through the drip shield. A reduction in the quantity of water flux through the drip shield reduces the potential for advective transfer and subsequent release and transport of radionuclides from the waste packages. Ignoring the process of evaporation in this analysis therefore bounds (maximizes) the impacts of the seepage flux on waste packages.

Although some splashing or splattering can occur as water droplets impinge on the drip shield, the splash distance would be limited, and the water would effectively be redistributed over the top of the drip shield. If water droplets were to fall near the edge of the top plate, some splashes could fall onto the invert or lower walls of the drift and drain directly into the invert. This situation would minimize the degrading effects of water dripping on the drip shield and therefore is eliminated from consideration in order to bound the impacts of the seepage flux on waste packages.

5.7 NO PHYSICAL FILTRATION OR GRAVITATIONAL SETTLING OF COLLOIDS

Assumption: It is assumed that physical filtration and gravitational settling of colloids will not occur within the waste package and the drift.

Basis: Filtration processes may affect transport of radionuclide-bearing colloids in the waste and EBS. Colloid filtration as discussed here refers to the physical removal of colloids from a flow system by pore clogging, sieving, and straining. Filtration of colloids generally means the retention of colloids moving with the suspending fluid in pores, channels, and fracture apertures that are too small or dry to allow passage of the colloids.

In the *EBS RT Abstraction*, the assumption is made that all stable colloids formed within the waste package (the calculated colloid source term) exit the package and enter the invert without filtration. These colloids will then move through the invert material without being subjected to filtration until they reach the underlying UZ.

Filtration is excluded on the basis of low consequence. Since filtration within the waste package and the invert will actually occur to some extent, the modeling approach of neglecting filtration overestimates the potential impact of colloid-facilitated transport of radionuclides in the TSPA dose calculations and is considered bounding.

In the *EBS RT Abstraction*, it is assumed that all stable radionuclide-bearing colloids will not be subject to gravitational settling. Assuming that gravitational settling will not occur results in an overestimation of the potential consequences of colloid-facilitated transport of radionuclides and is considered bounding.

Confirmation Status: This assumption does not require confirmation because it is a bounding assumption that reduces the potential effectiveness of the invert as a transport barrier.

Use in the Model: This assumption is used in Section 6.5.1.2.

6. MODEL DISCUSSION

6.1 MODELING OBJECTIVE

The objective of the *EBS RT Abstraction* is to provide the conceptual model used to determine the time-dependent flux of radionuclides from the EBS to the unsaturated zone in the TSPA. In particular, this model is used to quantify such releases from a failed waste package and the subsequent transport of those radionuclides through the EBS to the emplacement drift wall/unsaturated zone interface. The basic time-dependent inputs to the *EBS RT Abstraction* in TSPA calculations consist of the drift seepage influx, the environmental conditions in the drift (temperature, relative humidity, and water chemistry), and the degradation state of the EBS components. Outputs consist of the rates of radionuclide fluxes to the unsaturated zone as a result of advective and diffusive transport, radionuclide solubility, retardation, the degree of liquid saturation of the waste form and invert materials, and the impact of colloids on potential radionuclide transport. The *EBS RT Abstraction* is implemented directly into the TSPA GoldSim model to compute the release rates; details of the implementation are provided in Section 6.5.3.

6.1.1 Engineered Barrier System Components

The EBS consists of the emplacement drift, waste form, cladding, drip shield, the waste package on an emplacement pallet, and an invert constructed with steel supports and filled between the steel framework with crushed tuff (BSC 2005 [DIRS 173978], Table A-1). The *EBS RT Abstraction* focuses on the drip shield, waste package, and invert. Each of the components of the EBS is designed to act as a barrier to prevent or delay the mobilization and release of radionuclides into the geologic environment (see Section 6.7 for a summary of barrier capabilities). For example, the drip shield is designed to redirect any seepage that flows into the drift away from the waste package. The invert supports the waste package and emplacement pallet. It acts as a barrier to diffusive transport of radionuclides in liquids if the liquid saturation in the crushed tuff is low. Figure 6.1-1 presents a typical cross-section of an emplacement drift and the major components of the EBS.

The drip shield is fabricated from titanium, a corrosion-resistant material to provide long-term effectiveness. The waste package outer corrosion barrier is comprised of Alloy 22. The major corrosive processes are stress corrosion cracking in the closure lid welds of the waste package, localized corrosion in the waste package outer corrosion barrier, and general corrosion for both the drip shield and waste package.

Once the drip shield fails (i.e., is initially breached), a portion of the total dripping flux can drip onto the waste package. It is possible for breaches to occur at the gap between adjacent waste packages. If breaches in the drip shield occur at the gap between two drip shield segments, which happens to be above a gap between waste packages, the dripping flux would fall directly to the invert, avoiding the waste package. The possibility that breaches in the drip shield can occur over a gap, allowing liquid to bypass the waste package, is not considered in the *EBS RT Abstraction*.

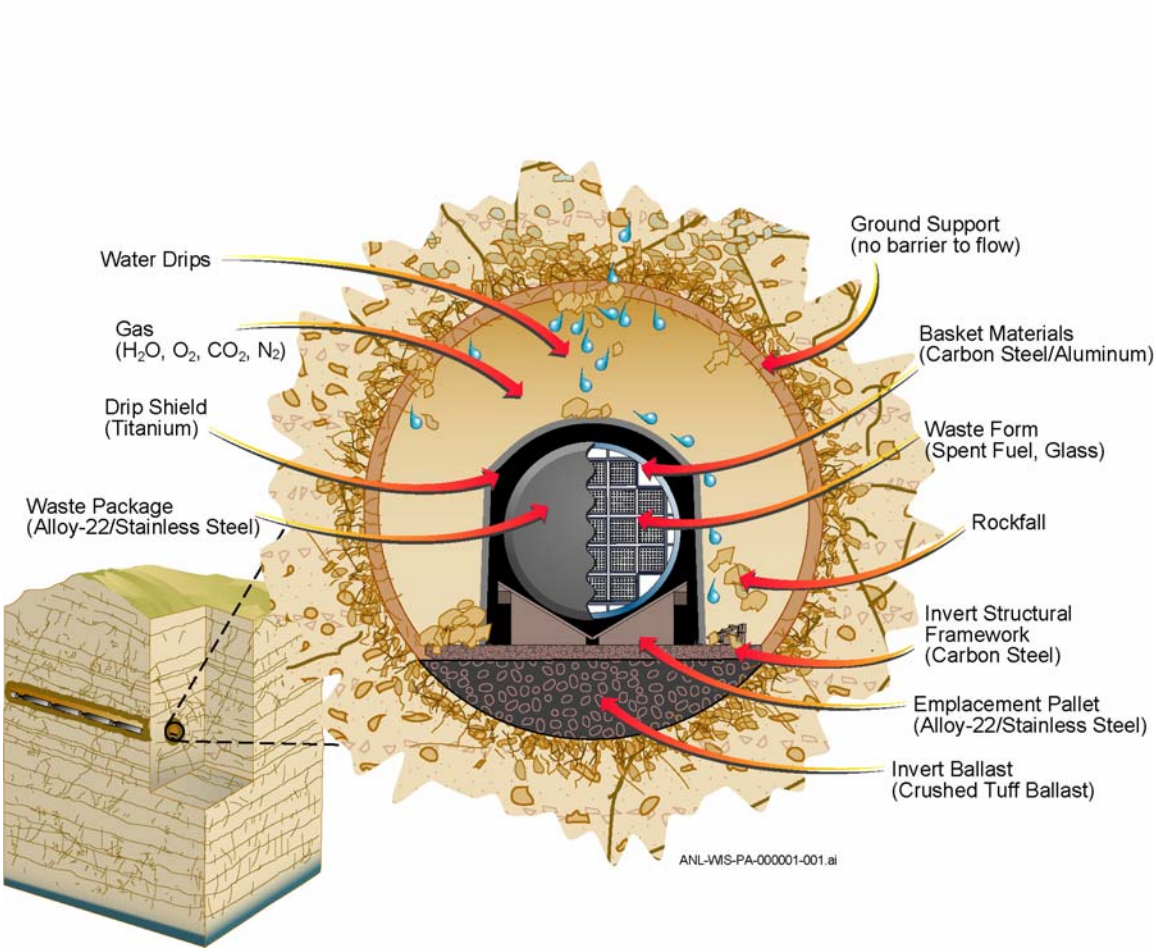

Figure 6.1-1. Schematic Diagram of a Typical Emplacement Drift and the Major Components of the EBS

After the waste package fails (breached by corrosion, seismic damage, igneous intrusion, or early failure mechanisms), a portion of the water that flows through the drip shield can enter the waste package, mobilizing radionuclides in any degraded waste form, and transporting these radionuclides into the unsaturated zone. Diffusion is the primary transport mechanism when the flux into the waste package is small or zero, or if stress corrosion cracks are the only penetrations through the waste package. Advective transport is important when the dripping flux occurs. In this case, advective fluxes can pass through the breaches in the drip shield and waste package.

6.1.2 Scenario Classes for TSPA

A modeling case is a well-defined, connected sequence of features, events, and processes (FEPs) that can be thought of as an outline of a possible future condition in the repository system. Modeling cases can be designated as undisturbed, in which case the performance would be the expected or nominal performance of the system. Or, modeling cases can be designated as disturbed, if altered by disruptive events, such as human intrusion, or by natural phenomena, such as volcanism or nuclear criticality. A scenario class is a set of related modeling cases that share sufficient similarities to aggregate them usefully for the purposes of screening or analysis.

The scenario classes included in TSPA are the nominal scenario class, igneous scenario class, and seismic scenario class.

The three scenario classes are described briefly below. The *EBS RT Abstraction* applies to the nominal scenario class. Further information on the Igneous Scenario Class may be found in *Atmospheric Dispersal and Deposition of Tephra from a Potential Volcanic Eruption at Yucca Mountain, Nevada* (BSC 2004 [DIRS 170026]) and *Dike/Drift Interactions* (BSC 2004 [DIRS 170028]). Further information on the Seismic Scenario Class may be found in *Seismic Consequence Abstraction* (BSC 2005 [DIRS 173247]) and *Characterize Framework for Seismicity and Structural Deformation at Yucca Mountain, Nevada* (BSC 2004 [DIRS 168030]).

Nominal Scenario Class—The nominal scenario class for TSPA encompasses all of the FEPs that are screened in, except for those FEPs related to igneous or seismic activity. This scenario class therefore incorporates the important effects and system perturbations caused by climate change and repository heating that are projected to occur over the 10,000-year regulatory-compliance period. In addition, the nominal scenario class considers that the waste packages and drip shields will be subject to EBS environments and will degrade with time until they are breached and expose the waste forms to percolating groundwater. Then the waste forms will degrade, releasing and mobilizing radionuclides that subsequently will be transported out of the repository. Radionuclides released from the repository then will be transported to the saturated zone by the groundwater percolating through the unsaturated zone below the repository, and then transported to the accessible environment by water flowing in the saturated zone.

The nominal scenario class is represented by two modeling cases. The first modeling case is for those waste packages that degrade by corrosion (general corrosion, stress corrosion cracking, and localized corrosion) under expected repository conditions. The second modeling case is for those waste packages that fail early due to manufacturing and material defects and pre-emplacement operations including improper heat treatment.

Igneous Scenario Class—The igneous scenario class describes performance of the repository system in the event of igneous activity that disrupts the repository and is represented by two modeling cases: (1) igneous intrusion into the repository emplacement drifts that results in release of radionuclides to the groundwater and (2) volcanic eruption through the repository resulting in release of radionuclides to the atmosphere. Both modeling cases assume that the igneous event consists of a magmatic penetration of the repository at some time after permanent closure.

The igneous intrusion modeling case assumes that an igneous dike intersects drifts of the repository and destroys drip shields and waste packages in those drifts intruded by magma, exposing the waste forms to percolating water and mobilizing radionuclides. The released radionuclides can then be transported out of the repository, and flow down through the unsaturated zone to the saturated zone, and then be transported through the saturated zone flow and transport system to the accessible environment. Radionuclide releases occur only as a result of igneous interactions with EBS components and not as a result of drip shield or waste package corrosion processes or early waste package failure.

The volcanic eruption modeling case assumes that the magma flow associated with a dike intersects the repository and destroys a limited number of waste packages, transports waste from the destroyed waste packages to the land surface through one or more eruptive conduits, and then discharges tephra and entrained waste into the atmosphere and transports it downwind.

Seismic Scenario Class— The seismic scenario class describes performance of the repository system in the event of seismic activity that could disrupt the repository system. The seismic scenario class represents the direct effects of vibratory ground motion and fault displacement associated with seismic activity by considering the effects of the seismic hazards on drip shields, waste packages, and cladding. The seismic scenario class also takes into account changes in seepage, waste package degradation, and flow in the engineered barrier system that might be associated with a seismic event. The conceptual models and abstractions for the mechanical response of engineered barrier system components to seismic hazards are documented in *Seismic Consequence Abstraction* (BSC 2005 [DIRS 173247]).

The seismic scenario class is represented by two modeling cases. The first modeling case includes those waste packages that fail solely due to the ground motion damage associated with the seismic event. Only stress corrosion cracks appear on the waste packages from ground motion damage; these only allow diffusive transport of radionuclides. The presence of damaged areas and possible stress corrosion cracks on the drip shields are excluded from the TSPA model (*Seismic Consequence Abstraction,* BSC 2005 [DIRS 173247], Sections 6.5.4 and 6.3.6). The primary cladding failure mechanism from vibratory ground motion is perforation due to accelerations when a waste package impacts an emplacement pallet or when there is an end-to-end impact between adjacent waste packages. The failed cladding fraction varies as a function of peak ground velocity.

The second modeling case includes only those waste packages that fail due to fault displacement damage. The drip shields over the waste packages that are damaged by fault displacement are completely degraded. Therefore, this group of waste packages could also be potentially damaged by crown seepage-induced localized corrosion after the seismic event has occurred. The cladding is fully failed in this modeling case while the damage area from the fault displacement on the waste package varies. The resulting damage is modeled as allowing flow into the waste package (if seepage is present) and allowing advective and diffusive transport out of the waste package.

6.2 FEATURES, EVENTS, AND PROCESSES INCLUDED IN THE MODEL

The development of a comprehensive list of FEPs potentially relevant to postclosure performance of the Yucca Mountain repository is an ongoing, iterative process based on site-specific information, design, and regulations. The approach for developing an initial list of FEPs, in support of TSPA-Site Recommendation (SR) (CRWMS M&O 2000 [DIRS 153246]), was documented in *The Development of Information Catalogued in REV00 of the YMP FEP Database* (Freeze et al. 2001 [DIRS 154365]). The initial features, events and processes (FEP) list contained 328 FEPs, of which 176 were included in TSPA-SR models (CRWMS M&O 2000 [DIRS 153246], Tables B-9 through B-17). To support TSPA, the FEP list was re-evaluated in accordance with *The Enhanced Plan for Features, Events, and Processes (FEPs) at Yucca Mountain* (BSC 2002 [DIRS 158966], Section 3.2), resulting in the LA FEP list

(DTN: MO0407SEPFEPLA.000 [DIRS 170760]). Table 6.2-1 provides a list of FEPs that are included in TSPA models described in this model document, summarizes the details of their implementation in TSPA, and provides specific references to sections within this document. Screening arguments for both included and excluded FEPs are summarized in *Engineered Barrier System Features, Events, and Processes* (BSC 2005 [DIRS 173781]). The following excluded FEPs listed in the TWP (BSC 2005 [DIRS 173617], Table 1) as being associated with this report are summarized in *Engineered Barrier System Features, Events, and Processes* (BSC 2005 [DIRS 173781]) and are not addressed in this report:

- 2.1.06.05.0A – Mechanical degradation of emplacement pallet
- 2.1.08.01.0B – Effects of rapid influx into the repository
- 2.1.08.14.0A – Condensation on underside of drip shield
- 2.2.07.06.0A – Episodic/pulse release from repository
- 2.2.07.21.0A – Drift shadow forms below repository.

Table 6.2-1. Included FEPs for This Report

FEP No.	FEP Name/FEP Description	Section Where Disposition Is Described
2.1.06.06.0A	Effects of drip shield on flow	6.3.2.4 6.5.1.1
2.1.08.04.0A	Condensation forms on roofs of drifts (drift-scale cold traps)	6.3
2.1.08.04.0B	Condensation forms at repository edges (repository-scale cold traps)	6.3
2.1.08.05.0A	Flow through invert	6.3 6.5
2.1.08.06.0A	Capillary effects (wicking) in EBS	6.3 6.5
2.1.08.07.0A	Unsaturated flow in the EBS	6.3 6.5
2.1.09.05.0A	Sorption of dissolved radionuclides in EBS	6.3.4.2 6.5.1.2 6.5.3
2.1.09.08.0A	Diffusion of dissolved radionuclides in EBS	6.3.1.2 6.3.4.1 6.5.1.2 6.5.3.1
2.1.09.08.0B	Advection of dissolved radionuclides in EBS	6.3.1.2
2.1.09.19.0B	Advection of colloids in EBS	6.3.4.4 6.5.1.2 6.5.3
2.1.09.24.0A	Diffusion of colloids in EBS	6.3.4.4 6.5.1.2 6.5.3
2.1.11.09.0A	Thermal effects on flow in the EBS	6.3.1.1
2.2.07.06.0B	Long-term release of radionuclides from the repository	6

6.3 BASE CASE CONCEPTUAL MODEL

6.3.1 Introduction and Overview

6.3.1.1 EBS Flow Abstraction

The primary source of inflow to the EBS is the dripping flux from the crown (roof) of the drift and includes seepage flux and any condensation that may occur on the walls of the drift above the drip shield. The seepage flux is driven by downward infiltration through the existing fracture system at Yucca Mountain. The seepage flux is conceptualized to flow from discrete fractures above the roof of the drift, falling vertically downward, and is represented in the TSPA model through *Abstraction of Drift Seepage* (BSC 2004 [DIRS 169131]). Condensation on the drift walls is represented in the TSPA model through the *In-Drift Natural Convection and Condensation Model* (BSC 2004 [DIRS 164327]). A secondary source of inflow to the EBS is imbibition into the invert crushed tuff particles from the surrounding UZ rock matrix. The inflow from these sources can flow through the EBS along eight pathways, as shown in Figure 6.3-1.

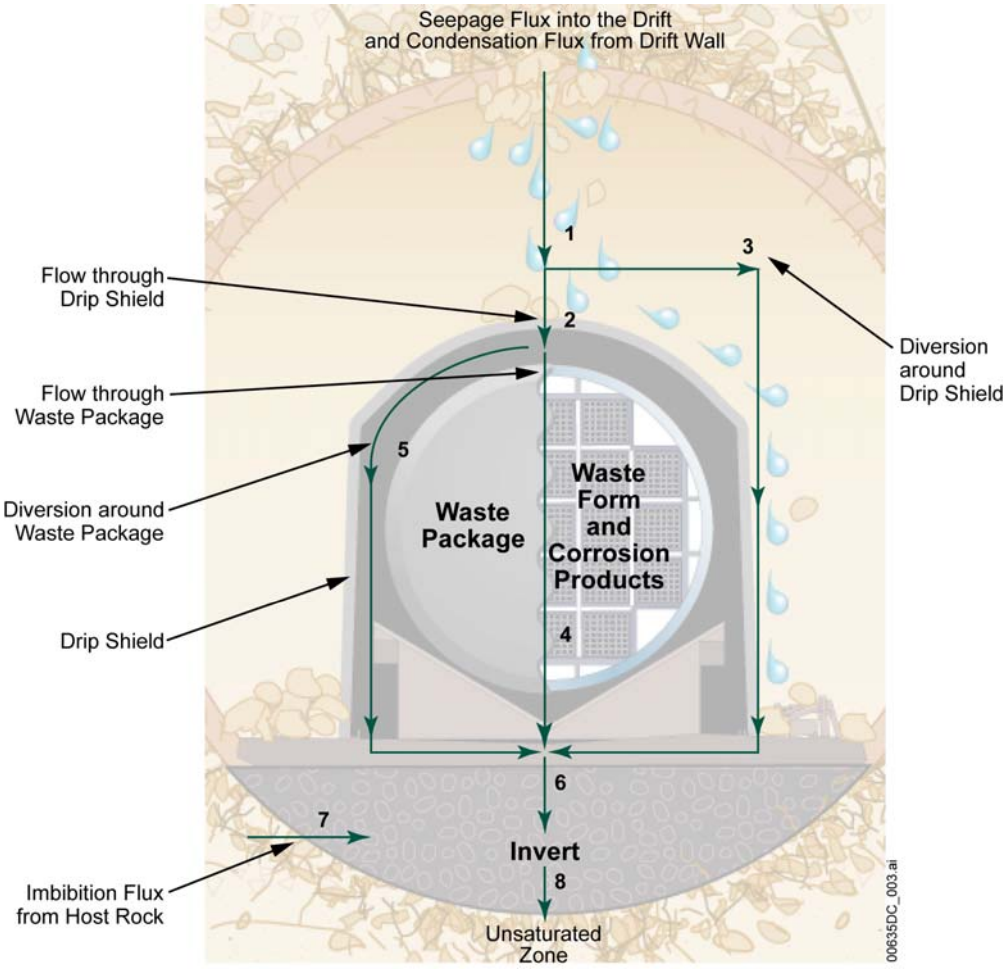

Figure 6.3-1. Schematic of the Potential Flow Pathways in the EBS

These pathways are time dependent, in the sense that total dripping flux, drip shield gaps, drip shield penetrations, and waste package penetrations will vary with time and local conditions in the repository.

The conceptual model for flow through the EBS includes three domains associated with radionuclides: the waste form domain (composed of either fuel rods, HLW glass, or DSNF), waste package corrosion products domain, and the invert domain. The waste form domain for the codisposal packages is divided into two subdomains, HLW glass and DSNF, due to different degradation characteristics of the waste form and associated transport parameters. The waste form domain is conceptualized to have a concentric cylindrical geometry for volume calculations, with one-dimensional flow. The waste form domain is part of the waste package that contains fuel rods or glass logs and DSNF, which undergo alteration to form a rind. The thickness of the rind changes as the degradation of the fuel rod or glass log continues; the DSNF degrades almost instantaneously and the rind thickness remains fixed. The second domain (corrosion products from degradation of steel internal components) fills the inside of a waste package within the Alloy 22 outer corrosion barrier, so its thickness is uncertain and can be as much as the radius of the waste package. The third domain (invert) is modeled as being in intimate contact with the waste package and has a thickness of 0.597 m (see Section 6.5.3). This is the average thickness of the invert, and appropriate for the one-dimensional transport calculation. Because the presence of the emplacement pallet is ignored, water and radionuclides pass directly from the waste package to the invert.

The waste form domain represents the source term for the TSPA. Source term abstractions are defined in other model reports or design documents for radionuclide solubility (BSC 2005 [DIRS 174566]), HLW glass dissolution rate (BSC 2004 [DIRS 169988]), cladding response (BSC 2005 [DIRS 172895]), and inventory by waste package type (BSC 2004 [DIRS 169472], Table 11). The source term represents input data or boundary conditions for the *EBS RT Abstraction* and is not discussed in this document.

The final output from the *EBS RT Abstraction* is the mass flux of radionuclides (kg yr^{-1}) from the EBS into the unsaturated zone. The parameters and formulas for calculating the water fluxes in the various pathways are summarized in Table 6.3-1.

flux through the drip shield that can enter a waste package. The flux splitting algorithm is important to TSPA because the liquid flux into the waste package determines in part the transport of radionuclides by advection, an important release mechanism from the waste package and from the repository.

Once the flux through the drip shield is known, the flux diverted around the drip shield, F_3, is calculated using a quasi-static continuity of flow approach:

$$F_3 = F_1 - F_2 . \qquad \text{(Eq. 6.3.2.4-1)}$$

Key features of the drip shield flux splitting algorithm include: (1) the dripping flux (seepage plus condensation) into the drift falls as droplets from the top of the drift onto the crown of the drip shield (Assumption 5.1); (2) droplets fall randomly along the length of the drip shield; (3) only flow through general corrosion patches is considered; (4) evaporation from the drip shield is neglected (Assumption 5.2); all of the seepage flux either flows through corrosion patches or drains down the sides of the drip shield; and (5) all water that flows through breaches in the drip shield flows onto or into the waste package.

Some aspects of the flux splitting algorithm have been defined or clarified by experiments. The breached drip shield experiments (BSC 2003 [DIRS 163406]) were performed to validate the drip shield flux splitting algorithm and to examine in more detail the real behavior of seepage water impinging on and flowing over a drip shield. The tests were conducted by dripping water onto a mock-up portion of a full-scale drip shield made of stainless steel. The mock-up section included slightly more than half of the shield from the top/center down the curvature to the side. The side was shortened along the longitudinal and vertical axes. Simulated corrosion patches-square holes 27 cm wide, the size of nodes in an earlier version of the WAPDEG corrosion model (CRWMS M&O 2000 [DIRS 151566], p. 36)–were cut into the drip shield at various locations to enable measurements of flow through breaches in the drip shield. Tests were performed with both smooth (machined stainless steel) and rough (silica anti-slip coating) surfaces. Data from the tests on the smooth surface were used to develop parameter values for the flux splitting submodel, whereas the rough surface test data were used to validate the submodel. Tests were conducted in a test chamber in an environment that would minimize evaporation (i.e., relative humidity of at least 80 percent). Water was dripped at various rates intended to cover the expected range of seepage rates within the repository. The dripping distance was the full-scale distance from the top of the drift to the crown of the drip shield, 2.17 m (BSC 2003 [DIRS 163406], Figure 10), based on repository design.

The tests that were conducted included (BSC 2003 [DIRS 163406]): (1) splash radius tests to determine the distance from the point of impact and a rough distribution of splattered water when drops impinge on the surface of the drip shield; (2) spread factor tests to determine the lateral rivulet spread distance from the drip impact point; (3) single patch splash tests to determine the amount of water that enters targeted breaches as a result of splashing; (4) single patch flow tests to determine the amount of water that flows down the surface of the drip shield and into patches; (5) multiple patch tests to collect both splashed water and rivulet flows that entered all affected patches; and (6) bounding flow rate tests to provide data for extreme drift seepage conditions to compare with the nominal seepage rate.

The factor f_{DS} accounts for the uncertainty in the submodel and is a sampled parameter in TSPA simulations. Sources of uncertainty include:

1. **Drip location with respect to the crown of the drip shield**–Drops that fall to either side of the crown will not divide exactly in half, as assumed by this submodel.

2. **Patch location**–Patches located on the crown will allow the entire dripping flux to pass through, whereas Equation 6.3.2.4-2 considers all patches to be located off the crown. For a given value of f_{DS}, Equation 6.3.2.4-2 underestimates the flux into crown patches because $f_{DS} < 1$, so $F_2 < F_1$, i.e., not all of the total dripping flux can flow through breaches. Since most of the randomly-located breaches occurring will not be located on the drip shield crown, this is a reasonable approximation, but not a bounding estimate of flow through drip shield breaches.

3. **Splattering distribution**–Although splattering of drops when they impinge on the drip shield is a random process, preferential directions or distributions could develop, for example, due to surface alteration as a result of corrosion or drift degradation (rockfall).

4. **Rivulet spread**–The breached drip shield experiments showed that a range of rivulet spread factors or spread angles can occur even on smooth surfaces. Surface roughness also affects the rivulet spread angle. Precipitation of salts or accumulation of dust on the drip shield surface could also affect rivulet flow.

5. **Interference among multiple patches**–Implicit in this submodel is that the patches do not interfere with each other, i.e., that no patch is lower on the drip shield surface than another patch. Patches located below another patch will see reduced or zero flux through the patch. By ignoring patch interference, water flux through the drip shield will be overestimated.

6. **Patches outside the footprint of the waste package**–Flux through these patches will pass directly to the invert. Since the conceptual model requires that all flow through the drip shield goes onto or into the waste package, Equation 6.3.2.4-2 will overestimate that flow.

7. **Evaporation from the surface of the drip shield**–Evaporation is neglected (Assumption 5.2); if it occurs, the flux through the drip shield is less than predicted by Equation 6.3.2.4-2.

8. **Size of corrosion patches**–The WAPDEG model assumes a fixed size and shape for all corrosion patches. In reality, the patches will vary widely in size and shape randomly as well as over time.

Bounds and a distribution for f_{DS} must be established for use in TSPA calculations. Because, under some of these uncertain conditions, the flux through the drip shield may be zero even when breaches exist, an appropriate lower bound on f_{DS} is zero. Under some other

circumstances mentioned above, the entire seepage flux could flow through the drip shield. Thus, an upper bound on f_{DS} cannot be specified *a priori*, but should be given by:

$$f_{DS} = \frac{1}{\frac{N_b \ell}{L_{DS}}\left(1+\frac{\tan\alpha}{2}\right)}, \qquad \text{(Eq. 6.3.2.4-3)}$$

which makes $F_2 = F_1$. Since the number of patches, N_b, varies over time, f_{DS} should be a function of time, with a starting value of zero and potentially reaching a value equal to the total number of nodes in the WAPDEG corrosion model of the drip shield (BSC 2004 [DIRS 169996]). A uniform distribution is appropriate given that the uncertainty is difficult to quantify. To ensure that the flux through the drip shield is not greater than the seepage flux, the flux through the drip shield is computed as:

$$F_2 = \min\left[F_1 \frac{N_b \ell}{L_{DS}}\left(1+\frac{\tan\alpha}{2}\right) f_{DS}, F_1\right]. \qquad \text{(Eq. 6.3.2.4-4)}$$

The uncertainty in spread angle α can be lumped in with f_{DS} since both would otherwise be sampled independently. A lumped uncertainty factor f'_{DS} is defined as:

$$f'_{DS} = \left(1+\frac{\tan\alpha}{2}\right) f_{DS}, \qquad \text{(Eq. 6.3.2.4-5)}$$

with the flux through the drip shield to be computed as:

$$F_2 = \min\left[F_1 \frac{N_b \ell}{L_{DS}} f'_{DS}, F_1\right]. \qquad \text{(Eq. 6.3.2.4-6)}$$

In Section 6.5.1.1.2.4, an upper bound on f'_{DS} is developed based on results of the breached drip shield experiments, and is used in the TSPA model.

6.3.3 Water Flux through the Waste Package (F_4)

The conceptual model for the TSPA is based on the assumed presence of continuous flow paths through the patches that penetrate the waste package. More specifically, in the TSPA conceptual model, vertical flow of seepage into the waste package, through the waste form, and out of the waste package is not impeded by the location of patches on the surface of the waste package. In other words, there is no long-term build-up and retention of liquid within the waste package for flow and transport. (An alternative conceptual model in which water fills the waste package before any water flows out–the "bathtub" model–is evaluated in Section 6.4.1). There is also no resistance to the flow through the waste form. The TSPA approach attempts to maximize the immediate release and mobilization of radionuclides, while retaining as much realism as justified by the data and understanding of the physical and chemical processes that take place.

crack is taken to be the lid thickness. Figure 6.3-3 is a schematic diagram of the geometry of the ellipsoidal cone crack.

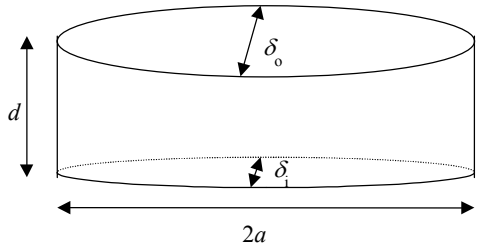

Figure 6.3-3. Schematic of the Dimensions for an Ellipsoidal Crack

A range of values of σ_a, the residual stress, and the maximum length $2a$ of a radial crack can be estimated. The region of high residual stress is identified from finite-element simulations (BSC 2004 [DIRS 172203], Section 6.4). The expected maximum length of a radial crack is approximately two times the lid thickness (BSC 2004 [DIRS 172203], Section 6.5.1). For an outer lid thickness of 25.4 mm (BSC 2004 [DIRS 167394]), the maximum crack length is approximately 50 mm. Table 6.3-3 gives the calculated gap width, based on Equation 6.3.3.1-1 and typical residual stresses at the inner and outer surface of the lid for a 21-PWR waste package (BSC 2004 [DIRS 172203], Table 6-9).

The cross-sectional area of the stress corrosion crack is important for transport by diffusion. The bounding (largest) cross-sectional area is defined by conditions at the outer surface of the 5-cm-long crack. The area of this ellipse is πab, where $2a$ is 5 cm and b is one-half of the larger gap width on the outer surface (in Table 6.3-3). The cross-sectional area of a single stress corrosion crack is then $\pi(0.025\text{ m})(9.8 \times 10^{-5}\text{ m})$ or $7.7 \times 10^{-6}\text{ m}^2$.

An updated analysis of stress corrosion cracking is given in *Stress Corrosion Cracking of the Drip Shield, the Waste Package Outer Barrier, and the Stainless Steel Structural Material* (BSC 2004 [DIRS 172203]). For the base conceptual model (BSC 2004 [DIRS 172203], Appendix B, Table B-2), the estimated crack opening is smaller than the crack opening of $7.7 \times 10^{-6}\text{ m}^2$ obtained in this section. Therefore, use of this value in TSPA calculations when stress corrosion cracking occurs will overestimate the rate of release of radionuclides compared with the updated values in (BSC 2004 [DIRS 172203]).

Table 6.3-3. Calculated Gap Width for a Range of Residual Stresses at 400°F (Approximately 200°C) in a 21-PWR Container

Parameter	Inner Surface	Outer Surface
Hoop stress, σ_a (BSC 2004 [DIRS 172203], Table 6-9)	231.1380 MPa	385.0522 MPa
Gap width for crack length $2a$ = 50 mm	118 μm	196 μm

Advective flow into stress corrosion cracks is unlikely because the waste package is not oriented in such a way that water can flow in. Dripping water is capable of contacting a stress corrosion crack only if the waste package is tilted upward. A possible mechanism for tilting is emplacement pallet collapse due to corrosion that causes one end of the waste package to fall off

(BSC 2005 [DIRS 173944], Section 6.3) indicate that the available heat can evaporate incoming water for several thousand years. However, although evaporation is expected to occur, complexities in the internal geometry of the waste packages (particularly the response of any water pooled at the bottom of the package and the potential presence of small conduits for water vapor to escape through stress corrosion cracks) make it difficult to say definitively that all incoming water is evaporated.

The expected evaporation in the waste package is ignored in the TSPA. This approach is bounding because evaporation might eliminate advection as a transport mechanism. In addition, by ignoring evaporation from a waste package, it becomes possible to specify a water saturation of 1.0 (fully saturated) inside a failed waste package whenever dripping occurs. If evaporation were accounted for, the water saturation inside a waste package would generally be less than 1.0, which would reduce the amount of radionuclides that could dissolve in the water and be advectively transported from the waste package. Lower water saturations would also reduce estimates of diffusive releases, since both the diffusion coefficient and the cross-sectional area for diffusion would be less. Thus, without these simplifying assumptions, the amount of radionuclides transported from a waste package would be expected to be less.

As a simplification, it is assumed that no radionuclide transport occurs when the temperature in the waste package is above 100°C (Assumption 5.5), when a continuous film of water needed for transport is not expected to exist.

6.3.3.2 Water Flux through and around the Breached Waste Package (F_4 and F_5)

The flux through (into and out of) the waste package, F_4, is conceptualized to be the flux through patches, which originates from the flux thorough the drip shield (F_2). Advective flux of water through stress corrosion cracks is unlikely and therefore is neglected (Section 6.3.3.1.2.1). A quasi-steady state approach is used. The presence of a gap between adjacent waste packages is neglected in the TSPA model. Dripping onto the waste package from condensation on the underside of the drip shield is screened out (BSC 2005 [DIRS 173781], Section 6.2.43).

A flux splitting algorithm analogous to the drip shield flux splitting algorithm (Section 6.3.2.4) is developed here. The analogy is appropriate based on similarities in geometry and assumptions regarding the source of liquid flux falling onto the waste package. The surface of the waste package is a horizontal cylinder, as is the top of the drip shield, the primary difference that impacts liquid flow on the curved surface being that the radius of curvature of the waste package is smaller than that of the drip shield. Thus, flow behavior on the surface of the waste package should be similar to that on the drip shield. In particular, if any water is available, it is expected to flow over the surface of the waste package in rivulets rather than as film flow, based on findings of the breached drip shield experiments (BSC 2003 [DIRS 163406]).

Whereas drip locations on the drip shield could reasonably be confined to the crown of the drip shield (because the drift seepage flux will most likely originate from the crown of the drift), the drip locations may be more widely dispersed on the waste package. This is the case for drips that fall from breaches in the drip shield, which are randomly located on the drip shield. Since breaches (mainly general corrosion patches) in the waste package are also randomly located, the fraction of dripping flux falling on the waste package that flows into the waste package might be

regions of the drip shield. Rivulets flowing from those drip locations may simulate more closely the behavior on a surface having a smaller radius, such as a waste package. Because the waste package has a smaller radius and more curvature than the drip shield surface, more of the surface is sloped to such a degree that water will readily flow down it by gravity. Only a larger cylindrical surface (the drip shield mock-up) was available on which to observe gravity flow behavior. Observations away from the crown, where the slope is steep enough to initiate flow as readily as on a more highly curved surface, are appropriate analogs to measurements on an actual smaller cylinder. An analysis of drip shield experimental data for off-crown drip locations (Section 6.5.1.1.3) gives a mean spread angle of 13.7° and a range from 5.5° to 22.0°. In analogy to f_{DS}, an upper bound on f_{WP} can be obtained using the minimum rivulet spread angle α of 5.5° and the known values for N_{bWP} (BSC 2004 [DIRS 169996]), $2\ell_{WP}$, and L_{WP}:

$$f_{WP} = \frac{1}{\frac{N_{bWP}\ell_{WP}}{L_{WP}}\left(1+\frac{\tan\alpha}{2}\right)}. \qquad \text{(Eq. 6.3.3.2-2)}$$

As with the drip shield, the term $\left(1+\frac{\tan\alpha}{2}\right)$, which is uncertain itself, can be factored in with f_{WP} to simplify the model, resulting in:

$$F_4 = \min\left[F_2\left(\frac{N_{bWP}\ell_{WP}}{L_{WP}}\right)f'_{WP}, F_2\right], \qquad \text{(Eq. 6.3.3.2-3)}$$

where

$$f'_{WP} = \left(1+\frac{\tan\alpha}{2}\right)f_{WP} \qquad \text{(Eq. 6.3.3.2-4)}$$

is assigned a uniform distribution. In Section 6.5.1.1.3, an upper bound on f'_{WP} is developed based on results of the breached drip shield experiments. The range for f'_{WP} based entirely on experimental results is used in TSPA.

Finally, the flux that is diverted around the waste package, F_5, is calculated using continuity of the quasi-static flow around and into the waste package:

$$F_5 = F_2 - F_4. \qquad \text{(Eq. 6.3.3.2-5)}$$

6.3.3.3 Condensation on the Drip Shield

Condensation of water on the underside of the drip shield is discussed in *Engineered Barrier System Features, Events, and Processes* (BSC 2005 [DIRS 173781], Section 6.2.43, FEP Number 2.1.08.14.0A). A review of the temperature profiles calculated using the results described in *In-Drift Natural Convection and Condensation Model* (BSC 2004 [DIRS 164327],

the corrosion products, sorption and desorption onto colloids, and colloid stability. The concentrations in the invert domain depend on the radionuclide solubility limits, colloid stability in the invert, the transfer of radionuclides between the corrosion products domain and the invert, and the boundary concentrations at the invert-unsaturated zone interface. The boundary condition at the unsaturated zone interface is implemented by defining multiple grid cells in the unsaturated zone that provide a diffusive path length that is sufficiently long such that the concentration at the outlet of the farthest cell from the drift wall can realistically be assigned a value of zero (Section 6.5.3.6).

The emphasis in this *EBS RT Abstraction* is on transport of radionuclides through the EBS after the radionuclides are mobilized. This abstraction does not define related elements of the TSPA, such as corrosion processes, radionuclide solubility limits, waste form dissolution rates and concentrations of colloidal particles, that are generally represented as boundary conditions or input parameters for the *EBS RT Abstraction*. This abstraction provides the algorithms for determining radionuclide transport in the EBS using the flow and radionuclide concentrations determined by other elements of the TSPA.

6.3.4.1 Invert Diffusion Submodel

The TSPA model requires an abstraction for the effective diffusion coefficient in granular materials as a function of radionuclide, porosity, saturation, temperature, and concentration. This submodel is intended specifically to apply to the invert. The abstraction is as follows:

- Use the free water diffusion coefficient for self-diffusion of water, 2.299×10^{-5} cm^2 s^{-1} (Mills 1973 [DIRS 133392], Table III), as a bounding value for all radionuclides at 25°C.

- Modify the free water diffusion coefficient for the porosity and liquid saturation of the invert. The modification for porosity and saturation is based on Archie's law and experimental data for granular media, and is presented in Section 6.3.4.1.1.

- Further modify the diffusion coefficient for variation of the invert temperature using the formulation in Section 6.3.4.1.2. The invert temperature is provided by the *Multiscale Thermohydrologic Model* (BSC 2005 [DIRS 173944]).

- Ignore the increase in the diffusion coefficient with increasing ionic strength of concentrated solutions (see Section 6.3.4.1.3). The maximum modification for a highly concentrated solution of potassium iodide is a factor of 1.27. This factor is almost within the bounding approximation inherent in using the self-diffusion coefficient for all radionuclides. It is neglected for the TSPA.

6.3.4.1.1 Modification of Diffusion Coefficient for Porosity and Saturation of the Invert

The modified diffusion coefficient for a partly saturated porous medium can be estimated from Archie's law and the relationship between electrical conductance and diffusivity in a liquid. This relationship enables diffusion coefficients to be obtained from experimental measurements of the electrical conductivity of samples of the porous medium. From these measurements, an

θ = volumetric moisture content (percent).

The slope of the *X*-*Y* relationship is found to be 1.863, leading to the following linear equation for *Y* as a function of *X*:

$$Y = 1.863X$$

$$\log_{10}\left(\frac{\phi S_w D_I}{D_0}\right) = 1.863\left(\log_{10}\theta - 2\right), \qquad \text{(Eq. 6.3.4.1.1-20)}$$

or

$$\phi S_w D_I = D_0 \phi^{1.863} S_w^{1.863} = D_0\left(\frac{\theta}{100}\right)^{1.863}. \qquad \text{(Eq. 6.3.4.1.1-21)}$$

The statistical fit for the effective invert diffusion coefficient has uncertainty, which is represented by the scatter of data points around the fit in Figure 6.3-4. This uncertainty is approximated by a normal distribution for the residuals (data–model) in log-log space. This normal distribution of residuals has a mean value of 0.033 and a standard deviation of 0.218. The uncertainty can be incorporated into the statistical fit as an additional factor on the full statistical fit.

$$\phi S_w D_I = D_0 \phi^{1.863} S_w^{1.863} 10^{ND(\mu=0.033,\sigma=0.218)} \qquad \text{(Eq. 6.3.4.1.1-22)}$$

where *ND* represents a normal distribution with a mean, μ, of 0.033 and a standard deviation, σ, of 0.218. *ND* is in the exponent because the residuals are calculated in the log-log space of the statistical fit. This statistical fit is the submodel for the invert diffusion coefficient to be used for TSPA. Since the normal distribution is theoretically unbounded, unrealistic values for the diffusion coefficient could potentially be obtained. To avoid this potential problem, the implementation in TSPA will use a truncated normal distribution, limited to plus or minus three standard deviations from the mean.

Figure 6.3-4 presents the statistical fit (solid line) and the upper and lower bounds (dashed lines) at three standard deviations above and below the fit. The dashed lines encompass almost all the data points, because ± 3 standard deviations includes 99.7 percent of the area under a normal distribution. Equation 6.3.4.1.1-22, therefore, accurately represents the uncertainty in the diffusivity data for the TSPA calculations.

Because the saturation exponent (1.863) is less than the generally accepted value (2), the fit to the data provides less of a bounding estimate for the effective diffusion coefficient than if the accepted value were used. However, the estimate using Equation 6.3.4.1.1-22 is realistic instead of simply bounding the diffusion coefficient because it is developed from measured data rather than using the general behavior of unconsolidated sand as its basis. Furthermore, being based on a large number of measured data, the uncertainty in effective diffusion coefficient using

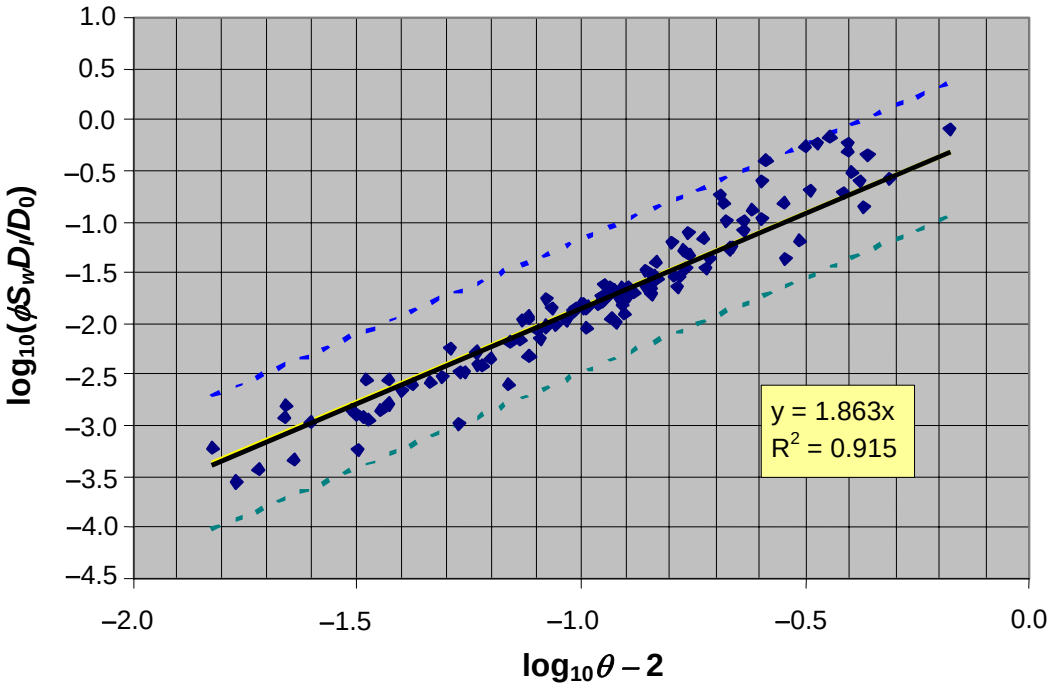

Source: Conca And Wright 1992 [DIRS 100436], Figure 2; Conca et al. 1993 [DIRS 170709], Figure 2.

NOTE: The dashed lines correspond to three standard deviations above and below the statistical fit to the data.

Figure 6.3-4. Uncertainty in the Statistical Fit for the Effective Diffusion Coefficient

For each realization of the TSPA calculations, the normal distribution is sampled, thereby incorporating the uncertainty of the experimental data into the diffusivity.

6.3.4.1.2 Modification for Temperature

The diffusivity D_T is proportional to absolute temperature and inversely proportional to viscosity η_T; i.e., $D_T \propto T/\eta_T$ (Cussler 1997 [DIRS 111468], p. 114). It follows that if the diffusivity is known at some temperature T_0, the diffusivity at temperature T can be found by:

$$\frac{D_T}{D_{T_0}} = \frac{\frac{T}{T_0}}{\frac{\eta_T}{\eta_{T_0}}}, \qquad \text{(Eq. 6.3.4.1.2-1)}$$

where D_T is the diffusion coefficient ($m^2\ s^{-1}$) at temperature T (K), D_{T_0} is the diffusion coefficient ($m^2\ s^{-1}$) at temperature T_0 (K), η_T is the viscosity of water (Pa s) at temperature T (K), and η_{T_0} is the viscosity of water (Pa s) at temperature T_0. The dependence of viscosity on temperature T (K) (293.15 K ≤ T ≤ 373.15 K) is given by (Weast and Astle 1981 [DIRS 100833], p. F-42):

6.3.4.1.3 Modification for Concentrated Aqueous Solutions

Data in *American Institute of Physics Handbook* (Gray 1972 [DIRS 138541], Table 2p-2) show that the majority of the diffusion coefficients increase with increasing solution strength. For example, the diffusion coefficient of sodium iodide increases from 1.616 in a dilute solution to 1.992 for a 3 M solution and the coefficient for potassium iodide increases from 2.00 in a dilute solution to 2.533 at 3.5 M. The percent increase for potassium iodide, 26.7 percent, is the greatest of any in Gray's Table 2p-2, (Gray 1972 [DIRS 138541]) excluding HCl. HCl has been excluded from consideration because, being volatile, it is not representative of the type of radionuclides released from the waste package.

Although the diffusion coefficients of aqueous solutions increase with increasing ionic strength, the self-diffusion coefficient of water is still higher. Therefore, using the self-diffusion coefficient for water is a bounding value for all radionuclides at a given temperature. The modification for concentrated aqueous solutions is therefore neglected in the TSPA.

6.3.4.2 Retardation in the Engineered Barrier System

In this section, parameters are developed to enable the impact of sorption processes on radionuclide transport through the EBS to be quantified. Transport through the EBS is affected by the adsorption and desorption of radionuclides on the materials in the waste package and invert. Adsorption describes the uptake of a radionuclide by a solid surface when in contact with a radionuclide-laden aqueous solution. This uptake typically occurs when a bond is formed by surface sites that have a chemical affinity for the radionuclide. Progressive inflow of fluids with low radionuclide concentrations would thermodynamically favor desorption of the original population of sorbed radionuclides back into solution, a process referred to as reversible sorption. Fully reversible sorption and desorption of radionuclides is often described by a linear isotherm, using a sorption distribution coefficient (K_d).

Irreversible sorption refers to the tendency in natural systems for desorption to be incomplete. In other words, the amount of sorbed contaminant available for desorption in natural systems is typically less than the total sorbed mass due to chemical and physical processes occurring at or beneath the mineral surface. Irreversible sorption is described by a reaction rate coupled with some limit on the amount of sorption that is possible.

Sorption processes are referred to as adsorption if the process occurs on the surface or absorption if the process occurs beneath the surface. Retardation in the EBS results from adsorption of radionuclides on surfaces of corrosion product or tuff particles that comprise a porous bulk mass.

This section defines a conceptual model and parameters for transport through the degraded EBS, including appropriate K_d values and a description of irreversible sorption of radionuclides. In addition to adsorption of radionuclides, water is expected to adsorb on corrosion products inside a breached, degraded waste package. This adsorbed water will provide a diffusive transport pathway under conditions where no seepage occurs into the drift. This in-package diffusion submodel is described in more detail in Section 6.3.4.3. Section 6.5.1.2 and Appendix B show the mathematical incorporation of the K_d approach in the transport model.

water saturation in corrosion products, while goethite and HFO properties are used for modeling corrosion product surface chemistry (specifically, irreversible sorption). Because the water vapor adsorption isotherms (expressed as water layer thickness) for HFO and goethite are similar to that of hematite (Section 6.3.4.3.1), the hematite isotherm (Jurinak 1964 [DIRS 154381], p. 486) is representative of the mixed iron oxide assemblage and is used to compute the water content in the corrosion products. The specific surface areas of HFO and goethite are generally greater than that of hematite (Langmuir 1997 [DIRS 100051], Table 10.2), meaning that the water content and the potential for radionuclide diffusion is greater at any given relative humidity for ferrihydrite and goethite than for hematite. However, the diffusion rate is dependent on the dissolved concentration of radionuclides in the corrosion products. The mass of radionuclides in solution is given by the waste form degradation rate. Because the water content or volume will tend to be less using hematite specific surface area rather than those of goethite or HFO, the given mass of radionuclides will result in the radionuclide concentration being higher for hematite corrosion products. Consequently, releases will be overestimated by using hematite properties for water adsorption calculations.

6.3.4.2.2 Sorption Parameters for the Invert

In the invert, radionuclide sorption can potentially take place on the crushed tuff ballast material and on products of corrosion of the metallic components such as steel support beams and copper conductor bars. In the *EBS RT Abstraction*, sorption onto the crushed tuff is included so as to be consistent with the model for sorption onto tuff in UZ transport (BSC 2004 [DIRS 164500], Section 6.1.2.3). As a bounding approach, sorption of radionuclides on corrosion products in the invert is ignored (Assumption 5.6).

6.3.4.2.2.1 Sorption onto Crushed Tuff in the Invert

Sorption onto the crushed tuff is included in the EBS transport abstraction. K_d values and distributions for nine selected radionuclides are presented in Table 4.1-15 (DTN: LA0408AM831341.001 [DIRS 171584]); K_d values for sorption of carbon, iodine and technetium on tuff are zero. The ranges of K_d values for sorption onto devitrified tuff are used because the crushed tuff in the invert will be the same tuff that is removed when the drifts are bored; most of the repository will be developed in the TSw33 through TSw36 stratigraphic units, which are composed of devitrified tuff. The K_d values selected are summarized in Table 6.5-6. Correlations of K_d values among various radionuclides for sorption on tuff are given by a correlation matrix presented in Table 4.1-16. Invert K_d values are implemented in TSPA by first computing unsaturated zone K_d values for devitrified tuff and then assigning those values to the invert.

6.3.4.2.2.2 Sorption onto Corrosion Products in the Invert

Invert corrosion products will tend to be localized and widely spaced, with the possibility being that seepage from the waste package could completely miss corrosion products in the invert. In this case, even small K_d values could overestimate the amount of retardation of radionuclides in the invert. Furthermore, invert corrosion products will have a smaller sorptive capacity than waste package corrosion products simply because the masses of sorptive corrosion products in

the invert are much less than in the waste packages. Therefore, as a bounding approach, sorption of radionuclides on corrosion products in the invert is ignored (Assumption 5.6).

To compare with the mass of sorbing material in the waste packages, the mass of sorbing material in the invert is estimated below using the data from *Repository Subsurface Emplacement Drifts Steel Invert Structure Sect. & Committed Materials* (BSC 2004 [DIRS 169776], Committed Materials table). The iron content of the steel invert support beams, stiffeners, base plates, gantry runway beams, runway beam cap plates, stub columns and top plates, miscellaneous stiffener plates, and the gantry rails is included in this calculation. The iron in the steel set ground support, the rock bolts, and the welded wire fabric steel has been ignored, even though the corrosion products from these components may fall on the invert.

As in Table 6.3-4 (Section 6.3.4.2.3.1), the mass of corrosion products is estimated by assuming that iron converts to Fe_2O_3 during the corrosion process. The mass of A 588 carbon steel per unit length of drift in the invert is 893 kg m^{-1} (BSC 2004 [DIRS 169776], Committed Materials table), having an iron content of 859 kg m^{-1} (using an iron content of 96.16 percent for the composition of A 588 steel; ASTM A 588/A 588M-01 [DIRS 162724], Table 1). The mass of A 759 steel in the gantry rails is 134 kg m^{-1} (BSC 2004 [DIRS 169776], Committed Materials table), which has an iron content of 97.47 percent (ASTM A 759-00 [DIRS 159971]), or 131 kg m^{-1}. The total iron content of the invert is then 990 kg m^{-1}, which converts to 1,415 kg m^{-1} of Fe_2O_3. As a comparison, the average mass of Fe_2O_3 in the invert under a 21-PWR or 44-BWR waste package, having a nominal length of 5.02 m (BSC 2004 [DIRS 169472], Table 1), would be 7,100 kg, or approximately one-third the amount of iron corrosion products inside a waste package (Table 6.3-4). Thus, while not negligible, the sorptive capacity of the invert is small compared to that of the waste packages, and ignoring retardation by corrosion products in the invert (Assumption 5.6) will overestimate radionuclide transport.

The impact of copper in the invert on retarding iodine and technetium is discussed here to complete the analysis of neglecting retardation by corrosion products in the invert and thus overestimating radionuclide transport. The amount of elemental copper in the drift is given by the nominal weight of the solid copper conductor bar rail, 4.0 kg m^{-1} (BSC 2001 [DIRS 154441], Section 3.1.7), plus the copper in the communication cable, which is 50 percent by weight of the total cable weight of 2.00 kg m^{-1} (BSC 2001 [DIRS 154441], Sections 3.1.9 and 3.2.1.3). The total weight of elemental copper per meter of drift is then [4.0 + (0.5)(2.00)] or a total of 5.0 kg m^{-1}. These values are based on the nominal mass of elemental copper, rather than the upper bound values, to avoid overestimating potential sorption on copper. The mass of elemental copper is not explicitly represented in the TSPA model, but its presence when oxidized is noted because of its role as a potential sorber for iodine and technetium.

The mass of copper is large relative to the mass of iodine and technetium. Using a waste package length of 5.024 m for the CSNF waste package (BSC 2004 [DIRS 169472], Table 1), there is nominally 25.1 kg (395 mol) of elemental copper in the invert per CSNF waste package. This value (25.1 kg) can be compared to approximately 7.64 kg (77.2 mol) of technetium-99 and 1.75 kg (13.6 mol) of iodine-129 per CSNF waste package (DTN: SN0310T0505503.004 [DIRS 168761]). Thus, there is more elemental copper than iodine or technetium using a mass or molar basis. Similarly, the 5 DHLW/DOE SNF - Short codisposal waste package has a length

design changes for the 5 DHLW/DOE Short waste package (see Section 4.1.3, preceding Table 4.1-18), the mass of iron in that waste package is larger using the current design (IED 800-IED-WIS0-00601-000-00A, BSC 2005 [DIRS 173501], Table 7) than for the earlier design version (BSC 2004 [DIRS 167207], Table 5). In addition, in the calculation of the corrosion product mass (see Figure A-2), a mass of 1 kg for the Interface Ring for the 5 DHLW/DOE Short waste package is erroneously used; the correct value is 44.6 kg. Lastly, the mass of the spread ring was increased from 31.9 kg in the earlier design version (BSC 2004 [DIRS 167207], Table 5) to 33.8 kg in the current design (BSC 2005 [DIRS 173501], Table 7). Using the updated 5 DHLW/DOE Short waste package design data and correcting the Interface Ring mass result in an increase in the estimated mass of corrosion products, from 14,230 kg (Table 6.3-4) to 14,320 kg (updated, corrected value). The difference (0.6 percent) is negligible, so the earlier estimate of 14,230 kg shown in Table 6.3-4 is suitable for TSPA calculations.

In a revision to the 21-PWR and 44-BWR waste package design (Anderson 2004 [DIRS 171637], BSC 2004 [DIRS 170710], BSC 2004 [DIRS 170838]), the Neutronit used for the absorber plates is replaced with a nickel-chromium-molybdenum-gadolinium alloy, N06464 (ASTM B 932-04 [DIRS 168403]), denoted as Ni-Gd Alloy. The mass of Neutronit in a 21-PWR waste package (2,120 kg; see Table 6.3-4) is replaced by 2400 kg of Ni-Gd Alloy. The mass of Neutronit in a 44-BWR waste package (2,990 kg; see Table 6.3-4) is replaced by 3,290 kg of Ni-Gd Alloy. Whereas Neutronit contains 66.06 percent iron (Kügler 1991 [DIRS 155761], p. 15), N06464 contains a maximum of 1.0 percent iron (ASTM B 932-04 [DIRS 168403]). In the analysis summarized in Table 6.3-4, only the iron in the waste package components contributes to the corrosion product mass that is used in water adsorption calculations in the in-package diffusion submodel, Section 6.3.4.3. This corrosion product mass also is used in the radionuclide sorption calculations. Using N06464 instead of Neutronit in a 21-PWR waste package would reduce the total iron mass from 13,600 kg to 12,220 kg; the equivalent mass of Fe_2O_3 would be reduced from 19,440 kg to 17,470 kg, a reduction of 10.1 percent. Using N06464 instead of Neutronit in a 44-BWR waste package would reduce the total iron mass from 15,550 kg to 13,610 kg; the equivalent mass of Fe_2O_3 would be reduced from 22,240 kg to 19,460 kg, a reduction of 12.5 percent.

For purposes of TSPA calculations, iron and corrosion product mass estimates are based on the earlier waste package design. For a 21-PWR waste package, the calculations use Revision 00C of *Design and Engineering, 21-PWR Waste Package Configuration* (BSC 2004 [DIRS 167394]) rather than Revision 00D (BSC 2004 [DIRS 170710]). For a 5 DHLW/DOE Short waste package, the calculations use Revision 00B of *D&E/PA/C IED Typical Waste Package Components Assembly* (BSC 2004 [DIRS 167207], Table 5), instead of Revision 00C (BSC 2004 [DIRS 169472], Table 5). The estimated masses of corrosion products in 44-BWR and Naval Long waste packages shown in Table 6.3-4 are not used directly in TSPA calculations.

a 21-PWR, 21,640 kg FeOOH vs. 19,440 kg Fe_2O_3; for a 5 DHLW/DOE Short, 15,940 kg FeOOH vs. 14,320 kg Fe_2O_3). The increase is obtained from the percentage change from the molecular weight of hematite (0.15969 kg mol^{-1}) to that of goethite or HFO (both having the chemical formula FeOOH with molecular weight of 0.08885 kg mol^{-1}), accounting for stoichiometry: $100 \times [(2 \text{ mol FeOOH/mol } Fe_2O_3) \times (0.08885)/(0.15969) - 1] = 11.3\%$. This increase in mass of corrosion products is approximately the same as the 10 to 12% *decrease* in corrosion product mass resulting from using the current waste package design instead of the previous design. Thus, using hematite as corrosion products together with the iron content of the previous waste package design approximately offsets treating corrosion products as goethite and HFO with the current waste package design.

6.3.4.2.3.2 Irreversible Sorption onto Waste Package Corrosion Products

Irreversible sorption of a limited number of radionuclides (Pu and Am only) is allowed to take place in recognition of field and laboratory observations that this process does occur. Uncertainty is accounted for by specifying a range and distribution for parameters governing the irreversible sorption model.

Recent reviews of field and laboratory measurements indicate that the fraction of sorbed plutonium that is available for desorption rarely exceeds 1 percent (Brady et al. 1999 [DIRS 154421], Appendix F, pp. 141 to 142; Davis and Kent 1990 [DIRS 143280]; see also Section 6.3.4.2). Observations of this sort have led to the concept that most of the plutonium sorbed onto soil materials and particularly iron oxyhydroxides is irreversibly attached. Recognition of the strong role of "irreversible sorption" is implicit in models for watershed transport (Graf 1994 [DIRS 154419]) that focus solely on particulate transport. At the Rocky Flats site in Colorado, soil plutonium is largely associated with the negatively charged organic macromolecular fraction and not with the more abundant iron oxides and clays (Santschi et al. 2002 [DIRS 170923]; Ibrahim and Salazar 2000 [DIRS 170882]). Litaor and Ibrahim (1996 [DIRS 161667]) used 0.01 M $CaCl_2$ as an extractant and measured plutonium in Rocky Flats soil to be 0.04 to 0.08 percent exchangeable. Transport of minute quantities of colloidal plutonium (10^{-14} M) over hundreds of meters was observed at the Nevada Test Site (Kersting et al. 1999 [DIRS 103282]), although the presence of organics may limit the relevance of these data to Yucca Mountain. Laboratory experiments of plutonium sorption onto iron oxide colloids have shown that approximately 1 percent of the initially sorbed plutonium can be desorbed into solution over a period of several months (Lu et al. 2000 [DIRS 166315]; BSC 2004 [DIRS 170025], Section 6.3.3.2), which is broadly consistent with field observations, although much shorter in time scale. However, because the time scales for all of these observations are much shorter than the regulatory time period for repository performance (10,000 years), parameters describing irreversible sorption of plutonium in TSPA calculations have a large uncertainty.

Although the field studies describe contaminant plumes that appear to be up to 50 years old, these occurrences of plutonium have not been studied, nor data collected, during that period. In addition, the mechanism(s) of attachment have not been addressed in these studies. Possible mechanisms of plutonium sorption and desorption are described in Section 6.6.7. In that section an alternative conceptual model is presented that incorporates a two-site model of iron oxyhydroxide substrates, based on published studies, that is supported by the data from Lu et al.

(2000 [DIRS 166315]). A plausible mechanism for the strong sorption of plutonium is described in Section 6.6.7 based on the reduction of Pu(V) to Pu(IV) at the surface of the iron oxyhydroxide substrates. However, it is not known if this process explains strong sorption of plutonium over long periods of time. In any case, neither this mechanism nor any other has been invoked to explain the field occurrences of plutonium nor, until recently, the laboratory data (Lu et al. 2000 [DIRS 166315]) that suggest slow desorption.

Effectively irreversible uptake may be the dominant control over contaminant transport in soils. Evidence for soil sequestering of bomb-pulse plutonium and americium and of uranium, iodine, technetium, cesium, and strontium from ore processing and reactor operations has been documented in the literature (Coughtrey et al. 1983 [DIRS 132164]). Pu and Am sorb more strongly than the others listed (see BSC 2004 [DIRS 170025], Section 6.3.3.1).

Estimates of the mean fraction of irreversible sorption for various radionuclides on soil are derived in *Site Screening and Technical Guidance for Monitored Natural Attenuation at DOE Sites* (Brady et al. 1999 [DIRS 154421], Appendix F, pp. 141 to 142). The value of the irreversible fraction for the EBS will differ from that for soils and will depend on the material that the specific radionuclide encounters, the speciation of the radionuclide, and other factors in the material and chemical environment. For the TSPA model, irreversible sorption of Pu and Am is included, with appropriate fractions of the total mass adsorbed being based on field observations. The implementation of the irreversible radionuclide sorption component of the EBS transport model is described in Section 6.5.3.4.

For the irreversible sorption submodel, the composition of the iron oxyhydroxide corrosion products is modeled as goethite, ranging from 45 – 80 percent, with the balance being HFO (Section 6.3.4.2.1). The goethite and HFO content has a uniform distribution. Justification for these composition ranges is as follows.

Ferrihydrite will convert to the more stable phase goethite under repository conditions so the latter will most likely be the dominant phase after long periods of time. Under controlled laboratory conditions, this conversion occurs rapidly, with time frames on the order of days to even months depending on temperatures and solution composition. A study by Hamzaoui et al. (2002 [DIRS 173866]), for example, on the transformation of ferrihydrite to goethite at alkaline conditions for a given range of temperatures indicates that full conversion will occur in a period of about 80 hours at pH 11 and about 20 hours at pH 12.2 and a temperature of 40°C. A similar result at pH 12.2 was obtained by Cornell and Giovanoli (1988 [DIRS 173864]) but at a temperature of 70°C, where full conversion to goethite was obtained in about 24 hours. Hamzaoui et al. (2002 [DIRS 173866]) also show that transformation rates increases with increasing pH. The studies by Cornell and Giovanoli (1988) and Cornell et al. (1989 [DIRS 173865]) indicate that the presence of some metals in solution and organics tends to retard the transformation of HFO to more crystalline phases. Slower rates are expected at ambient temperatures and near-neutral pH conditions. Schwertmann et al. (2000 [DIRS 173863]) studied long-term transformation of ferrihydrite to more crystalline oxyhydroxides at pH 4-7 and 25°C. Their results show that the presence of other metals in soils, such as Al, can slow down the conversion process. Even at low metal concentration, the full transformation process can be on the order of many months. However, whereas laboratory data show fast conversion rates from ferrihydrite to goethite, field-type corrosion experiments under

consistent with that adopted for HFO ($Fe_2O_3 \cdot H_2O$) along with the conversion factor of 89 g HFO/mol Fe by Dzombak and Morel (1990 [DIRS 105483]). Therefore, the adopted chemical formula for ferrihydrite/HFO in this analysis is FeO(OH), which is equivalent to that of goethite. Adoption of this chemical composition is consistent with that used in the HFO sorption analysis presented by Dzombak and Morel (1990 [DIRS 105483]). The close correspondence of the adopted chemical formula for ferrihydrite/HFO when compared to the range of reported compositions given above for ferrihydrite (Cornell and Schwertmann 2003) supports the use of this chemical formula in this report.

The sorptive capacity of the corrosion products is directly proportional to the surface area of the solids. Data for the specific surface area of goethite and HFO are compiled in Table 4.1-10 and qualified for use in TSPA in Section 4.1.2. These data provide a range of values to be sampled in TSPA for both goethite and HFO. The data in Table 4.1-10 are used to develop a discrete distribution, shown in Table 6.3-6. To calculate the discrete probability distribution, the data in Table 4.1-10 were first sorted into ascending order. Multiple occurrences of the same number were removed from the sorted data list, but their occurrence frequency was assigned for probability calculation. The probability levels were calculated by dividing the frequency of the each data number by the total number of original data points in the data list. The specific surface area of HFO is given by a single value, 600 $m^2 g^{-1}$ (Dzombak and Morel 1990 [DIRS 105483], Table 5.3; Hofmann et al. 2005 [DIRS 173711], Table 2).

Irreversible sorption of radionuclides occurs only on specific sites on the surface of corrosion product particles. The number of sites per unit area of surface, or site density (typically in units of sites nm^{-2}), determines the total quantity of radionuclides that can be adsorbed. Site density data for goethite and HFO are compiled in Table 4.1-10 and qualified for use in TSPA in Section 4.1.2. Site density data for goethite in Table 4.1-10 in units other than sites nm^{-2} are converted to sites nm^{-2} in Table 6.3-4a.These data provide a range of values to be sampled in TSPA for both goethite and HFO. The data in Table 4.1-10 are used to develop discrete distributions, shown in Table 6.3-6, by applying the same technique used for goethite specific surface area.

where S_{HA} (Table 4.1-12) and S_{total} (Table 4.1-13) are high-affinity and total sites, respectively. This operation is done for each value of S_{total} listed in Table 4.1-13 (see DTN: SN0508T0503305.003, Spreadsheet 'sorption data.xls', Worksheet 'HFO % of high affinity sites'). That is, S_f is calculated using the set of values listed in Table 4.1-12 for each value of given in Table 4.1-13. For example, the range of values in Table 4.1-12 are all divided by a total site density of 0.2 (see Table 6-3.5) and the operation is repeated for the subsequent total site density in Table 4.1-13.

The objective of this approach is to capture an all-encompassing range of percentage of high-affinity sites for the given bounds of total site densities for HFO tabulated by Dzombak and Morel (1990 [DIRS 105483]). This approach reduces bias in the eventual sampling range of high-affinity site densities for a given set of total site density values. The percentage of high-affinity sites for HFO are listed in Table 6.3-5.

The percentage of high-affinity data are used to develop discrete distributions for goethite and HFO for sampling in TSPA by applying the same technique used for goethite specific surface area and site densities; the distributions are shown in Table 6.3-6.

The values currently used in TSPA for goethite and HFO specific surface area, site density, and high-affinity site percentages, and the discrete distributions for these parameters, are based on preliminary DTN: SN0503T0503305.001. Four data values in this DTN are incorrect. In addition, the data currently used in preliminary DTN: SN0503T0503305.001 contain up to 15 significant digits, whereas the source data in Tables 4.1-10, 4.1-11, and 4.1-12 are accurate to one to three digits. The parameter values for the discrete distributions in Table 6.3-6 are given to three significant digits, while the probability levels are reported to five decimal places. Details of the data errors and the discrete distributions currently used in TSPA are described in Appendix J.

The capacity (in moles of high-affinity sites per gram of corrosion products) for irreversible sorption on stationary corrosion products is computed based on these four parameters, combining the capacity of goethite and HFO:

$$\frac{10^{16}}{N_A}\left[\omega_G \bar{s}_G + (1-\omega_G)\bar{s}_{HFO}\right]\left[\omega_G N_{S,G} + (1-\omega_G)N_{S,HFO}\right]\left[\omega_G f_{HA,G} + (1-\omega_G)f_{HA,HFO}\right]$$

(Eq. 6.3.4.2.3.2-2)

where:

ω_G = mass fraction of corrosion products as goethite (dimensionless)
$\bar{s}_G$ = specific surface area of goethite ($m^2\ g^{-1}$)
$\bar{s}_{HFO}$ = specific surface area of HFO ($m^2\ g^{-1}$)
$N_{S,G}$ = sorption site density for goethite (sites nm^{-2})
$N_{S,HFO}$ = sorption site density for HFO (sites nm^{-2})
$f_{HA,G}$ = percentage of high-affinity sites for goethite (percent)
$f_{HA,HFO}$ = percentage of high-affinity sites for HFO (percent)
N_A = Avogadro's number (sites mol^{-1}).

The factor of 10^{16} includes a conversion factor from nm^2 to m^2 and from percentage of high-affinity sites to fraction of high-affinity sites.

Table 6.3-6 shows discrete probabilities for various values of several parameters. The sum of these parameters is 1.0, and the cumulative sum at any parameter value is the cumulative (probability) distribution function, CDF.

From the parameter values given in Table 6.3-6, the sorption capacity of corrosion products ranges from 3.90×10^{-6} mol g^{-1} to 2.18×10^{-3} mol g^{-1}. To put these values into perspective, the amount of radionuclides capable of being irreversibly sorbed can be estimated for a 21-PWR. The inventory of Pu and Am and their isotopes is 83.6 kg per CSNF waste package (DTN: SN0310T0505503.004 [DIRS 168761]). Using an approximate atomic weight of 240 g mol^{-1} (to represent various Pu and Am isotopes), this inventory of Pu and Am in a fully-degraded 21-PWR containing 19,440 kg corrosion products (as Fe_2O_3, from Table 6.3-4)

internal components within the waste package outer corrosion barrier, where the solids consist of the fuel rods and Fe_2O_3, is 1 - (3.710 + 1.513)/9.622 = 0.46.

Another approach to estimating the waste package porosity in a fully degraded state includes the nonferrous constituents of the steel components, which are not included in the 19,440 kg of Fe_2O_3 corrosion products in a 21-PWR in Table 6.3-4. The mass of these constituents in a 21-PWR is 4,920 kg (from Table 6.3-4). As seen in Table 4.1-14, the bulk of the nonferrous constituents is chromium and nickel, which comprise 18 percent and 14 percent, respectively, of 316 stainless steel (DTN: MO0003RIB00076.000 [DIRS 153044]), so the nonferrous portion can be approximately considered to be composed of just these two metals, proportioned as 56 weight percent Cr and 44 weight percent Ni. These metals will corrode to form Cr_2O_3, having a density of 5,220 kg/m^3 (Lide 2000 [DIRS 162229], p. 4-54) and a molecular weight of 0.151990 kg/mol (Lide 2000 [DIRS 162229], p. 4-54), and NiO, having a density of 6,720 kg/m^3 (Lide 2000 [DIRS 162229], p. 4-75) and a molecular weight of 0.074692 kg/mol (Lide 2000 [DIRS 162229], p. 4-75). These two metals, when fully oxidized, will occupy 1.181 m^3 of volume within the outer corrosion barrier. Then the bulk porosity of the fully degraded internal components within the waste package outer corrosion barrier, where the solids consist of the fuel rods, Fe_2O_3, Cr_2O_3, and NiO, is: 1 - (3.710 + 1.513 + 1.181)/9.622 = 0.33. The porosity of corrosion products themselves, Fe_2O_3, Cr_2O_3, and NiO distributed among the fuel rods, is: 1 - (3.710 + 1.181)/8.109 = 0.40.

The various approaches in this section to estimating the bulk porosity of waste package corrosion products result in porosities ranging from 0.33 to 0.54. For comparison, the porosity of unconsolidated geologic materials ranges from 0.25 to 0.70 (Freeze and Cherry 1979 [DIRS 101173], Table 2.4).

Lamination and flaking of corrosion products is expected to redistribute this material within the waste package pore space (Knight 1982 [DIRS 106733], p. 50), rather than leave it uniformly distributed throughout the waste package void volume. If the oxide settles to the bottom of a waste package, the physical geometry of the granular iron oxide that has settled can be represented by that of tightly packed sand, which has a solid content of 58 percent (Brown and Richards 1970 [DIRS 131479], Table 2.2), or a porosity of 0.42 (CRWMS M&O 1997 [DIRS 102824], p. 29). This value (0.42) for corrosion products porosity within a waste package has been used in criticality studies (CRWMS M&O 1997 [DIRS 102824], p. 29) and in an independent performance assessment of the Yucca Mountain repository (EPRI 2000 [DIRS 154149], p. 6-21 to 6-22). A porosity of 0.4 has been used in other criticality studies (YMP 1998 [DIRS 104441], p. C-23 to C-25) and in a model of diffusive releases from breached waste packages (Lee et al. 1996 [DIRS 100913], p. 5-67). Although some uncertainty exists and small-scale variability is likely, for the waste package as a whole, a fixed value of 0.4 is used for the porosity of corrosion products in TSPA.

The calculations just discussed do not account for water adsorbed on the spent fuel itself because this water constitutes the “rind” water (i.e., water in the conceptual waste form domain). The rind water does not directly affect diffusion to the exterior of the waste package because the fuel is the source, rather than part of the corrosion products that comprise the diffusive path to the exterior.

The surface area inside a waste package can be computed as a function of time, if the degradation rates of the basket components and the stainless steel inner vessel are known. The calculation is complicated by the different compositions of each component of the waste package. Spatial variability in degradation rates due to variations in accessibility to water vapor further complicate the picture. However, an average corrosion rate for a 21-PWR waste package provides a reasonable approximation from which surface areas and quantities of adsorbed water can be computed.

The complete degradation of a 21-PWR waste package gives an estimated upper bound on the surface area available for adsorption. The total amount of Fe_2O_3 in a 21-PWR waste package (from Table 6.3-4) is 19,440 kg Fe_2O_3. Using a specific surface area of 9.1 $m^2\ g^{-1}$ for the oxide (Jurinak 1964 [DIRS 154381], p. 480), the estimated upper bound for total surface area for adsorption in a 21-PWR waste package is 1.8×10^8 m^2/package.

The corrosion rates for the two types of steel are known with some uncertainty, as shown by the data presented in Table 4.1-1 for carbon steel and for stainless steel (DTN: MO0409SPAACRWP.000 [DIRS 172059]). The data set used is for corrosion rates at 60°C in simulated dilute well J-13 water. The average corrosion rate for carbon steel is 77.43 $\mu m\ yr^{-1}$, with a standard deviation of 8.83 $\mu m\ yr^{-1}$ (DTN: MO0409SPAACRWP.000 [DIRS 172059]). An empirical cumulative distribution function developed in DTN: MO0409SPAACRWP.000 [DIRS 172059] is used for parameter CS_Corrosion_Rate to be sampled in TSPA. The TSPA implementation in GoldSim requires that the cumulative distribution functions (CDFs) cover the entire range of probabilities of 0.0 to 1.0. To accommodate this, another row for the zero-th percentile is added using a corrosion rate that is slightly lower than the minimum in the empirical cumulative distribution function (ECDF); this row is 65.76 $\mu m\ yr^{-1}$ and zero probability.

The mean corrosion rate for Stainless Steel Type 316L is 0.248 $\mu m\ yr^{-1}$, with a standard deviation of 0.146 $\mu m\ yr^{-1}$ (DTN: MO0409SPAACRWP.000 [DIRS 172059]). The data set used is for corrosion rates in fresh water for the temperature range of 50°C to 100°C. An ECDF developed in DTN: MO0409SPAACRWP.000 [DIRS 172059] is used for parameter SS_Corrosion_Rate to be sampled in TSPA. As with carbon steel, the TSPA implementation in GoldSim requires that the CDFs cover the entire range of probabilities of 0.0 to 1.0. To accommodate this, another row for the zero-th percentile is added using a corrosion rate that is slightly lower than the minimum in the ECDF; this row is 0.03699 $\mu m\ yr^{-1}$ and zero probability.

From these rates and the thicknesses of the steel components, the lifetime of each type of steel is computed. From Table 6.3-4 above, carbon steel comprises about one-third of the total mass of steel in a CSNF waste package (30 percent in a 21-PWR; 33 percent in a 44-BWR). Based on this fraction, the surface area is interpolated over time. The implementation of this interpolation scheme in TSPA is presented in Section 6.5.3.2.

Although this interpolation provides a reasonable means for approximating the surface area of the interior of a waste package over time as it degrades, there is still uncertainty as to the actual surface area. The corrosion rates themselves are uncertain. In addition, many factors affect the surface area of the corrosion products. The chemical and physical conditions under which corrosion takes place impacts the morphology of the corrosion products. Seismic occurrences

The effective diffusion coefficient, D_s, as defined and used in this section, implicitly includes the effects of tortuosity. The area used for TSPA calculations depends on the scenario class and is presented in Section 6.5.3.1. The length of the diffusive path is also variable because the radionuclide sources may develop at random locations within a waste package, and the path length will depend on the geometry of the film connecting the source to a breach. Finally, the effective diffusion coefficient itself depends on the complex interactions of source term composition, water chemistry, porosity, water saturation, and temperature, none of which can be characterized in a deterministic fashion. Thus, each term in the above equation—A, Δx, and parameters affecting D_s and S_w—needs to be sampled or specified for each modeling case, and a reasonable range and distribution for each has to be determined. All terms are interrelated through the geometry used for the waste package interior, and all are effectively a function of relative humidity and time.

In CSNF waste packages, the water saturation in the corrosion products is set to 1.0 in a seep environment. In a no-seep environment, the effective water saturation in the corrosion products in CSNF waste packages results from adsorbed water, as described in the rest of this section. In CDSP waste packages, the water saturation in the corrosion products is set to 1.0 in both a seep and no-seep environment.

Archie's law, discussed in Section 6.3.4.1.1, gives the diffusion coefficient as a function of porosity and saturation in a partly saturated, granular medium as:

$$\phi S_w D_s = D_0 \phi^{1.3} S_w^2 \qquad \text{(Eq. 6.3.4.3.5-2)}$$

where D_0 is the free water diffusion coefficient ($m^2\ s^{-1}$). The diffusion coefficient D_s again is an effective value that implicitly includes the effect of tortuosity in a porous medium. The exponents in Archie's law are typical values, and will vary for different materials (Bear 1988 [DIRS 101379], p. 116). Whereas exponents of 1.863 are used for invert materials, based on experimental measurements of diffusion coefficients for crushed rock, the typical values (1.3 and 2) are used throughout this section to estimate in-package diffusion coefficients for corrosion products.

The effective water saturation within the corrosion products, $S_{we,CP}$, can be obtained as a function of RH by dividing the water volume by the pore volume of the corrosion products. The water volume is given by the adsorbed water film thickness multiplied by the surface area covered by water. The film thickness is $t_f \theta_a$, where t_f is the thickness of a water monolayer (Equation 6.3.4.3.2-6), and θ_a is the number of monolayers of coverage, a function of RH. The porosity of corrosion products is ϕ_{CP}.

The surface area of the corrosion products ($m^2\ Fe_2O_3$), given by:

$$\begin{aligned} s_{CP} &= m_{CP} \bar{s}_{CP} \\ &= \rho_{FeOx} V_{CP} \bar{s}_{CP} \left(\frac{1 - \phi_{CP}}{\phi_{CP}} \right). \end{aligned} \qquad \text{(Eq. 6.3.4.3.5-3)}$$

may have reversibly sorbed radionuclides. The waste form colloids may have irreversibly attached (embedded) or reversibly attached (sorbed) radionuclides. The corrosion products colloids may have irreversibly attached (strongly sorbed) or reversibly attached (weakly sorbed) radionuclides. The stability and mass concentrations of colloids are functions of the ionic strength and pH of the groundwater or local liquid chemistry in the waste package and invert. Both groundwater and waste form colloids are modeled using smectite mineralogy, and therefore sorption distribution coefficients (K_d) values associated with radionuclide sorption onto smectite colloids are used in the TSPA model (BSC 2004 [DIRS 170025], Table 6-6). The K_d values for colloids used in the TSPA calculations are presented in Table 6.3-11.

The potential mass of radionuclides irreversibly attached (embedded) to the waste form colloids (BSC 2004 [DIRS 170025], Section 6.3.3.3) is determined from reactions within the waste package. The mass of radionuclides reversibly attached to all three types of colloids is determined primarily by three parameters:

- Mass concentration of dissolved (aqueous) radionuclide in the liquid
- Mass concentration of colloid material in the liquid
- Radionuclide distribution coefficient (K_d) of a specific radionuclide on a specific colloid mineralogical type.

The potential concentrations of colloids in the drifts and EBS have also been assessed (BSC 2004 [DIRS 170025]). In a DOE-funded research project at the University of Nevada at Las Vegas to evaluate the corrosion of scaled-down miniature waste packages, the data indicate a preponderance of amorphous corrosion products released as colloids, including magnetite (Fe_3O_4), lepidocrocite (FeOOH), and goethite (FeOOH) (DTN: MO0302UCC034JC.003 [DIRS 162871]; BSC 2004 [DIRS 170025], Section 6.3.1.3).

Colloidal transport of radionuclides occurs by advective and diffusive processes. Advective transport moves colloids (and the associated radionuclides) at approximately the same velocity as the liquid flux through the EBS. Longitudinal dispersion, which could potentially enable colloids to travel faster than the bulk average liquid velocity, is ignored because of the short travel distance through the EBS (see Section 6.3.1.2). Diffusive transport moves colloids due to the concentration gradient and the medium diffusive properties. In the absence of a rigorous theory of solute diffusion in liquids, order of magnitude estimates may be made on the basis of hydrodynamic theory. Based on the Stokes-Einstein equation (Bird et al. 1960 [DIRS 103524], p. 514, Equation 16.5-4), the diffusivity of a solute in a liquid is inversely proportional to the radius of the diffusing particles.

Rates of diffusion of colloidal particles can be estimated by scaling those experimentally determined free water diffusion coefficients for dissolved actinides to dissolved colloidal materials on the basis of size (Stokes-Einstein relationship) as follows:

$$D_{coll} = D_{ion}\left(\frac{r_{ion}}{r_{coll}}\right), \qquad \text{(Eq. 6.3.4.4-1)}$$

Table 6.3-11. Sorption Distribution Coefficient (K_d) Values and Interval Probabilities Used for Reversible Radionuclide Sorption on Colloids in TSPA Calculations

Radionuclide	Colloid	K_d Value Range (ml g^{-1})	K_d Value Intervals (ml g^{-1})	K_d Value Interval Probabilities
Pu	Iron Oxyhydroxide	10^4 to 10^6	$<1 \times 10^4$ 1×10^4 to 5×10^4 5×10^4 to 1×10^5 1×10^5 to 5×10^5 5×10^5 to 1×10^6 $> 1 \times 10^6$	0 0.15 0.2 0.5 0.15 0
	Smectite	10^3 to 10^6	$< 1 \times 10^3$ 1×10^3 to 5×10^3 5×10^3 to 1×10^4 1×10^4 to 5×10^4 5×10^4 to 1×10^5 1×10^5 to 5×10^5 5×10^5 to 1×10^6 $> 1 \times 10^6$	0 0.04 0.08 0.25 0.2 0.35 0.08 0
Am, Th, Pa	Iron Oxyhydroxide	10^5 to 10^7	$< 1 \times 10^5$ 1×10^5 to 5×10^5 5×10^5 to 1×10^6 1×10^6 to 5×10^6 5×10^6 to 1×10^7 $> 1 \times 10^7$	0 0.15 0.2 0.55 0.1 0
	Smectite	10^4 to 10^7	$< 1 \times 10^4$ 1×10^4 to 5×10^4 5×10^4 to 1×10^5 1×10^5 to 5×10^5 5×10^5 to 1×10^6 1×10^6 to 5×10^6 5×10^6 to 1×10^7 $> 1 \times 10^7$	0 0.07 0.1 0.23 0.2 0.32 0.08 0
Cs	Iron Oxyhydroxide	10^1 to 10^3	$< 1 \times 10^1$ 1×10^1 to 5×10^1 5×10^1 to 1×10^2 1×10^2 to 5×10^2 5×10^2 to 1×10^3 $> 1 \times 10^3$	0 0.13 0.22 0.55 0.1 0
	Smectite	10^2 to 10^4	$< 1 \times 10^2$ 1×10^2 to 5×10^2 5×10^2 to 1×10^3 1×10^3 to 5×10^3 5×10^3 to 1×10^4 $> 1 \times 10^4$	0 0.2 0.25 0.5 0.05 0

DTN: SN0306T0504103.006 [DIRS 164131], Table 1.

NOTE: In engineered barrier system calculations, upper bound of K_d ranges for plutonium (Pu) and americium (Am) on iron oxyhydroxide reduced by a factor of 100 to be compatible with mechanistic sorption model described in *Waste Form and In-Drift Colloids-Associated Radionuclide Concentrations: Abstraction and Summary* (BSC 2004 [DIRS 170025], Section 6.3.3.2). Thus the K_d values for Pu and Am on iron oxyhydroxide are effectively fixed at 10^4 and 10^5, respectively.

and stainless steels within the waste package. The iron oxyhydroxides are known to be excellent sorbers (as indicated by their high K_d values) of many radionuclide species. In this alternative conceptual model, sorption is modeled as being completely reversible for all radionuclides and represented by linear adsorption isotherms in the form of K_d values. The K_d values allow retardation factors to be computed for transport through the EBS.

K_d values for 13 radionuclides are discussed in Section 6.6.6.

6.4.7 Pu Sorption from Stationary Corrosion Products and Colloids

The TSPA model accounts for limited plutonium desorption from iron oxyhydroxides by incorporating an irreversible sorption component. In contrast, this alternative conceptual model (ACM) accounts for the slow desorption of plutonium observed in experiments investigating absorption and desorption of plutonium from iron oxyhydroxide. Postulated mechanisms of plutonium sorption are described and the experimentally observed desorption is interpreted in the context of these mechanisms. K_d values are calculated for application to plutonium transport in the EBS and comparison with the TSPA model base case. This ACM is not incorporated into the base-case model because the durations of sorption-desorption experiments are short relatively to the repository time scale, the mechanisms of plutonium sorption are not yet well understood, and data on plutonium sorption and desorption are not available for high pH ranges.

This model is described in detail in Section 6.6.7.

6.5 MODEL FORMULATION FOR BASE CASE MODEL

6.5.1 Mathematical Description of Base Case Conceptual Model

A solute transport model typically consists of two component models: a model to solve the flow equation and another to solve the transport equation (Anderson and Woessner 1992 [DIRS 123665], p. 327). The solution of the flow equation yields the flow velocities or flow rates. These flow rates are input to the transport model, which predicts the concentration distribution in time and space. Development of the EBS flow model and the EBS transport model are discussed separately in the next two subsections.

6.5.1.1 EBS Flow Model

The EBS flow model is essentially a mass balance on water in the EBS. Because the microscopic details of processes that occur in the EBS are not important on a drift or waste package scale, an appropriate starting point for developing the EBS flow model is a general macroscopic balance on water within a drift (Bird et al. 1960 [DIRS 103524], p. 686):

$$\frac{dm_w}{dt} = -\Delta w_w + w_w^m + r_w. \qquad \text{(Eq. 6.5.1.1-1)}$$

Here, m_w (kg) is the instantaneous total mass of water within the walls of a drift, which encompass the EBS. This equation states that the rate of change of water mass in the EBS is equal to the mass rate of flow out of minus the mass rate of flow into the EBS (Δw_w [kg s^{-1}]),

plus w_w^m (kg s^{-1}), the net mass flow rate of water across bounding surfaces into the EBS by mass transfer (e.g., condensation or evaporation transfer water across a liquid surface, which is a boundary between gas-phase flow and transport and liquid-phase flow and transport), plus the rate of production of water by chemical reactions, r_w (kg s^{-1}). Per Assumption 5.4, production or consumption of water by chemical reactions is assumed to be zero, resulting in:

$$\frac{dm_w}{dt} = -\Delta w_w + w_w^m . \qquad \text{(Eq. 6.5.1.1-2)}$$

At steady state or when the mass of water in the EBS changes slowly, the time derivative can be set to zero:

$$-\Delta w_w + w_w^m = 0 . \qquad \text{(Eq. 6.5.1.1-3)}$$

The alternative bathtub conceptual model, using Equation 6.5.1.1-2 for the waste package, is screened out as an alternative conceptual model in Section 6.6.1. By neglecting changes in the density of the water within a drift as it passes through the EBS, Equation 6.5.1.1-3 can be divided by the density of water, ρ_w (kg m^{-3}), to transform it into a volume balance involving volumetric flow rates:

$$-\Delta F_w + F_w^m = 0 , \qquad \text{(Eq. 6.5.1.1-4)}$$

where $F_w = w_w / \rho_w$ is the volumetric flow rate (m^3 s^{-1}), and the superscript *m* still refers to mass transfer processes. Since both $-\Delta F_w$ and F_w^m represent a net inflow minus outflow, Equation 6.5.1.1-4 simply states that outflow is equal to inflow. This is the general form of the water mass balance that is used for individual flow paths in the EBS in the *EBS RT Abstraction*. It is applicable to the EBS as a whole as well as to individual components of the EBS. In particular, the terms Δw_w and w_w^m can be broken down into the separate and distinct flow paths listed in Section 6.3.1.1.

The volumetric flow rate of water into the top of the EBS is referred to as the total dripping flux, designated F_1 in Table 6.3-1, and is comprised of seepage flux into the top of the drift and condensation on walls of the drift. The seepage flux is computed in the GoldSim TSPA model using *Abstraction of Drift Seepage* (BSC 2004 [DIRS 169131]), and condensation on the drift walls is represented in the TSPA model through the *In-Drift Natural Convection and Condensation Model* (BSC 2004 [DIRS 164327]); these are inputs or sources of inflow into the EBS flow model.

Over the entire EBS, Equation 6.5.1.1-4 becomes

$$F_1 + F_7 = F_8 , \qquad \text{(Eq. 6.5.1.1-5)}$$

where F_1 is the total dripping flux into the top of the drift and F_7 is the imbibition flux into the invert; see Figure 6.3-1. F_8 is the flow rate of water leaving the invert and entering the unsaturated zone.

Table 6.5-4. Water Collected in Drip Shield Experiment Q(film); Drip Location: Patch 4, 8 cm Right of Center, Crown

Collection Station	Initial Mass (g)	Final Mass (g)	Net Water Mass (g)	Water Collected in Each Group of Collection Stations (g)
Input Water	-50.32	-228.52	-178.20	178.20
Gutter 1-1	7.652	16.434	8.782	36.351
Gutter 3-1	7.611	8.677	1.066	
Gutter 3-2	7.600	23.213	15.613	
Gutter 3-3	7.612	8.899	1.287	
Gutter 3-4	7.521	17.124	9.603	
Breach 2	107.02	109.00	1.98	24.00
Breach 4	107.60	129.62	22.02	
Drip Shield OUT 1	7.634	8.738	1.104	72.685
Drip Shield OUT 2	7.578	19.681	12.103	
Drip Shield OUT 3	7.574	34.446	26.872	
Drip Shield OUT 4	7.702	40.308	32.606	

DTN: MO0207EBSATBWP.023 [DIRS 163402].

One other cause for the discrepancies between experimental and predicted flow fractions is that, in the model, all dripping flux flows down the drip shield surface. In the experiments, a large amount of water remained on the drip shield as splattered drops that had not yet grown large enough to flow down the surface. For example, Table 6.5-4 shows the amount of water collected in the first experiment listed in Table 6.5-2. Of the 178.2 g of water that was dripped onto the surface, only 60.35 g was collected from the breaches or drainage gutters, whereas 72.685 g, or 41 percent, remained on the surface ("Drip Shield OUT" entries). This is a source of uncertainty in the experimental results that could be reduced by increasing the duration of the experiment far beyond the one-hour length of the test, but is inherent in the experiment and cannot be eliminated. The result is that less of the dripping flux actually flowed down the drip shield surface than is predicted by the model. This also causes the model to overestimate the fraction that flows into breaches, and, therefore, overestimates the transport of radionuclides.

Results presented in Table 6.5-2 and Table 6.5-3 show a large uncertainty in the fraction of rivulet flow that enters breaches. The integrated fraction of flow into breaches, which is the desired result, is not readily discerned from the uncertainty in the inflow fractions, even though the flows obtained experimentally are more clearly quantified.

Another approach, which is used to develop an uncertainty factor for use in TSPA, is to apply the integrated flow fraction approach to a drip shield whose length is about as wide as the splash diameter. If the rivulet source is dispersed along the crown, the integrated flow into a breach, Equation 6.5.1.1.2-34, can be applied. However, instead of the full drip shield length, the splash diameter is used for L_{DS}. Thus, for the breached drip shield experiments, L_{DS} has a range that is double the measured range for "inner cluster" splash radius (25 to 48 cm, as discussed at the beginning of this section, Section 6.5.1.1.2.4), or 50 to 96 cm.

The sampled parameter is then f'_{DS}, and the drip shield flux splitting algorithm is:

$$F_2 = \min\left[F_1 \frac{N_b \ell}{L_{DS}} f'_{DS}, F_1 \right], \qquad \text{(Eq. 6.5.1.1.2-37)}$$

which is identical to Equation 6.3.2.4-6. Using the higher value of maximum for f'_{DS} of 0.85 is both more reliable, being based on experimental data, and overestimates releases of radionuclides by predicting a higher water flow rate through the drip shield. The range for f'_{DS} to be used in TSPA is 0 to 0.85. A uniform distribution is appropriate for f'_{DS} because insufficient data are available to define any other distribution.

6.5.1.1.3 Water Flux through a Breached Waste Package

The submodel for flow through a breached waste package is conceptually identical to the submodel for flow through a breached drip shield. Key features listed at the start of Section 6.5.1.1.1 apply to both the drip shield and waste package cases. The waste package and drip shield flow submodels differ in two important respects: (1) the radius of curvature of the waste package is less than that of the drip shield; and (2) the nominal corrosion patch size as modeled by WAPDEG (BSC 2004 [DIRS 169996]) is smaller for a waste package than for the drip shield. These differences have no affect on the formulation of the waste package flow model. However, they have an affect on the values of uncertainty parameters that are part of the model. Because experiments were performed on a breached drip shield mock-up but not on a breached waste package mock-up, application of drip shield data to the waste package flow model introduces additional uncertainty in development of the model; however, these uncertainties cannot be quantified.

The water flux through a breached waste package, F_4, as developed in Section 6.3.3.2, is given by:

$$F_4 = \min\left[F_2 \frac{N_{bWP} \ell_{WP}}{L_{WP}} f'_{WP}, F_2 \right], \qquad \text{(Eq. 6.5.1.1.3-1)}$$

where F_2 is the flux through the breached drip shield. This is a simplification of a more rigorous expression:

$$F_4 = \min\left[F_2 \frac{N_{bWP} \ell_{WP}}{L_{WP}} \left(1 + \frac{\tan\alpha}{2} \right) f_{WP}, F_2 \right], \qquad \text{(Eq. 6.5.1.1.3-2)}$$

which explicitly accounts for the rivulet spread angle α. Because α is an uncertainty parameter itself, it can be lumped in with the parameter f_{WP} to give f'_{WP}. Equation 6.5.1.1.3-2 is considered first in order to examine the dependence on α.

flux splitting model in Section 6.5.1.1.2, values of f_{expt} are computed. The flow data are analyzed in Microsoft Excel spreadsheet: Flux Split Waste Package Model, Worksheet: f calculations, which is documented in Appendix D. In Microsoft Excel spreadsheet: Flux Split Waste Package Model, Worksheet: Summary, documented in Appendix D, tables analogous to Tables 6.5-2 and 6.5-3 are presented.

An uncertainty factor f_{WP} that can be obtained by replacing the fraction F_4 / F_2 with f_{expt}:

$$f_{WP} = \frac{F_4 / F_2}{\frac{\ell}{L_{WP}}\left(1 + \frac{\tan\alpha}{2}\right)} = \frac{f_{expt}}{\frac{\ell}{L_{WP}}\left(1 + \frac{\tan\alpha}{2}\right)}. \qquad \text{(Eq. 6.5.1.1.3-3)}$$

The range of values for f_{WP} is obtained by evaluating it with the appropriate minimum and maximum values of L_{WP} and α so as to minimize and maximize f_{WP}. The half-width of the patch used in the experiments ($\ell = 13.5$ cm) is used to evaluate f_{WP}. The minimum value of f_{WP}, using $L_{WP} = 50$ cm and $\alpha = 22.0°$, is $f_{WP} = 3.081 f_{expt} = 0.909$ using the mean value of 0.295 for f_{expt}. The maximum value of f_{WP}, using $L_{WP} = 96$ cm and $\alpha = 5.5°$, is $f_{WP} = 6.784 f_{expt} = 2.001$ using the mean value of 0.295 for f_{expt}.

A much lower range could also be justified by using the median inflow fraction of 0.014 instead of the mean (0.295) to define f_{WP}. In this case, f_{WP} would range from 0.043 to 0.095, which demonstrates the large degree of uncertainty in the experimental measurements and the resulting flux splitting submodel.

The values for f_{WP} discussed in this section actually represent a range for the maximum value of f_{WP}, since the minimum must be zero. If the factor (1 + ½ tan α) that accounts for the rivulet spread angle is lumped in with f_{WP}, the sampled uncertain factor f'_{WP} has an upper bound (using the maximum rivulet spread angle, $\alpha = 22°$) of 2.41. The range for f'_{WP} to be used in TSPA is 0 to 2.41. The parameter f'_{WP} is assigned a uniform distribution.

6.5.1.2 EBS Transport Model

The EBS transport model consists of mass balances on radionuclides. The transport model is more complex than the flow model for two basic reasons. First, the transport model is necessarily transient because the mass of each radionuclide at any particular location is dependent on its history (i.e., how far it has traveled, the quantity remaining at the source, and the extent of radioactive decay or ingrowth). Second, several complex interacting processes occur in transport, including dissolution and precipitation, sorption, advective transport,

diffusion, and colloid-facilitated transport. The term "colloid-facilitated transport" includes numerous phenomena, including adsorption and desorption of radionuclides onto mobile and immobile colloids, capture of colloids by solid surfaces and the air-water interface, filtering, dispersion, and diffusion. Transport can take place at any degree of water saturation greater than zero, so the model has to account for water saturation. Dissolution and precipitation may occur at finite rates or sufficiently fast to reach equilibrium. Solubility limits that determine whether, or to what extent, these processes occur are dependent on the chemical environment of the EBS. The EBS transport model applies to the waste package, the invert, and the invert/UZ interface.

Mass Balance for Dissolved and Reversibly and Irreversibly Sorbed Radionuclides in the Aqueous Phase

As with the flow model, the details of pore structure within the EBS are not important, and macroscopic mass balances using phenomenological rate expressions are appropriate. The starting point is the equation of continuity, or mass balance equation, for each *dissolved* radionuclide species *i* (Bird et al. 1960 [DIRS 103524], p. 561):

$$\frac{\partial \rho_i}{\partial t} = -\nabla \cdot \boldsymbol{J}_i + Q_i^m + r_i \,. \qquad \text{(Eq. 6.5.1.2-1)}$$

Here, ρ_i is the mass concentration of dissolved radionuclide species *i* (kg *i* m^{-3} bulk volume), $\boldsymbol{J}_i$ is the mass flux vector (or mass specific discharge) (kg m^{-2} s^{-1}) of dissolved radionuclide species *i* in the mobile water phase and accounts for advection, hydrodynamic dispersion, and diffusion of the dissolved radionuclide species *i*. The term Q_i^m is the net rate on a bulk volume basis (kg m^{-3} s^{-1}) of the various mass transfer processes, including reversible and irreversible sorption onto solid stationary materials in the EBS, dissolution and precipitation, and the various colloid-facilitated transport processes. The reaction term, r_i, accounts for radioactive decay and ingrowth on a bulk volume basis (i.e., production by decay of the parent of *i*) (kg m^{-3} s^{-1}). Each of these terms is expanded and described in more detail below, then simplified as appropriate for application in the TSPA model.

It is convenient to develop the transport model following the approach normally taken in the literature (Corapcioglu and Jiang 1993 [DIRS 105761], pp. 2217 to 2219; Choi and Corapcioglu 1997 [DIRS 161621], p. 306), with an emphasis on colloid-facilitated transport, since the complexity of those processes tends to dominate the analysis. First, Equation 6.5.1.2-1 is rewritten in terms of concentrations of radionuclides in an unsaturated porous medium. The density, or mass concentration, of dissolved radionuclide species *i* is given by:

$$\rho_i = C_i \phi S_w \,, \qquad \text{(Eq. 6.5.1.2-2)}$$

mass; the irreversibly sorbed radionuclides are sorbed onto the surface of these colloids, rather than being embedded within the colloid matrix, as are the radionuclides associated with the waste form colloids. The ground water colloids exist in the corrosion products and invert domains, and their concentrations are dependent on the local domain chemistry. The ground water colloids transport only reversibly sorbed radionuclide mass. The iron oxyhydroxide corrosion products are immobile and found only in the corrosion products domain. These corrosion products support both reversibly sorbed and irreversibly sorbed radionuclide mass; however, as a bounding approach, reversible sorption is ignored by setting the K_d values to zero (BSC 2005 [DIRS 174695]). Since corrosion products are immobile, all radionuclide mass sorbed to corrosion products is not transported but is retarded.

All of the features of the EBS radionuclide transport abstraction are accounted for in Equations 6.5.1.2-38, 6.5.1.2-36, 6.5.1.2-41, and 6.5.1.2-42 (or the one-dimensional versions of these equations, Equations 6.5.1.2-46, 6.5.1.2-49, 6.5.1.2-47, and 6.5.1.2-48, respectively), including invert diffusion, retardation in the waste package, in-package diffusion, and transport facilitated by reversible and irreversible colloids. Implementation of these equations into TSPA involves additional simplifications and restrictions that are discussed in Section 6.5.3.

6.5.1.3 Nomenclature

Symbols used in Sections 6, 7, and 8 are summarized in Table 6.5-5.

Table 6.5-5. Nomenclature

Variable	Definition	Units	Where First Used
A	Cross sectional area of diffusive or flow pathway	m^2	Eq. 6.5.1.2-5
A_f	Diffusive area of UZ fracture cell	m^2	Eq. 6.5.3.5-21
A_g	Surface area of crushed tuff granule	m^2	Section 6.6.4.1
A_I	Invert cross sectional area (circle segment)	m^2	Eq. 6.5.3.3-2
A_I	Diffusive area of invert cell	m^2	Eq. 6.5.3.5-21
A_{Is}	Intercepted flow area of a drift over the length of one waste package	m^2	Eq. 6.5.3.3-12
$A_{I/UZ}$	Diffusive area between invert and UZ cells	m^2	Eq. 6.5.3.3-4
A_m	Diffusive area of UZ matrix cell	m^2	Eq. 6.5.3.5-21
A_{scc}	Cross sectional area of stress corrosion crack	cm^2	Eq. 6.6.2-8
$A_{scc,eff}$	Effective cross sectional area of stress corrosion crack	cm^2	Section 6.6.2
A_{UZ}	Projected area of UZ normal to vertical flux	m^2	Eq. 6.5.3.6-1
A_w	Cross sectional area of water molecule	m^2	Table 4.1-9; Eq. 6.3.4.3.2-6
a	One-half the length of a stress corrosion crack	m	Eq. 6.3.3.1-1
a	Constant in equation for binary diffusion coefficient	dimensionless	Eq. 6.6.2-6
a	Empirical parameter in Archie's law	dimensionless	Eq. 6.3.4.1.1-1

Table 6.5-5. Nomenclature (Continued)

Variable	Definition	Units	Where First Used
ϕ	Porosity	$m^3\ m^{-3}$	Eq. 6.3.4.2.2-1
ϕ_{CP}	Porosity of corrosion products	$m^3\ m^{-3}$	Eq. 6.3.4.3.5-3
ϕ_f	Porosity of UZ fractures	$m^3\ m^{-3}$	Eq. 6.5.1.2-52
ϕ_I	Bulk porosity of invert	$m^3\ m^{-3}$	Eq. 6.5.1.2-25
ϕ_{inter}	Porosity of invert intergranular continuum	$m^3\ m^{-3}$	Eq. 6.5.3.3-10
ϕ_{intra}	Porosity of invert intragranular continuum	$m^3\ m^{-3}$	Eq. 6.5.3.3-7
ϕ_m	Porosity of saturated tuff matrix	$m^3\ m^{-3}$	Eq. 6.5.1.2-51
ψ	Moisture potential	$J\ kg^{-1}$	Eq. 6.6.5.1-2
ψ_e	Air-entry moisture potential	$J\ kg^{-1}$	Eq. 6.6.5.1-2
ψ_{es}	Air-entry moisture potential at a bulk density of 1,300 kg m^{-3}	$J\ kg^{-1}$	Eq. 6.6.5.1-3
ω_G	Mass fraction of corrosion products as goethite	dimensionless	Eq. 6.3.4.2.3.2-1
ω_i	Mass fraction of radionuclide species *i* released per unit mass of waste form	$kg\ kg^{-1}$	Eq. 6.6.1.1.1-1
∇	Del operator: $\boldsymbol{i}\frac{\partial}{\partial x}+\boldsymbol{j}\frac{\partial}{\partial y}+\boldsymbol{k}\frac{\partial}{\partial z}$, where ***i***, ***j***, and ***k*** are unit vectors in the *x*-, *y*-, and *z*-directions, respectively	m^{-1}	Eq. 6.5.1.2-1

BET = Brunauer, Emmett and Teller; CP = corrosion products; COV = coefficient of variance; DSNF = defense spent nuclear fuel; FHH = Frenkel-Halsey-Hill adsorption isotherm equation.

6.5.2 Base Case Model Inputs

Table 6.5-6 summarizes model inputs used in the *EBS RT Abstraction* that are sampled in the TSPA model calculations. The uncertainty associated with each parameter is indicated by the range and distribution shown for the parameter and is discussed in this section. The type of uncertainty is listed for each parameter. Aleatoric uncertainty refers to uncertainty for which sufficient knowledge is unobtainable because features, events, and processes involve chance occurrences. This type of uncertainty cannot be reduced through further testing and data collection. Epistemic uncertainty arises from a lack of knowledge about a parameter because the data are limited or there are alternative interpretations of the available data. The parameter is variable because an analyst does not know what the precise value of the parameter should be, but the state of knowledge about the exact value of the parameter can increase through testing and data collection.

6.5.2.1 Invert Diffusion Coefficient

The invert diffusion coefficient is used to calculate the rate of diffusion of radionuclides through the invert, after they have been released from the waste package. The uncertainty in the invert diffusion coefficient is epistemic. The values were derived from measured values of diffusion coefficients in various granular materials, including tuff. However, the data were scattered. This was particularly true at lower values of volumetric water content, where experimental difficulties are more pronounced – achieving uniform and consistent degrees of water saturation is difficult, resulting in uncertainties in the actual water content. The use of electrical conductivity measurements as an analog for diffusivity becomes more uncertain at low water content due to uncertainty in the electrical connectivity between electrodes and the porous material as well as between the particles themselves. The reported uncertainty approximates a normal distribution for the residuals in the statistical fit to the experimental data. Uncertainty in the porosity of the invert is included in the greater uncertainty associated with the measurements of the diffusion coefficient, which were made on a variety of geologic materials having a range of porosities; thus the porosity uncertainty can be considered to be accounted for in the effective diffusion coefficient.

6.5.2.2 Irreversible Sorption onto Iron Oxyhydroxides

The irreversible sorption model developed in Section 6.3.4.2.3.2 involves six parameters for which the uncertainty is both epistemic and aleatoric. These parameters are the specific surface area of goethite, the relative abundance of goethite (compared to HFO) in stationary corrosion products, the sorption site densities of goethite and HFO, and the percentage of high-affinity sorption sites for goethite and HFO. The epistemic uncertainty in sorption site densities and the percentage of high-affinity sorption sites arises from the difficulty in making precise measurements of these properties. One result of this experimental epistemic uncertainty is the inability to assign greater weight to individual experiments, so discrete distributions are used that give equal weight to all experimental results. Aleatoric uncertainty is due to the unpredictable variability in the circumstances and environment under which the iron oxyhydroxides will be formed in the repository, which will result in variations in specific surface area, relative abundance of goethite, and sorption properties.

6.5.2.3 Sorption Distribution Coefficients for Calculating Invert Sorption

Sorption on crushed devitrified tuff in the invert also involves some epistemic uncertainty for most radionuclides. The exceptions are C, I, and Tc, which do not sorb measurably on tuff (K_d values are zero). As with K_d values for sorption on corrosion products, the invert K_d values also involve some aleatoric uncertainty due to the evolving chemistry of the seepage water and changes resulting from chemical processes that occur as EBS components degrade. Invert K_d values are correlated as shown in Table 4.1-16 (DTN: LA0311AM831341.001 [DIRS 167015]). In the implementation of sorption distribution coefficients in the invert in TSPA, the devitrified tuff K_d values developed for the UZ submodel are assigned to the invert.

6.5.2.4 In-Package Diffusion Submodel

The general corrosion rates for carbon steel and stainless steel are known with some uncertainty, as shown in the data presented in Table 4.1-1 (DTN: MO0409SPAACRWP.000 [DIRS 172059]). An empirical cumulative distribution function developed in DTN: MO0409SPAACRWP.000 [DIRS 172059] is used for parameter CS_Corrosion_Rate to be sampled in TSPA. An empirical cumulative distribution function developed in DTN: MO0409SPAACRWP.000 [DIRS 172059] is used for parameter SS_Corrosion_Rate to be sampled in TSPA. In view of the large range in the measured data even among multiple samples under identical conditions, some epistemic uncertainty exists in corrosion rates. In addition, the future physiochemical environment of the waste package interior will influence corrosion rates, as evidenced by the variability in rates under different conditions (DTN: MO0409SPAACRWP.000 [DIRS 172059]). Thus, aleatoric uncertainty also exists in the corrosion rates owing to the uncertain future waste package environment.

The parameters Diff_Path_Length_CP_CSNF and Diff_Path_Length_CP_CDSP are developed in Sections 6.5.3.1.1 and 6.5.3.1.2. These are the diffusion path lengths from the internal waste package corrosion products domain to the invert domain of the EBS transport abstraction for CSNF (e.g., 21-PWR and 44_BWR) and codisposal (CDSP) (e.g., 5 DHLW/DOE SNF – Short) waste packages, respectively. The radionuclide source (failed fuel rods or glass logs) and the porous corrosion products are treated as being uniformly distributed throughout the volume of the breached waste package. Breached fuel rods or glass logs may lie adjacent to the interior of a breach in the waste package or nearby. Some aleatoric uncertainty exists in the location of the radionuclide source embedded in the corrosion products. The minimum path length is the thickness of the waste package outer corrosion barrier, 0.02 m for CSNF waste packages and 0.025 m for codisposal waste packages. The maximum is the radius of a waste package, 0.859 m for CSNF waste packages and 1.063 m for codisposal waste packages. A uniform distribution is appropriate for this parameter.

The parameter Surface_Area_CP, the specific surface area of corrosion products, is developed in Section 6.3.4.3.3, where uncertainties are discussed. This parameter accounts for the uncertainty in the computed surface area of corrosion products that is available for water adsorption inside a breached waste package. The calculated mass of corrosion products is multiplied by their specific surface area to compute the bulk surface area. The uncertainties are both aleatoric and epistemic. Unpredictable processes or events may occur that impact the morphology of corrosion products and alter their surface area, including seismic events, collapse of waste package internal structures, and changes in seepage rates. The nature of corrosion products formed under the conditions in a breached waste package in a humid environment, from a mixture of various types of steel, and their behavior in response to events and process that may occur is also uncertain. Due to the sparseness of the data for the specific surface area of corrosion products, only a uniform distribution can be justified for this parameter.

6.5.2.5 EBS-UZ Boundary Condition Implementation in TSPA

The EBS-UZ boundary condition implementation, discussed in Section 6.5.3.6, is applied when the EBS transport abstraction is discretized and implemented in GoldSim. This model provides the radionuclide concentration boundary condition at the invert-UZ boundary such that the

far-field concentration is approximately zero. To compute this boundary condition, a portion of the UZ is modeled, so input parameters for the UZ are used and therefore become EBS transport input parameters. The uncertainty in sampled parameters is discussed in this section; details about how UZ parameters are used are provided in Section 6.5.3.6.

Most of the parameters used for the EBS-UZ boundary condition implementation are taken from the output of *Drift-Scale Radionuclide Transport* (BSC 2004 [DIRS 170040]), in which specification of the ranges and distributions for the parameters is discussed. The parameters were developed for the discrete fracture-matrix partitioning model (BSC 2004 [DIRS 170040]). Although the modeling approach used in the *EBS RT Abstraction* is different, the parameter values remain unchanged. The parameter values are given in DTN: LB0307FMRADTRN.001 ([DIRS 165451], Folder: U0230_excel_files.zip). These parameters were developed for the lower, mean, and upper bound flow fields for the glacial transition climate and recommended for use in TSPA for the entire duration of the simulation. The glacial transition lower, mean, and upper infiltration cases cover a range of conditions that encompass all of the monsoon climates and all but the present-day lower infiltration climate. Furthermore, most of the regulatory compliance period (2,000 to 10,000 years) is modeled as being under glacial transition climate. Because of the predominance in time and wide range of the glacial transition infiltration cases, these three cases are used as representative for the low, mean, and high infiltration cases for the entire compliance period.

6.5.2.5.1 Matrix and Fracture Percolation Fluxes

Similar to the approach taken in *Drift-Scale Radionuclide Transport* (BSC 2004 [DIRS 170040]), in the EBS-UZ interface model, the parameter uncertainty is included through uniform sampling of the 433 different repository locations that have been assigned model parameters such as fracture and matrix flux and water saturation values. These values have been taken from the output of the UZ flow model for the repository host rock; see Sections 6.4.5 and 6.4.6 of *Drift-Scale Radionuclide Transport* (BSC 2004 [DIRS 170040]) for additional information. The sampled parameters that are based on repository locations are sampled such that if a flux for a certain location is considered then the saturation for the same location is also used.

6.5.2.5.2 Fracture Frequency

The fracture frequency distribution for each UZ model layer is presented in Table A-1 of *Drift-Scale Radionuclide Transport* (BSC 2004 [DIRS 170040], Appendix A, Table A-1). Since approximately 80 percent of the waste emplacement drift area is occupied by the TSw35 (Topopah Spring welded tuff lower lithophysal) unit of the UZ model (Appendix H of *Drift-Scale Radionuclide Transport*, BSC 2004 [DIRS 170040]), and because of the small variation in fracture frequency among various units, it is sufficient to use the fracture frequency distribution for TSw35 as given in Table A-1 of *Drift-Scale Radionuclide Transport* (BSC 2004 [DIRS 170040], Appendix A, Table A-1).

6.5.3 Summary of Computational Model

The object of the EBS radionuclide transport abstraction is to determine the rate of radionuclide releases from the EBS to the unsaturated zone. In the EBS transport model, the EBS is spatially partitioned into the following domains: (1) waste form, consisting of, for example, fuel rods, HLW glass, and DSNF; (2) waste package corrosion products; and (3) invert. In addition, the UZ immediately underlying the invert is conceptualized as a dual continuum consisting of (4) UZ matrix continuum and (5) UZ fracture continuum. The inclusion of a portion of the UZ is needed for an accurate calculation of the invert-to-UZ interface fluxes by providing a diffusive path length that is sufficiently long such that the concentration at the outlet of the UZ can realistically be assigned a value of zero.

In the waste form domain, degradation processes occur, including breaching and axial splitting of fuel rods, dissolution of SNF and HLW glass, and formation of waste form colloids wherever applicable. Dissolved species are transported by advection and/or diffusion to the waste package corrosion products domain. The primary interactions in the corrosion products domain involving radionuclide species are irreversible sorption onto stationary corrosion products, reversible and irreversible sorption of dissolved species onto iron oxyhydroxide colloids, and reversible sorption onto groundwater colloids and waste form colloids (when present). In the invert domain, radionuclides released from the corrosion products domain are transported by advection and diffusion, and interact with the crushed tuff by adsorption processes. The properties of each domain, including the volume, porosity, water saturation, diffusion cross sectional area, and diffusive path length, affect the rate of advective and diffusive transport of radionuclides through the domain. The invert domain interfaces with both continua of the UZ. The properties of the domains are defined in the following sections.

6.5.3.1 Waste Form and Waste Package Diffusion Properties

This section summarizes the general approach, major assumptions, main steps in the computational algorithm, and the stochastic parameters for the in-package diffusion submodel for TSPA. The mathematical equations for the in-package diffusion submodel are described in Section 6.3.4.3

The general approach for the commercial SNF (21-PWR and 44-BWR) waste packages is to consider two pathways for diffusion: (1) through porous waste form products inside the package, and (2) through porous corrosion products filling the bottom of the waste package. Starting from the time when a package is first breached, the extent of degradation is determined. This parameter is the basis for estimating the amount of corrosion products present inside a package, and allows the water saturation and effective diffusion coefficient to be computed.

Implementation of the three-domain EBS abstraction requires that properties be specified for each domain, including the volume, diffusive cross-sectional area, the diffusive path length, porosity, water saturation, and the procedure for calculating the diffusion coefficient. These properties must be specified for each type of waste package (CSNF and codisposal waste packages) and for the drip and no-seep environments.

6.5.3.1.1 CSNF Waste Packages Properties

This section discusses the CSNF waste package properties in the following two domains: CSNF waste form and CSNF corrosion products.

6.5.3.1.1.1 CSNF Waste Form Domain

In CSNF waste packages, the waste form domain consists of fuel rods. Except for ^{14}C, which is released from fuel hardware at the time of waste package breach (DTN: SN0310T0505503.004 [DIRS 168761]), radionuclides are released only from failed rods. Fuel rods initially fail either by perforations in the cladding as a result of corrosion or by damage in handling or in seismic events; however, it is assumed that the fuel rod cladding instantly splits along its length when the waste package fails (BSC 2005 [DIRS 172895], Assumption 5.3). Fuel rods split when the SNF reacts with the oxygen and moisture inside the waste package, forming metaschoepite. The resulting material, having a greater volume than SNF (mostly UO_2), causes the fuel rod to split open. The configuration of the failed rod is a mostly intact tube with the slit along the length exposing the SNF inside.

The reacted SNF constitutes a porous "rind" that is modeled as saturating quickly and completely with water, both in a seep and no-seep environment. The volume of the rind as a function of time and the rind porosity are provided by *Cladding Degradation Summary for LA* (BSC 2005 [DIRS 172895]). Radionuclides dissolve in the water that fully saturates the pore volume of the rind.

The diffusive area of the waste form domain is the total exposed surface area of the SNF in all of the axially split fuel rods, i.e., the area of the slit times the number of failed fuel rods. This area is provided by *Cladding Degradation Summary for LA* (BSC 2005 [DIRS 172895]).

The diffusive path length is the thickness of the rind, which is a function of time as the SNF reacts to form metaschoepite.

The diffusion coefficient is computed using Archie's law (Equation 6.3.4.3.5-2), with the porosity of the rind and the assigned water saturation of 1.0. As discussed in Section 6.5.3.5, the discretized mass balance equations use a diffusive conductance, which is a harmonic average of diffusion coefficient terms (including diffusivity, porosity, saturation, diffusive path length, and cross-sectional area for diffusion; see Equation 6.5.3.5-7), in this case, for the waste form and corrosion products domains. Since the TSPA model, GoldSim (GoldSim Technology Group 2002 [DIRS 160579]) computes the diffusive conductance, only the diffusion coefficients need to be input, rather than the diffusive conductances themselves.

6.5.3.1.1.2 CSNF Corrosion Products Domain

The second domain consists of the corrosion products inside the waste package. The mass of corrosion products (m_{CP}) is given as a function of time by Equation 6.5.3.2-5 below. In Section 6.3.4.3.4, a porosity (ϕ_{CP}) of 0.4 for corrosion products is shown to be appropriate. For purposes of calculating the water content of a breached waste package, the corrosion products

- In the igneous intrusive modeling case, the entire waste package is breached, and the waste package and cladding provide no further protection to the waste forms (BSC 2004 [DIRS 168960], Section 6.7.1). Transport begins with transport through the invert.

- In the igneous eruptive modeling case, the entire inventory of affected waste packages is made available for release to the air as ash. The EBS transport model does not apply.

In all scenario classes, the corrosion products diffusive path length is a sampled parameter (see Table 6.5-6) ranging from 0.02 m (the thickness of the CSNF waste package outer corrosion barrier) to 0.859 m (the outside radius of a 21-PWR) (BSC 2004 [DIRS 169472], Table 1).

6.5.3.1.2 Codisposal Waste Packages Properties

Codisposal waste packages consist of five cylindrical canisters containing HLW glass (glass "logs") surrounding a central canister of defense spent nuclear fuel (DSNF). After the codisposal waste package is breached, the HLW glass slowly degrades to a clay-like alteration product. However, the DSNF is modeled as degrading instantaneously (within a single TSPA time step) once the waste package is breached (BSC 2004 [DIRS 172453], Section 8.1). In addition to the on-going fuel degradation, the steel support framework inside the waste package also corrodes gradually, allowing the HLW glass logs to collapse onto each other such that the general cylindrical shape of the logs is retained. On the other hand, since DSNF is modeled as degrading instantaneously with no credit taken for the canister, it is expected that DSNF will not retain its cylindrical geometry, and may mix with the steel degradation products (iron oxyhydroxides) as a porous medium. With this assumption of the internal configuration of a degraded codisposal waste package, two separate waste form subdomains are conceptualized, one for HLW and the other for DSNF. The transport characteristics in each waste form subdomain are expected to be different.

Since the EBS transport model is a one-dimensional model, the two waste form subdomains are modeled sequentially, such that the HLW subdomain is upstream of the DSNF subdomain. The mass released from the degradation of HLW glass moves to the DSNF subdomain by advection and/or diffusion and is then transported to the corrosion product domain. This sequential representation is consistent with the conceptualization that the DSNF will degrade quickly and mix with the down-gradient steel corrosion products while the HLW glass logs will retain their cylindrical geometry and remain up-gradient of the corrosion products. The seepage flux through the waste package is also conceptualized to pass in series so that each waste form subdomain and the corrosion product domain have the same seepage flux.

The diffusive area in the HLW waste form subdomain, for the mass transport calculation, is calculated to be the combined initial surface areas of the five glass logs. The diffusive area in the DSNF waste form subdomain is set equal to the diffusive area of the corrosion product domain, which varies by the scenario class being modeled. This is reasonable because the corroded mass of uranium oxide, formed from degradation of DSNF waste form, is expected to mix with the iron oxyhydroxides formed from corrosion of steel components inside the waste package and be dispersed throughout the waste package, occupying the same area. In the

$$\theta_{inter} = \theta_r + \frac{(\theta_s - \theta_r)}{\left[1 + (\psi\alpha)^n\right]^m}, \qquad \text{(Eq. 6.5.3.3-14)}$$

Parameters in Equation 6.5.3.3-14 are:

θ_r = residual volumetric water content in the invert (percent)
= 5.0 (BSC 2005 [DIRS 173944], Appendix X, Table X-7)

θ_s = saturated volumetric water content in the invert (percent)
= 45.0 (BSC 2005 [DIRS 173944], Appendix X, Table X-7)

α = van Genuchten air-entry parameter (bar^{-1})
= 624. bar^{-1} (BSC 2005 [DIRS 173944], Appendix X, Table X-7)

n = van Genuchten n value (dimensionless)
= 8.013 (BSC 2005 [DIRS 173944], Appendix X, Table X-7)

m = van Genuchten m value (dimensionless)
= 0.875 (BSC 2005 [DIRS 173944], Appendix X, Table X-7)

With the algorithm and parameters described in this section, the bulk volumetric water content in the invert is obtained.

6.5.3.4 Irreversible Sorption onto Iron Oxyhydroxide Colloids and Stationary Corrosion Products

Irreversible sorption of Pu and Am onto iron oxyhydroxide colloids and stationary corrosion products in the corrosion product domain is included in the TSPA model, as described in Section 6.3.4.2.3.2. A linear forward rate constant, k_i, for irreversible sorption reactions is needed for the source terms in the mass balances for radionuclides that undergo irreversible sorption. In Equation 6.5.1.2-46, the mass balance for dissolved and reversibly sorbed radionuclide species *i*, the forward rate constant appears in a term that removes dissolved radionuclides from solution. In Equations 6.5.1.2-47 and 6.5.1.2-48, the mass balances for irreversibly sorbed radionuclide species *i* on mobile iron oxyhydroxide colloids and stationary corrosion products, respectively, the forward rate constant appears in a term that increases the concentration of irreversibly sorbed radionuclide species *i*.

In the no-seep case or where iron oxyhydroxide colloids are unstable, the forward rate constant is randomly sampled from a range developed in *Waste Form and In-Drift Colloids-Associated Radionuclide Concentrations: Abstraction and Summary* (BSC 2004 [DIRS 170025], Section 6.3.3.2) from experimental data of 0.01 $m^3\ m^{-2}\ yr^{-1}$ to 0.24 $m^3\ m^{-2}\ yr^{-1}$, with a log-uniform distribution (DTN: SN0309T0504103.010 [DIRS 165540]).

For the seep case and where colloids are stable, the forward rate constant k_i describing irreversible sorption to iron oxyhydroxide corrosion products and colloids (Equations 6.5.1.2-13 and 6.5.1.2-18, respectively) is computed as a fitting parameter to match a specified target flux out ratio for the corrosion products domain (BSC 2004 [DIRS 170025], Section 6.3.3.2). The

target flux out ratio (Ω) is the ratio of radionuclide flux exiting the corrosion product domain that is transported by colloids to the total radionuclide flux exiting the corrosion product domain (in dissolved state or sorbed onto colloids). The mass of radionuclides in the fluid exiting the corrosion products domain is expected to be proportioned such that the mass of radionuclide species *i* both reversibly and irreversibly sorbed onto all colloids is some fraction of the total mass of radionuclide species *i* exiting the system in all forms–aqueous, reversibly sorbed, and irreversibly sorbed. Observations in nature, such as the transport of Pu from the Benham test site (Kersting et al. 1999 [DIRS 103282]) indicate that this fraction is about 95 percent.

This is expressed as:

$$\Omega = \frac{\text{colloid mass flux out}}{\text{total mass flux out}} = 0.95 . \qquad \text{(Eq. 6.5.3.4-1)}$$

This target flux out ratio value of 95 percent is uncertain with an uncertainty range of 0.9 to 0.99 and a uniform distribution associated with it (BSC 2004 [DIRS 170025], Table 6-12, p. 6-72). It also may be a function of time, since the observation time for the Benham test is only about 50 years. In TSPA, irreversible sorption occurs only for Pu and Am.

The dependence of the forward rate constant on the target flux out ratio is obtained from an analytical solution of a finite difference approximation of transport in the corrosion products domain. The function for evaluating the forward rate constant is given by Equation B-72 in Appendix B.

This treatment applies in a seep environment. The calculated forward rate constant is constrained to be less than or equal to the experimentally derived maximum value of the sampled range for the no-seep environment, $0.24\ m^3\ m^{-2}\ yr^{-1}$ (DTN: SN0309T0504103.010 [DIRS 165540]). This approach is adopted because honoring the experimentally derived value is deemed more appropriate than honoring the target flux out ratio.

6.5.3.5 Discretization and Development of Computational Model for TSPA

The continuum mass balance equations for EBS transport model are described and developed in Section 6.5.1.2. The one-dimensional mass balance equation describing transport of dissolved and reversibly sorbed radionuclide species *i* is provided by Equation 6.5.1.2-46. The one-dimensional mass balance equations for irreversibly sorbed radionuclide species *i* on iron oxyhydroxide colloids and corrosion products are given by Equations 6.5.1.2-47 and 6.5.1.2-48, respectively. The solution of these continuum-form mass balance equations is approximated for the purpose of numerical modeling by the solution of discrete forms of these equations using a finite-difference approach. This requires the discretization of the time derivative (or mass accumulation term) and the advective and diffusive terms for both dissolved and colloidal transport. All other source terms and decay terms do not require discretization in either time or space.

Numerical modeling of the EBS radionuclide transport is performed using the GoldSim software (Golder Associates 2003 [DIRS 166572]) cell pathway capability, available in the GoldSim Contaminant Transport Module. The cell pathway acts as a batch reactor, where radionuclide

mass is assumed to be instantaneously and completely mixed and partitioned among all media (fluid or solid) within the cell. Both advective and diffusive transport mechanisms can be explicitly represented using the cell pathways. When multiple cells are linked together via advective and diffusive mechanisms, the behavior of the cell network is mathematically described using a coupled system of differential equations, and is mathematically equivalent to a finite difference network. GoldSim numerically solves the coupled system of equations to compute the radionuclide mass present in each cell and the mass fluxes between cells as a function of time. Both initial and boundary conditions for a cell can be defined explicitly, and systems of varying geometry can be modeled.

Within a computational cell network, each cell is allowed to communicate by advection and/or diffusion with any other cell. This concept is crucial in implementing the bifurcation of diffusive fluxes across an interface between a single continuum domain and a dual continuum domain, such as at the interface between the invert domain and the unsaturated zone. Each computational cell is provided with parameters describing water volumes, diffusive properties, and advective and diffusive flux links to other cells. Between any two cells, the diffusive flux can be bidirectional, depending on the concentration gradient, while the advective flux is unidirectional. The output of a cell is given in terms of the advective and diffusive mass fluxes for radionuclide species *i* and its concentration at the cell center.

The number of cells in the finite-difference network and the discretization of the cells is chosen in such a way as to capture the unique physical and chemical properties of the EBS components with respect to radionuclide transport. The abstractions are in the form of logic statements and stochastic distributions that provide a method for linking various cells in the network. Implementation of the EBS flow and transport model for TSPA uses the output of the drift seepage model (BSC 2004 [DIRS 169131]), the models for drip shield and waste package degradation (BSC 2004 [DIRS 169996]), the EBS physical and chemical environment model (BSC 2005 [DIRS 173727]), the thermal-hydrologic environment model (BSC 2005 [DIRS 173944]), and the waste form degradation and mobilization model (BSC 2004 [DIRS 172453]); *Defense HLW Glass Degradation Model* (BSC 2004 [DIRS 169988]); and *CSNF Waste Form Degradation: Summary Abstraction* (BSC 2004 [DIRS 169987]). The flow through various cells is based on the continuity equations and conservation of mass, as discussed in Section 6.3. An overview of the computational model for TSPA, as implemented using GoldSim, is provided below.

Radionuclide transport through the waste package is modeled by spatially discretizing the waste package into two domains: an upstream waste form domain and a downstream corrosion products domain. As implemented using GoldSim, a single waste form cell represents the entire volume of the CSNF waste form domain, and two waste form cells represent the two CDSP waste form subdomains (HLW and DSNF subdomains, which together comprise the single CDSP waste form domain), while a single corrosion products cell represents the entire volume of the corrosion products domain. These are illustrated in Figure 6.5-4 below by the EBS portion of the cell network – waste form cell, corrosion products cell, and invert cell.

The waste form cell receives mass from a specialized GoldSim "Source" cell, which models the waste package failure, degradation of the waste form, and release of the inventory for possible transport through the EBS. The "Source" cell provides the specified flux boundary condition for

The UZ fluxes result in defining three diffusive conductances from the flux expressions:

$$\hat{D}_{If}\left(C_{iI}-C_{if}\right)=\frac{\hat{D}_I\hat{D}_f}{\hat{D}_I+\hat{D}_f+\hat{D}_m}\left(C_{iI}-C_{if}\right), \qquad \text{(Eq. 6.5.3.5-18)}$$

$$\hat{D}_{Im}\left(C_{iI}-C_{im}\right)=\frac{\hat{D}_I\hat{D}_m}{\hat{D}_I+\hat{D}_f+\hat{D}_m}\left(C_{iI}-C_{im}\right), \qquad \text{(Eq. 6.5.3.5-19)}$$

$$\hat{D}_{mf}\left(C_{im}-C_{if}\right)=\frac{\hat{D}_m\hat{D}_f}{\hat{D}_I+\hat{D}_f+\hat{D}_m}\left(C_{im}-C_{if}\right), \qquad \text{(Eq. 6.5.3.5-20)}$$

where

$\hat{D}_{If}$ = effective diffusive conductance between invert cell and UZ fracture cell ($cm^3\ s^{-1}$);

$\hat{D}_{Im}$ = effective diffusive conductance between invert cell and UZ matrix cell ($cm^3\ s^{-1}$);

$\hat{D}_{mf}$ = effective diffusive conductance between UZ fracture and matrix cells ($cm^3\ s^{-1}$).

In order to accommodate the GoldSim representation of diffusive conductance as a two-term expression, the diffusive conductances of radionuclide species *i* are written as:

$$\hat{D}_{If}=\frac{1}{\dfrac{L_I}{\left(\phi S_w DA\right)_I\left[\dfrac{\left(\phi S_w D\right)_f}{\left(\phi S_w D\right)_f+\left(\phi S_w D\right)_m}\right]}+\dfrac{L_f}{\left(\phi S_w DA\right)_f}}, \qquad \text{(Eq. 6.5.3.5-21)}$$

$$\hat{D}_{Im}=\frac{1}{\dfrac{L_I}{\left(\phi S_w DA\right)_I\left[\dfrac{\left(\phi S_w D\right)_m}{\left(\phi S_w D\right)_f+\left(\phi S_w D\right)_m}\right]}+\dfrac{L_m}{\left(\phi S_w DA\right)_m}}, \qquad \text{(Eq. 6.5.3.5-22)}$$

$$\hat{D}_{mf}=\frac{1}{\dfrac{L_f}{\left(\phi S_w DA\right)_f\left[\dfrac{L_I\left(\phi S_w D\right)_m}{L_I\left(\phi S_w D\right)_m+L_m\left(\phi S_w D\right)_I}\right]}+\dfrac{L_m}{\left(\phi S_w DA\right)_m}}. \qquad \text{(Eq. 6.5.3.5-23)}$$

Although the above approach is rigorous, it is complex and difficult to implement in the TSPA model. A second approach that is easier to understand and simpler to implement, while

providing the same results as the above approach, is presented here and is implemented in TSPA. This approach requires introduction of an interface cell, located between the invert cell and the UZ cells. This interface cell provides an approximate interface concentration and the resulting flux split at the invert-to-UZ cell interface. The interface cell is conceptualized as a very thin slice of the invert cell. This implies the interface cell takes on the invert diffusive properties, with the exception of diffusive length. Let the diffusive length within the interface cell be some small fraction (a scale factor) of the invert diffusive length, say, Interface_Scale_Factor = 10^{-6}:

$$L_{I-int} = 10^{-6} L_I . \qquad \text{(Eq. 6.5.3.5-24)}$$

As in Equation 6.5.3.5-7, the diffusive conductance between the invert cell and the invert interface cell is calculated as the harmonic average:

$$\hat{D}_{I/I-int} = \frac{1}{\frac{L_I}{(\phi S_w DA)_I} + \frac{L_{I-int}}{(\phi S_w DA)_{I-int}}} . \qquad \text{(Eq. 6.5.3.5-25)}$$

For diffusion between the interface cell and the UZ fracture and matrix cells, the diffusive conductances of radionuclide species *i* are, respectively,

$$\hat{D}_{I-int/f} = \frac{1}{\frac{L_{I-int}}{(\phi S_w DA)_{I-int}} + \frac{L_{UZ}}{(\phi S_w DA)_f}} , \qquad \text{(Eq. 6.5.3.5-26)}$$

$$\hat{D}_{I-int/m} = \frac{1}{\frac{L_{I-int}}{(\phi S_w DA)_{I-int}} + \frac{L_{UZ}}{(\phi S_w DA)_m}} . \qquad \text{(Eq. 6.5.3.5-27)}$$

The interface cell concentration of radionuclide species *i* is computed as part of the cell network solution. Because the transport mass balance equations conserve mass, the mass flux leaving the interface cell must equal the sum of the mass fluxes entering the two UZ cells. The solution provides the flux continuity across the interface between the invert interface cell and UZ cells. This formulation expects the flux exiting the invert cell (or entering the interface cell) is approximately equal to the flux exiting the interface cell. This approximation is dependent on the diffusive length within the interface cell. The error in this approximate solution approaches zero as the diffusive length of the interface cell approaches zero.

6.5.3.6 EBS-UZ Boundary Condition Implementation in TSPA

For TSPA, a semi-infinite zero-concentration boundary condition is used for the EBS-UZ interface. This is approximated by applying an effective zero-concentration boundary at approximately three drift diameters below the invert-UZ boundary into the UZ. In an alternative approach, a zero-concentration boundary condition can be used at the interface between the invert and the UZ, which will result in an unrealistically high diffusive gradient through the

where D_{ms} is the effective UZ matrix diffusion coefficient ($cm^2\ s^{-1}$), θ_m is the matrix water content (percent), and k_{me} is the matrix effective permeability (m^2) (BSC 2004 [DIRS 170040], Equation 6-57):

$$k_{me} = k_{rm} k_m , \qquad \text{(Eq. 6.5.3.6-3)}$$

where k_{rm} is the relative permeability of unsaturated zone tuff matrix (dimensionless), which is a sampled parameter (Table 6.5-6), and k_m is the intrinsic permeability of unsaturated zone tuff matrix (m^2) from Table 4.1-8. The value obtained for the effective UZ matrix diffusion coefficient is applied to the fracture diffusion coefficient as recommended by the *Drift-Scale Radionuclide Transport* (BSC 2004 [DIRS 170040], Section 6.4.5, p. 6-42). The sampling of the input parameters is described in Section 6.5.2.

The diffusive area between the fracture and matrix continua is computed by multiplying the bulk volume by the fracture interface area, which provides the connection area per unit bulk volume. This diffusive area is further reduced by the fracture-matrix interface reduction factor, given as $S_{ef}^{1+\gamma}$, where S_{ef} is the effective fracture saturation, and γ is the active fracture parameter (BSC 2004 [DIRS 169861]). The effective fracture saturation (S_{ef}) is computed as:

$$S_{ef} = \frac{S_{wf} - S_{wfr}}{1 - S_{wfr}}, \qquad \text{(Eq. 6.5.3.6-4)}$$

where S_{wf} is the fracture water saturation, and S_{wfr} is the fracture residual saturation.

The mass flux of radionuclides from the invert domain to the dual continuum UZ, computed at the boundary of the EBS-UZ interface (between the invert cell and the adjacent UZ matrix and fracture cells), is passed to the UZ transport model for TSPA calculations as described in *Particle Tracking Model and Abstraction of Transport Processes* (BSC 2004 [DIRS 170041]). In addition to the total mass flux, the relative fraction of the mass going into each of the fracture and the matrix cells at the EBS-UZ boundary is required by the UZ transport model. This fracture-matrix partitioning of mass is calculated on the basis of the mass fraction going into the fracture continuum (compared to the matrix continuum) from the invert domain in the EBS-UZ interface model. This partitioning is time dependent and captures the temporal processes active in the EBS, such as varying radionuclide concentrations in the waste form, corrosion products, and invert domains, and the changing water flux through various subcomponents of the EBS. Furthermore, this partitioning is computed by solving the mass transport equations for the EBS and part of the UZ as a coupled system with appropriate boundary conditions and adopting a modeling approach using the dual continuum invert model saturation results presented in *Multiscale Thermohydrologic Model* (BSC 2005 [DIRS 173944]), and the dual continuum transport model for the UZ (BSC 2004 [DIRS 170041]).

Sorption of radionuclides to the UZ matrix continuum is modeled by applying the devitrified tuff K_d values from the UZ submodel. For sorption calculations, the mass of UZ matrix continuum is

calculated as: $V_b \rho_b (1 - \phi_f)$, where V_b is the bulk volume of the matrix cell considered (m^3), ϕ_f is the fracture porosity (fraction), and ρ_{bm} is the dry bulk density of TSw35 matrix (kg m^{-3}).

All three types of colloids are transported from the invert to the UZ cells. Groundwater colloids are present in all four layers. The iron oxyhydroxide and waste form colloids with reversibly sorbed radionuclides are modeled to be present in only the first two layers of the middle column, making the groundwater colloid the only type of colloid available for far-field transport, consistent with colloid-facilitated transport modeled in the UZ as described in *Particle Tracking Model and Abstraction of Transport Processes* (BSC 2004 [DIRS 170041]).

6.6 MODEL FORMULATION FOR ALTERNATIVE CONCEPTUAL MODELS

6.6.1 Bathtub Flow Model

The conceptual model for the TSPA is based on the presence of continuous flow paths through the patches and stress corrosion cracks that penetrate the waste package. More specifically, the TSPA model conceptualizes that vertical flow of seepage into the waste package, through the waste form and out of the waste package is not impeded by the location of patches and stress corrosion cracks on the surface of the waste package. There is no long-term build-up and retention of liquid within the waste package for flow and transport. There is also no resistance to the flow through the waste form. The TSPA approach attempts to maximize the immediate release and mobilization of radionuclides into the local groundwater environment. This approach is referred to as the "flow through" geometry.

An alternative conceptual model to the "flow through" geometry is the "bathtub" geometry (Mohanty et al. 1996 [DIRS 130419]). The bathtub geometry allows seepage to collect within the waste package before being released to the EBS. In theory, a bathtub geometry could result in the sudden release of a large pulse of radionuclides when a package overflows with liquid or when a second patch appears abruptly beneath the water line.

The "bathtub" effect would be most important during the period when only a few patches or cracks have penetrated the drip shield and waste package. In this situation, there may be penetrations through the top of the waste package while the bottom surface remains intact, leading to retention of liquid. At later times, the presence of multiple penetrations makes a "flow-through" geometry the more likely configuration.

The response of the bathtub geometry is evaluated for a primary case and for three secondary cases. The primary case includes consideration of two limiting conditions on radionuclide releases: dissolution rate limited and solubility limited. Tc is typical of dissolution rate limited radionuclides. The Tc released due to waste dissolution can always be dissolved in the available water because the solubility limit of Tc is high (BSC 2005 [DIRS 174566], Section 6.14). Np is typical of the solubility limited type of radionuclide, where the release of Np from dissolution is limited by its low solubility (BSC 2005 [DIRS 174566], Section 6.6).

The results for the primary case are based on a closed form analytic solution with constant values of inflow rate, dissolution rate, and solubility. The three secondary cases consider a step change in inflow rate, such as would occur from a climatic change, a step change in water chemistry, or

Substituting this definition into the left-hand side of Equation 6.6.1.2.1-2 gives:

$$\frac{d\beta}{dt} = -\frac{q_{in,new}}{V_{tub}}\beta. \qquad \text{(Eq. 6.6.1.2.1-4)}$$

The solution to Equation 6.6.1.2.1-4 with initial condition $\beta = 1$ at $t = 0$ is:

$$\beta = \exp\left(-\frac{q_{in,new}}{V_{tub}}t\right), \qquad \text{(Eq. 6.6.1.2.1-5)}$$

which corresponds to an exponential decay of C_i from $C_{i,old}$ to $C_{i,new}$.

If the inflow rate were to increase, the concentration would decrease. In a flow-through model, the concentration would instantaneously decrease, whereas in the bathtub model, the concentration would exponentially relax to the new concentration. The flow-through model is then not bounding for concentration released into the EBS. The mass of radionuclide mobilized is identical, as implied by Equation 6.6.1.2.1-1, but the dissolved concentration varies with the amount of fluid flowing through the system. However, the TSPA model passes mass to the unsaturated zone, rather than concentration, so the difference between the flow through model and the bathtub model for this case is not critical to performance.

Finally, a change in inflow rate during the initial period, when the bathtub is filling, only affects the value of t_{fill} and hence the delay until the bathtub fills, after which it behaves as described in Section 6.6.1.1.

In summary, the response of the bathtub model to a change in inflow rate is identical to that of the flow-through model for solubility-limited radionuclides. For dissolution-rate-limited radionuclides, the response of the bathtub model is less bounding than the flow-through model when the inflow rate decreases (and concentration increases). If the inflow rate increases (resulting in a decrease in the outflow concentration of radionuclides), the bathtub model is more bounding than the flow-through model for dissolution-rate-limited radionuclides.

6.6.1.2.2 Change in Inflow Chemistry

Consider a step change in inflow chemistry after the bathtub has filled. Initially, there will be minor changes in concentration within the bathtub because the bulk of the water retains the original inflow composition. Eventually the "old" groundwater is flushed out and replaced with the "new" inflow, resulting in new concentrations within the bathtub.

Equations 6.6.1.2.3-1 and 6.6.1.2.3-2 have the same value for radionuclide concentration, C_i, in the retained liquid because the chemistry of the groundwater is independent of patch location. Implicit in Equations 6.6.1.2.3-1 and 6.6.1.2.3-2 is that the second patch in the alternative conceptual model occurs after the volume of liquid in the waste package in the primary model has reached steady state.

The flow-through model produces an average release continuously, while the bathtub model with the alternative flow path produces zero release initially, followed by a high pulse that soon returns to the same flux as the flow-through model. In other words, the flow-through model represents a time average of the response of the bathtub model. From this viewpoint, the potential difference between F_{alt} and F_{pri} is partly mitigated by the sorption and diffusion processes in the unsaturated and saturated zones. The potential difference between F_{alt} and F_{pri} is also small if the second patch appears shortly after the first penetration because there is less retained liquid.

This alternative can also be thought of as being equivalent to the appearance of additional penetrations in the waste package. This analogy is appropriate because additional penetrations in the waste package increase the inflow flux into the waste form, resulting in higher releases to the EBS. The main effect of the alternative patch geometry model is to generate the increase earlier. This is not considered a major difference because there is a wide range of variability in corrosion rates for the TSPA model (BSC 2004 [DIRS 169996]). The effect of the alternative patch geometry model can then be reasonably considered to be captured within this variability.

The results and observations in this section (6.6.1.2.3) and throughout Section 6.6.1 are appropriate for the general boundary conditions considered here. In other words, this comparison is based on the full fluid flux into the waste package having access to all radioisotopes in the waste. The model implemented in TSPA, in which radionuclides are mobilized in a mass of corrosion products around the fuel pellets, partly mitigates the differences discussed here. This mitigation occurs because a large fluid flux will not transport radionuclides at the solubility limit if the mass in solution is limited by the pore volume in a mass of corrosion products. The situation is then similar to that mentioned at the end of Section 6.6.1.2.1, where mass transfer to the unsaturated zone is the dominant issue, rather than dissolved concentration.

6.6.1.3 Summary

The response of the bathtub geometry has been evaluated for a primary case, with constant boundary conditions and material properties, and for three secondary cases. Analyses for the three secondary cases consider a step change in inflow rate, a step change in inflow chemistry, and a change in flow geometry as would occur if a patch suddenly appeared beneath the waterline. All cases include consideration of two types of radionuclide release mechanisms: dissolution-rate-limited and solubility-limited. The comparisons are based on closed form analytic solutions.

The key conclusions from the evaluation follow:

- The bathtub model introduces a time delay in the release of radionuclides from the waste package to the EBS in comparison to the flow-through model for the primary case. The base case flow-through model overestimates releases of radionuclides in relation to the bathtub geometry for the primary case because there is no delay in release of radionuclides to the EBS.

- The response of the bathtub model to a step change in inflow rate (secondary case 1) is identical to the flow-through model for solubility-limited radionuclides. The response of the bathtub model for dissolution-rate-limited radionuclides is to delay the change in concentration and mass flux associated with the new inflow rate. The base case flow-through model overestimates releases of radionuclides with respect to the bathtub geometry for the case of decreasing inflow, when the concentration of radionuclide increases. The case of increasing radionuclide concentration is of primary interest from a performance or regulatory viewpoint since this case will result in greater releases.

- The response of the bathtub model to a step change in inflow chemistry (secondary case 2) is to delay the change in concentration and mass flux associated with the new inflow chemistry. Analytical models cannot define the exact time delay, which is sensitive to nonlinear chemical effects when inflows mix. Limiting cases, when solubility increases or decreases by several orders of magnitude, have been examined to define a first order approximation to the response of the chemical system.

  The base case flow-through model overestimates releases of radionuclides relative to the bathtub geometry when solubility or dissolution rate increase with changing inflow chemistry. The flow-through model has an instantaneous change to the higher equilibrium value while the bathtub geometry delays the change as the initial inflow is flushed out of the waste package. Increases in radionuclide concentrations and fluxes are of primary interest from a performance or regulatory viewpoint, so the underestimation of releases of radionuclides in the flow-through model for decreasing solubility or dissolution rate can reasonably be excluded from the TSPA.

- The response of the bathtub model when a second patch opens instantaneously beneath the water level in the waste package (secondary case 3) has also been analyzed. The impact of the instantaneous opening is to release a pulse of radionuclides in comparison to the base case flow-through model. The impact of this alternative conceptual model is mitigated by the time delays introduced through sorption and diffusion in the unsaturated and saturated zones. In addition, the higher mass flux from the alternative flow path is similar to the impact from additional patches opening in the waste package. There is a wide range of variability in corrosion rates for the TSPA model, and the impact from the instantaneous opening is encompassed in the uncertainty in corrosion rates. The impact of this alternative flow model has therefore been screened out of TSPA analyses because of the potential mitigation from sorption and diffusion and because the variability of corrosion rates provides large uncertainty in radionuclide release rates from the waste package.

6.6.2 Limited Water Vapor Diffusion Rate into Waste Package

In this alternative conceptual model, a film of adsorbed water cannot form on the surface of corrosion products if the rate of water consumption by corrosion reactions is greater than the rate of diffusion of water vapor into the waste package. Until a film of water forms on internal corrosion products surfaces, diffusive releases of radionuclides through the adsorbed water cannot occur (according to the in-package diffusion submodel). Thus, the resistance to diffusion of water vapor through stress corrosion cracks delays releases until all of the corrodible materials inside a waste package are fully degraded. It is implicit in this alternative conceptual model that stress corrosion cracks appear before general corrosion patches form; this will not necessarily be the outcome of TSPA calculations.

The objective is to determine the length of time required to complete the corrosion of internal component steels, which is equivalent to the delay from the time a waste package is first breached by stress corrosion cracks until diffusive releases can first take place. This delay can potentially be important since it provides additional time for decay to reduce the concentration of radionuclides before they are released from a waste package. The rate of diffusion of water vapor through stress corrosion cracks into the waste package is estimated and compared with the rate of consumption of water by corrosion of steel internal components to show that diffusion rates are less than corrosion rates. Then, at the rate limited by diffusion, the time needed to corrode the steels completely is calculated to give the delay before diffusive releases of radionuclides can occur.

An example calculation is presented for a typical set of conditions in the drift and waste package to estimate the time lag between appearance of stress corrosion cracks and the earliest times when an adsorbed water film can first form through which radionuclides can diffuse. Suppose that the temperature of the waste package and drift air is 50°C, the relative humidity in the drift is 95 percent, and the relative humidity is zero inside the waste package. Letting the humidity be zero inside the waste package maximizes the water vapor concentration gradient between the exterior and interior of the waste package. The diffusion distance is $\Delta x = 2.54$ cm , the thickness of the waste package outer lid (BSC 2004 [DIRS 169472]; BSC 2004 [DIRS 167394], Detail A). This is the outer closure lid, made of Alloy 22, with a circumferential weld in which stress corrosion cracks may develop. The average diffusive distance is greater – half the length of the waste package interior, or about 240 cm for a 21-PWR (Note i in Table 6.3-9) – but the cross sectional area is less in the stress corrosion cracks than in the waste package, so diffusion through the cracks is the limiting segment of the path.

To calculate the diffusion rate, the concentration of water vapor in humid air is obtained from psychrometric data. Equations for the determination of psychrometric properties are given by Singh et al. (2002 [DIRS 161624]). At relative humidity *RH* (fraction) and temperature *T* (°C), the partial pressure of water p_w (Pa) is:

$$p_w = RH \cdot p_w^{\circ}, \qquad \text{(Eq. 6.6.2-1)}$$

table, the water vapor concentration, C_{wv}, is obtained from Equations 6.6.2-4 and 6.6.2-5 as a function of relative humidity and temperature. The water vapor flux through stress corrosion cracks, q, is given by Equation 6.6.2-8. The corrosion rate, r_{corr}, is the stoichiometrically equivalent rate of iron consumption that occurs when limited by the water vapor influx, q. The release delay is the time, t_{corr}, required to corrode from one side through 10 mm of carbon steel or 50.8 mm of stainless steel at the rate, r_{corr}.

This alternative conceptual model provides additional realism compared to the base model by accounting for the delay in formation of a diffusive pathway for transport of radionuclides due to water consumption by corrosion reactions. However, data and analyses are not available to support certain assumptions used in this alternative model. For example, it is not known whether water will in fact be consumed by corrosion reactions so preferentially that none will adsorb anywhere inside a breached waste package. In addition, this alternative conceptual model does not account for possible spatial variations in the extent of corrosion. As an example, if the iron near the breaches in the outer corrosion barrier is completely corroded before the iron far from a breach has even begun to corrode, then water adsorption could occur there, forming a diffusive release pathway before all of the iron in the waste package has been consumed. In that case, this model would be non-conservative. Because of the lack of data and potentially non-conservative results, this alternative conceptual model has not been implemented in the TSPA model.

Table 6.6-1. Summary of Release Delays Resulting from Limitations on Diffusion of Water Vapor Through Stress Corrosion Cracks

Drift *RH*	**0.8**	**0.9**	**0.95**	**0.99**	**1.00**
***T* = 50°C**, D_{AB} = 0.313 $cm^2\ s^{-1}$					
C_{wv} (mol cm^{-3})	3.67×10^{-6}	4.13×10^{-6}	4.36×10^{-6}	4.54×10^{-6}	4.59×10^{-6}
q (mol $H_2O\ yr^{-1}$)	27.5	30.9	32.7	34.0	34.4
r_{corr} (mol Fe yr^{-1})	18.3	20.6	21.8	22.7	22.9
t_{corr}, Carbon steel only, Fe_2O_3 stoichiometry, open stress corrosion cracks (yr)	5,380	4,780	4,530	4,350	4,300
t_{corr}, Carbon steel only, $Fe(OH)_3$ stoichiometry, open stress corrosion cracks (yr)	10,900	9,720	9,210	8,840	8,750
t_{corr}, Carbon steel only, Fe_2O_3 stoichiometry, ϕ_{scc} = 0.4 (yr)	13,400	12,000	11,300	10,900	10,800
t_{corr}, Carbon steel only, $Fe(OH)_3$ stoichiometry, ϕ_{scc} = 0.4 (yr)	26,900	23,900	22,600	21,700	21,500
t_{corr}, Stainless steel only, Fe_2O_3 stoichiometry, open stress corrosion cracks (yr)	6,530	5,810	5,500	5,280	5,230
t_{corr}, Stainless steel only, $Fe(OH)_3$ stoichiometry, open stress corrosion cracks (yr)	13,100	11,600	11,000	10,600	10,500
t_{corr}, Stainless steel only, Fe_2O_3 stoichiometry, ϕ_{scc} = 0.4 (yr)	16,300	14,500	13,800	13,200	13,100

iron with oxygen is lower than that of iron with water, so the steel components inside a waste package have a lesser affinity for oxygen than for water.

These calculations indicate that a more accurate mass balance for water and oxygen inside a waste package could reduce predicted releases of radionuclides to the invert, and thus releases to the accessible environment. Releases could be delayed for several thousand years compared with current estimates as the corrosion of fuel baskets and inner vessel components scavenges water and oxygen that diffuse through small stress corrosion cracks (providing general corrosion patches do not form first). Formation of a diffusive pathway could then be delayed until corrosion of iron-based materials is largely completed.

Despite the potential for delays in releases of radionuclides predicted by these models, uncertainty exists in the processes that are modeled. The assumption that no water is physically adsorbed until all steel is corroded is questionable, since adsorption is typically a fast process. On the other hand, if water consumption by corrosion does keep the relative humidity lower inside the waste package than outside, the effective water saturation could be less than when calculated using the humidity of the drift. If this occurs, calculated diffusion coefficients are simply lower than given by the in-package diffusion submodel, rather than zero, but for the time required for the internal components to corrode. The net effect is similar to what these alternative conceptual models predict. The corrosion rates that have been used are for aqueous conditions, which might exist on a microscopic scale. However, to be consistent with the assumption here that no adsorbed water film forms, rates in a low-humidity gaseous environment should be used. This increased realism would increase the time required for complete corrosion of the steel.

This alternative conceptual model provides additional realism compared to the base model by accounting for the delay in formation of a diffusive pathway for transport of radionuclides due to oxygen consumption by corrosion reactions. However, as with the alternative conceptual model for limited water vapor diffusion rate into waste package (Section 6.6.2), data and analyses are not available to support all of the assumptions used in this alternative model. Examples include to what extent oxygen is needed for corrosion and the extent to which water vapor will compete with or interfere in diffusion and corrosion reactions. This alternative conceptual model also does not account for possible spatial variations in the extent of corrosion. Because of the lack of data and potentially non-conservative results, this alternative conceptual model has not been implemented in the TSPA model.

6.6.4 Dual-Continuum Invert

The LA invert design (BSC 2004 [DIRS 169503]) uses crushed tuff as the invert ballast material. This material is actually comprised of two pore spaces – intragranular pore space (tuff particle matrix) and intergranular pore space. Although radionuclide transport by both advection and diffusion can occur in both pore spaces, the dominant flow and transport processes in each of these two pore spaces is generally different. In order to simulate flow and transport through the invert accurately, the invert may be conceptualized as overlapping dual continua and modeled using a dual-permeability approach (Šimůnek et al. 2003 [DIRS 167469], p. 22), wherein flow and transport occur in both pore spaces, and mass transfer takes place between the two pore spaces.

approximation is dependent on the diffusive length within the interface cell. The error in this approximate solution will approach zero as the diffusive length of the interface cell approaches zero.

At the invert-to-UZ interface, there is diffusive transport between both the invert cells and the UZ matrix and fracture cells. This implies four connections: from invert intergranular to UZ matrix, from invert intergranular to UZ fracture, invert intragranular to UZ matrix, and from invert intragranular to UZ fracture. An analysis similar to that for the diffusive conductances between the corrosion products cell and the dual invert cells (Equations 6.6.4.25-11 through 6.6.4.2-13) would provide expressions for diffusive conductances for each of the four diffusive flux links. However, for the TSPA, the approximation provided by introducing an interface cell when diffusing from a single to a dual continuum exits is used. An approximate solution is obtained by the introduction of two interface cells at the invert-UZ interface. This approach is identical to that used above for the interface between the corrosion products cell and the invert dual continuum cells. One interface cell represents a thin slice of the invert intergranular cell, and the other represents a thin slice of the invert intragranular cell. Let the length of both invert interface cells be a fraction (an Interface_Scale_Factor) of the invert diffusive length, say, Interface_Scale_Factor = 10^{-6}:

$$L_{invert\_int} = 10^{-6} L_{invert} . \qquad \text{(Eq. 6.6.4.2-18)}$$

The use of an Interface_Scale_Factor of 10^{-6} is examined in Section 6.6.4.4.

The diffusive conductance between the invert intergranular cell and the invert intergranular interface cell is:

$$\hat{D}_{inter/inter-int} = \frac{1}{\frac{L_{invert}}{(\phi S_w DA)_{inter}} + \frac{L_{invert\_int}}{(\phi S_w DA)_{inter}}} , \qquad \text{(Eq. 6.6.4.2-19)}$$

while the diffusive conductance between the invert intragranular cell and the invert intragranular interface cell is:

$$\hat{D}_{intra/intra-int} = \frac{1}{\frac{L_{invert}}{(\phi S_w DA)_{intra}} + \frac{L_{invert\_int}}{(\phi S_w DA)_{intra}}} . \qquad \text{(Eq. 6.6.4.2-20)}$$

The fluxes of radionuclide species *i* from the invert intergranular interface cell to the matrix-fracture UZ cells are computed with diffusive conductances:

$$\hat{D}_{inter-int/UZm} = \frac{1}{\frac{L_{invert\_int}}{(\phi S_w DA)_{inter}} + \frac{L_{UZ}}{(\phi S_w DA)_{UZm}}} , \qquad \text{(Eq. 6.6.4.2-21)}$$

6.6.4.3 Dual-Continuum EBS-UZ Boundary Condition

The EBS-UZ boundary condition implementation described in Section 6.5.3.6 is used to obtain a realistic concentration boundary condition at the invert-UZ interface. For the dual-continuum invert alternative model, the boundary condition implementation is modified to account for diffusive fluxes from each invert continuum to both UZ fractures and matrix. This implementation is represented in Figure 6.6-3.

The mass flux from either invert continuum flows into the top layer of the middle zone in the UZ. The intergranular invert advective flux flows into the top middle UZ fracture cell, while the intragranular invert advective flux flows into the top middle UZ matrix cell. Advective transfer of water between the two continua is ignored. The diffusive flux from each of the invert continua can go into both UZ continua based on the concentration gradient and effective diffusion coefficient. The advective flux flowing through the UZ fracture cells in the middle zone is given by the greater of the advective flux out of the invert and the steady state UZ fracture flux. The advective flux in the two outer zones is given by the steady state UZ flow in each continuum at the repository horizon; the drift shadow effects are ignored in the transport calculations as a bounding approximation.

The mass flux from the dual continuum invert domain to the dual continuum UZ, computed at the boundary of the EBS-UZ interface, would be passed to the UZ transport model, which is described in *Particle Tracking Model and Abstraction of Transport Processes* (BSC 2004 [DIRS 170041]). In addition to the total mass flux, the relative fraction of the mass going into each of the fracture and the matrix cells at the EBS-UZ boundary is required by the UZ transport model. This fracture-matrix partitioning of mass is calculated on the basis of the mass fraction going into the fracture continuum (compared to the matrix continuum) from the dual continuum invert domain in the EBS-UZ interface model. This partitioning is time dependent and captures the temporal processes active in the EBS, such as varying radionuclide concentrations in the waste form, corrosion products, and invert domains and changing water flux through various subcomponents of the EBS.

6.6.4.4 Verification of Dual Invert/Dual UZ Diffusive Flux Bifurcation

In this section, calculation of the diffusive flux from a single cell (corrosion products) to dual invert cells (intergranular invert and intragranular invert) and then to two UZ cells (UZ matrix and UZ fracture) is tested. These tests show that the approximations in the GoldSim implementation using an Interface_Scale_Factor of 1.0×10^{-6} are correct and that the implementation in GoldSim agrees with Microsoft Excel calculations.

In this verification test calculation, there is no diffusive communication between the dual continuum invert cells, and there is no diffusive communication between the UZ matrix/fracture cells. The corrosion products cell provides a diffusive flux to the dual continuum invert cells. Each invert cell provides a diffusive flux to both the UZ matrix and fracture cells. For this verification, at time zero, an initial mass of one gram is released in the corrosion products cell, while all other cells have initial mass of zero. Parameters controlling diffusion through this test network were not determined strictly from TSPA data, but were set so that measurable mass transport to all cells within the network occurs in a reasonable time frame. No parameters were

Figure 6.6-5 presents the GoldSim solution **S3** and the Microsoft Excel solution **S2**. The Microsoft Excel solution **S2** and GoldSim solution **S3** use an Interface_Scale_Factor of 1.0×10^{-6}. Figure 6.6-5 shows the mass in place for each of the five cells and demonstrates the excellent agreement between the Microsoft Excel solution and GoldSim solution. After 2 years, the maximum relative error for the corrosion products cell and the two invert cells is 0.2 percent, and the maximum relative error for the two UZ cells is 1.5 percent.

These results confirm that the bifurcation of diffusive flux from a single continuum (corrosion products domain) to a dual continuum (invert domain) and then to another dual continuum (UZ) is accurate and properly implemented in GoldSim.

6.6.4.5 Summary of Dual-Continuum Invert Alternative Conceptual Model

This alternative conceptual model treats the crushed tuff in the invert as a dual continuum comprised of two pore spaces – intragranular pore space (tuff particle matrix) and intergranular pore space. Although radionuclide transport by both advection and diffusion can occur in both pore spaces, the dominant flow and transport processes in each of these two pore spaces is generally different. The invert is conceptualized in this alternative conceptual model as overlapping dual continua using a dual-permeability approach, wherein flow and transport occur in both pore spaces, and mass transfer takes place between the two pore spaces. Despite the potential for increased accuracy compared to the base case, single-continuum model, insufficient data exist to validate diffusion coefficients in the individual continua. There are also insufficient data to confirm whether this is a bounding approach with respect to chemical behavior in the invert. Therefore, the single-continuum model is used in TSPA.

6.6.5 Alternative Invert Diffusion Coefficient Models

The following two alternative models for determining the diffusion coefficient in the invert are assessed in this section: the single-continuum invert diffusion coefficient model and the dual-continuum invert diffusion coefficient model.

6.6.5.1 Alternative Single-Continuum Invert Diffusion Coefficient Model

As an alternative to the Archie's law approach for determination of the diffusion coefficient for the single-continuum invert (Section 6.3.4.1), diffusion through the crushed tuff invert ballast is modeled using an approach that has been applied to diffusion in soils. Studies generally show that the bulk diffusion coefficients of soils at high water content decline with the moisture content and that a Millington-Quirk power law developed for high moisture content overpredicts the diffusion coefficient at low moisture content (Nye 1979 [DIRS 167377]; Olesen et al. 1999 [DIRS 154588]). The studies also show that, below a critical moisture content, the diffusion coefficient for granular materials becomes negligible (So and Nye 1989 [DIRS 170588]).

10^{-12} cm^2 s^{-1} is used to represent the diffusion coefficient. For saturated conditions ($\frac{\theta_{intra}}{100} = \phi_{intra}$, the intragranular porosity), the diffusion coefficient is set to a value corresponding to Equation 6.6.5.2-4. For unsaturated grains with moisture content above 8.9 percent, a power-law extrapolation from the saturated value is used. The overall model proposed for the intragranular diffusion coefficient is the following power law model:

$$D_{intra} = D_{ms}\left(\frac{\left(\frac{\theta_{intra}}{100}\right)}{\phi_{intra}}\right)^{p}, \qquad \theta_{intra} \geq \theta_{min}$$
$$D_{intra} = D_{limit}, \qquad \theta_{intra} < \theta_{min}, \qquad \text{(Eq. 6.6.5.2-5)}$$

where θ_{intra} is the intragranular moisture content (percent), ϕ_{intra} is the intragranular porosity (fraction), D_{limit} is the measurement limit, 10^{-12} cm^2 s^{-1}, and θ_{min} is equal to 8.9 percent. The exponent p is the slope of Equation 6.6.5.2-5 in a plot of $\log_{10}(D_{intra})$ versus $\log_{10}(\theta_{intra})$. This plot is a straight line (in log-log space) between points $\left(\frac{\theta_{min}}{100}, D_{limit}\right)$ and (ϕ_{intra}, D_{ms}). Thus, p is given by:

$$p = \frac{\log_{10}(D_{limit}) - \log_{10}(D_{ms})}{\log_{10}\left(\frac{\theta_{min}}{100}\right) - \log_{10}(\phi_{intra})}. \qquad \text{(Eq. 6.6.5.2-6)}$$

The dual porosity model for the invert diffusion coefficient follows by specifying values for the intergranular and intragranular diffusion coefficients. The intergranular diffusion coefficient is evaluated from Equation 6.6.5.1-5 and dividing by the intergranular porosity (i.e., Equation 6.6.5.2-3). The intragranular diffusion coefficient is evaluated from Equation 6.6.5.2-5. The effective bulk diffusion coefficient is determined from Equation 6.6.5.2-2.

6.6.5.3 Summary of Alternative Invert Diffusion Coefficient Conceptual Models

These conceptual models consider alternatives to Archie's law for determining the diffusion coefficient in the crushed tuff invert. One variation treats the invert as a single continuum, as in the base model; the second variation models the invert as a dual continuum comprised of two pore spaces – intragranular pore space (tuff particle matrix) and intergranular pore space. Despite the potential for increased accuracy compared to the base case single-continuum model using Archie's law, insufficient data exist to validate diffusion behavior at very low water contents. In addition, these alternative conceptual models do not provide upper bounds on diffusion coefficients, as the Archie's law approach does. Therefore, invert diffusion coefficients are computed in TSPA using Archie's law.

6.6.6 Reversible Sorption of Radionuclides onto Waste Package Corrosion Products

Reversible sorption of radionuclides onto stationary waste package corrosion products will occur to some extent. However, as a bounding approach in TSPA, reversible sorption of radionuclides onto stationary corrosion products has been eliminated, i.e., K_d values for all radionuclides are set to zero (see Section 6.3.4.2.3), and only irreversible sorption of Pu and Am is modeled as occurring on stationary corrosion products. The alternative conceptual model in this section describes the alternative approach of allowing for reversible sorption onto stationary corrosion products by using non-zero K_d values.

Descriptions of sorption based on a K_d are approximate because this approach is empirical, with little information about underlying mechanisms, and is therefore not easily extendable to different chemical environments and physical substrates (sorptive media). The use of a linear isotherm is also approximate because it does not predict saturation of the sorption sites with sorbed species that may include natural components of the groundwater. The mass of iron oxyhydroxides from waste package corrosion is large (Table 6.3-4), so each waste package provides many sites for sorption. For these reasons, the K_d approach is an order of magnitude measure of contaminant uptake in geologic environments (Davis and Kent 1990 [DIRS 143280]).

The use of the linear isotherm (K_d) approach to represent the subsequent release of radionuclides into fresh recharge (i.e., the desorption process) can be inconsistent with observations in geologic media. Typically, contaminants become more closely attached to a mineral surface after sorption, either adsorbed at high energy sites on the surface or absorbed through overcoating and buried due to other mineral surface reactions. The net result is that only a fraction of the original sorbed population remains available at the surface and able to react with adjacent solutions or be accessed by microorganisms. A linear isotherm (K_d) approach, on the other hand, assumes that all sorbed radionuclides are freely able to desorb from the substrate.

Sorption distribution coefficients are typically measured for groundwaters and substrates at ambient or near ambient temperatures. There are few experimental data for sorption distribution coefficients at the elevated temperatures that may occur in the EBS with either the repository design and operating mode described in *Yucca Mountain Science and Engineering Report* (DOE 2001 [DIRS 153849]) or an alternative thermal operating mode. In this situation, the available data for sorption distribution coefficients were used to define the ranges of K_d values for the earlier TSPA analyses, but it is not possible to distinguish alternative thermal operating modes. The effect of temperature on sorption coefficients was reviewed by Meijer (1990 [DIRS 100780], p. 17). Measured sorption coefficients onto tuffs were higher at elevated temperature for all elements studied: Am, Ba, Ce, Cs, Eu, Pu, Sr, and U. The conclusion was drawn that sorption coefficients measured at ambient temperatures should be applicable and generally bounding when applied to describing aqueous transport from a repository at elevated temperatures. This conclusion must be tempered by the possibility that elevated temperatures could result in changes in the near-field mineralogy and water chemistry that are not predictable by short-term laboratory and field experiments.

The large role of iron and aluminum oxyhydroxides minerals in controlling overall soil K_d values is explicitly recognized in the EPA documents. For this reason, one would expect EPA soil K_d values and EPRI iron oxyhydroxides K_d values to be similar and both to provide a reasonable approximation of retardation in the waste package corrosion products. There are some caveats, however, the most important one being that K_d values for a given material and radionuclide are approximate values that can vary widely depending on the specifics of the measurement (solid/solution ratio, radionuclide level, time allowed for equilibration). General coherence in an order-of-magnitude sense is the best that can be expected as the K_d approach does a poor job of reproducing actual transport profiles; see, for example, Bethke and Brady (2000 [DIRS 154437]) and Reardon (1981 [DIRS 154434]).

Table 6.6-7 gives K_d ranges describing retardation in the waste package corrosion products for the 13 radionuclides that were tracked in the earlier TSPA model, with the minimum K_d and maximum K_d being the ranges used in this alternative conceptual model. For all but iodine and technetium, the maximum K_d values are from DTN: LA0003AM831341.001 ([DIRS 148751], SEP table S00191_002). The maximum K_d value for iodine and technetium is chosen to be 0.6 ml g^{-1}, which is the approximate maximum K_d value for iodine and technetium specified for alluvium in saturated zone units in DTN: LA0003AM831341.001 ([DIRS 148751], SEP table S00191_001).

The minimum K_d values for carbon, cesium, iodine, radium, strontium, and technetium are the minimum K_d values specified in DTN: LA0003AM831341.001 ([DIRS 148751], SEP table S00191_002). In order to provide more of a bounding estimate of releases of radionuclides that have a large impact on dose, the minimum K_d values for actinium, americium, plutonium, and thorium are reduced by a factor of 10 from the minimum K_d values specified in DTN: LA0003AM831341.001 ([DIRS 148751] SEP table S00191_002). For the same reason, the minimum K_d value for protactinium is reduced by a factor of 5 from the minimum K_d value of 500 ml g^{-1} specified in DTN: LA0003AM831341.001 ([DIRS 148751], SEP table S00191_002); this minimum value is corroborated by *Evaluation of the Candidate High-Level Radioactive Waste Repository at Yucca Mountain Using Total System Performance Assessment, Phase 5* (EPRI 2000 [DIRS 154149], Table 6-9).

The minimum K_d value for neptunium is reduced by a factor of 500 from the minimum K_d value of 500 ml g^{-1} specified in DTN: LA0003AM831341.001 ([DIRS 148751], SEP table S00191_002); this minimum value is corroborated by *Evaluation of the Candidate High-Level Radioactive Waste Repository at Yucca Mountain Using Total System Performance Assessment, Phase 5* (EPRI 2000 [DIRS 154149], Table 6-9) and *Review of Geochemistry and Available K_d Values for Cadmium, Cesium, Chromium, Lead, Plutonium, Radon, Strontium, Thorium, Tritium (^3H), and Uranium.* Volume II of *Understanding Variation in Partition Coefficient, K_d, Values* (EPA 1999 [DIRS 170376], Table 5.17).

Table 6.6-7 also gives distributions for K_d values. For cesium, radium, and strontium, a beta distribution, as specified in Table 6.6-5 (DTN: LA0003AM831341.001 [DIRS 148751], SEP table S00191_002), is used in this alternative conceptual model. For carbon, iodine, protactinium, and technetium, a uniform distribution, as specified in Table 6.6-5 (DTN: LA0003AM831341.001 [DIRS 148751] SEP table S00191_001), is used in this alternative conceptual model. Whereas a uniform distribution is also specified in Table 6.6-5

This alternative conceptual model is not used as the base model in TSPA for several reasons. First, it does not account for limitations on the number of sites available for sorption. Second, it does not account for competition for sorption sites among the radionuclides that can sorb. Third, it does not account for competition for sorption sites with radionuclides such as Pu and Am that sorb irreversibly, which thereby reduce the number of sites available for reversible sorption.

6.6.7 Pu Sorption onto Stationary Corrosion Products and Colloids

As described in Section 6.3.4.2.3.2, the base case TSPA model accounts for limited Pu desorption from iron oxyhydroxides by incorporating an irreversibly sorbed component. This is based on available field and laboratory data, which suggest that Pu strongly sorbs onto iron oxyhydroxide substrates and does not desorb over time periods ranging from months (experimental studies), to approximately 50 years (field studies of Pu transport at contaminated sites).

Iron oxides and hydroxides are a primary sorptive sink for many metal ions and metal oxyion complexes in natural systems. Desorption studies have been done with ferrihydrite and goethite using Mn(II), Co(II), Ni(II), Cu(II), Pb(II), Zn(II), Cd(II), Cr(III), and the metal complexes arsenate, chromate, selenate, selenite, and uranyl; Pu(IV) and Pu(V) have also bee examined (Barney 1984 [DIRS 174702]; Schultz et al. 1987 [DIRS 173028]; Ainsworth et al. (1994 [DIRS 173033]); Payne et al., 1994 [DIRS 174707]; Coughlin and Stone 1995 [DIRS 173030]; Manning and Burau 1995 [DIRS 174725]; Davis and Upadhyaya 1996 [DIRS 173743]); Eick et al. 1999 [DIRS 174704]; Fendorf et al. 1996 [DIRS 173034]; Fendorf et al. 1997 [DIRS 173031]; Ford et al. 1997 [DIRS 174727]; Grossl et al. 1997 [DIRS 173032]; Sanchez et al. 1985 [DIRS 107213]; Lu et al. 1998 [DIRS 100946]; Lu et al 1998 [DIRS 174714]). Adsorption of these metal species onto iron oxyhydroxides is initially very rapid, reaching a steady-state concentration within minutes to hours; however, slow uptake commonly continues indefinitely. Desorption is also initially rapid, though generally slower than adsorption. It is often incomplete, with the fraction of readily desorbed metal a function of the metal/oxide contact (pre-equilibration) time, the time allowed for desorption, and, in some cases, the pre-equilibration pH (Schultz et al. 1987 [DIRS 173028]). Continued slow desorption is commonly observed for the duration of the experiment. For this reason, Schultz et al. (1987 [DIRS 173028]) have stated that the term “slowly reversible sorption” should be preferred over “irreversible sorption” when discussing metals that remain bound to the sorbent during desorption re-equilibration. In many cases, though, a fraction of the metal does appear to be irreversibly sequestered by the iron oxyhydroxide. As a result, there is a decrease in the labile, or readily available, fraction of metal ions in the system and a drop in the net metal toxicity. As the sorptive capacity of iron oxides is high, the development of an “irreversibly sorbed” metal fraction has been suggested to be an efficient mechanism for sequestering inorganic contaminants in natural environments (Brady et al. 1999 [DIRS 154421]).

However, the National Research Council (NRC) has taken the position that the assumption of irreversible sorption is tenuous, because there has been no agreement to date on the mechanism(s) responsible for permanent sequestration. The NRC published a report (NRC 2000 [DIRS 174394]) that stated that irreversible sorption models should not be applied to quantitative models of environmental contamination that aid decision-making on performance or exposure. With regard to the report on contaminant attenuation of Brady et al. (1999 [DIRS 154421]), the

products; sorption and retardation characteristics of radionuclides inside the waste package are discussed in this report (Section 6.3.4.2). When there is no advective transport, diffusive releases may still occur; a submodel for diffusion inside the waste package is presented (Section 6.3.4.3). With these models implemented in TSPA, the effectiveness of the waste package as a feature of the engineered barrier can be quantified with respect to radionuclide transport.

The invert consists of crushed tuff that can delay releases of radionuclides to the unsaturated zone. The invert limits diffusive transport of radionuclides out of the engineered barriers by maintaining unsaturated conditions under the waste package. The invert limits advective and diffusive transport of radionuclides by sorbing radionuclides onto crushed tuff. A simple model for computing the diffusion coefficient of the invert as a function of the porosity and water saturation is presented in this report (Section 6.3.4.1). This enables the effectiveness of the invert as a feature of the engineered barrier to be quantified when implemented in TSPA.

7. VALIDATION

Model validation for the *EBS Radionuclide Transport Abstraction* was performed in accordance with LP-2.29Q-BSC, *Planning for Science Activities*, and LP-SIII.10Q-BSC, *Models*, and follows the validation guidelines in the *Technical Work Plan for: Near-Field Environment and Transport: Engineered Barrier System: Radionuclide Transport Abstraction Model Report Integration* (BSC 2005 [DIRS 173617]).

LP-SIII.10Q-BSC, *Models*, requires that TSPA model components be validated for their intended purpose and stated limitations, and to the level of confidence required by the relative importance of the component to the potential performance of the repository system. Three levels of model validation are defined in LP-2.29Q-BSC, *Planning for Science Activities*, Attachment 3, with the level of validation increasing with an increasing level of model importance ranging from low to moderate to high. Models whose variation could lead to a potentially large effect on the estimate of mean annual dose (e.g., a change greater than 1 mrem yr^{-1}) should receive a high or Level III model validation. Models whose variation could lead to moderate effect on the estimate of mean annual dose (less than 1 mrem yr^{-1}, but greater than 0.1 mrem yr^{-1}) should receive Level II model validation. Level I validation is sufficient for models of less importance to the estimate of mean annual dose.

The levels of confidence required for the models of the *EBS RT Abstraction*, as stated in Section 2.2.2 of the TWP, are given as follows.

The required level of confidence for the EBS flow model is Level I. The required level of confidence for the EBS transport model is Level II. The required level of confidence for radionuclide transport from the waste package to the drift wall through the invert is Level I (also specified in Table 1 of LP-2.29Q-BSC, *Planning for Science Activities*). The EBS-UZ interface model of the *EBS RT Abstraction* provides input to the unsaturated zone radionuclide transport model as described in *Particle Tracking Model and Abstraction of Transport Processes* (BSC 2004 [DIRS 170041]). The appropriate level of confidence identified for unsaturated zone radionuclide transport is Level II. Therefore, Level II also represents appropriate level of confidence for the EBS-UZ interface model of the *EBS RT Abstraction*.

Confidence Building During Model Development to Establish Scientific Basis and Accuracy for Intended Use

For Level I validation, Section 2.2.3 of the TWP (BSC 2005 [DIRS 173617]) cites Attachment 3 of LP-2.29Q-BSC as guidance for documenting a discussion of decisions and activities for confidence building during model development. Additionally, the development of the model will be documented in accordance with the requirements of Section 5.3.2(b) of LP-SIII.10Q-BSC. The development of the *EBS RT Abstraction* model has been conducted according to these requirements and the requisite criteria have been met as discussed below:

1. *Selection of input parameters and/or input data, and a discussion of how the selection process builds confidence in the model [LP-SIII.10Q-BSC 5.3.2(b) (1) and LP-2.29Q-BSC Attachment 3 Level I (a)].*

7.1.1 Flux Splitting Submodel

The EBS flux splitting submodel, which is part of the *EBS RT Abstraction* flow model, determines the fraction of total dripping flux that will flow through the drip shield and/or waste package. This submodel is directly related to the waste isolation attribute (i.e., the limited release of radionuclides from engineered barriers). The amount of water flowing through engineered barriers, when combined with radionuclide solubility limits and diffusive transport, defines the mass flux of radionuclides that is mobilized for transport through the EBS to the unsaturated zone.

Level I validation is appropriate for the flux splitting submodel, because it is part of the process for radionuclide transport from waste package to the drift wall through the invert (see Section 7 above). In addition, the flux splitting submodel has the following features:

- The submodel is not extrapolated over large distances, spaces or time.
- The submodel has large uncertainties because of the chaotic nature of the flow of droplets or rivulets on corroded, roughened surfaces.
- Sensitivity analyses in the prioritization report *Risk Information to Support Prioritization of Performance Assessment Models* (BSC 2003 [DIRS 168796], Sections 3.3.6 through 3.3.11) show that the flux splitting abstraction will not have a large impact on dose in the first 10,000 years.
- The flux splitting submodel plays a minor role in TSPA. In the nominal scenario class, neither the drip shield nor the waste package fails due to general corrosion within the 10,000-year regulatory period (BSC 2004 [DIRS 169996], Section 7.2); if the TSPA model is run to compute the peak dose, which occurs beyond the 10,000-year regulatory period, then the flux splitting model will be used in the nominal scenario class. When the drip shield does fail (beyond the 10,000-year regulatory period in the nominal scenario class), it is modeled as failing completely in a single time step (BSC 2004 [DIRS 169996], Section 6.3). The early waste package failure modeling case is part of the nominal scenario class, where the drip shield does not fail within the 10,000-year regulatory period; thus, the flux splitting submodel is not used. In the igneous scenario class, neither the drip shield nor the waste package survives an igneous intrusion, so the flux splitting submodel is not used. Stress corrosion cracking of the drip shield occurs in the seismic scenario class, but since no advective flux is allowed through the cracks, the flux splitting submodel is not used. Thus, the flux splitting submodel is actually applied only in the seismic scenario class when seismic damage occurs to the waste package from fault displacement leading to fractional failure of the waste package.

This flux splitting submodel is validated through comparison to experimental data. A work plan entitled *Test Plan for: Atlas Breached Waste Package Test and Drip Shield Experiments* (BSC 2002 [DIRS 158193]) defines the experiments used for validation of this flux splitting submodel.

Products compartment represents the porous material that is formed after the basket materials are corroded. The Canister compartment represents the failed metal canisters. As with the GoldSim TSPA model, each compartment is treated as a mixing cell in which radionuclide concentrations are assumed to be uniform. Mass balances in each compartment account for the various processes that comprise the model, including transport by diffusion and advection, radioactive decay and ingrowth, sorption, dissolution, and precipitation.

In the EPRI model, EBS transport parameters are assigned fixed values. Both the Corrosion Products and corroded Canister compartments have a porosity of 0.42 (EPRI 2000 [DIRS 154149], p. 6-21), less than the initial porosity of a CSNF waste package, 0.58, as estimated in Section 6.3.4.3.4. The EPRI value accounts for the volume occupied by the oxide. A lower value for porosity overestimates releases of radionuclides. However, in the in-package diffusion submodel (Equation 6.3.4.3.5-6), the higher value of porosity increases the estimated diffusion coefficient by only a factor of 1.5, which is small compared to other uncertainties in the model.

The EPRI model assumes a fixed water saturation of 0.35 in both the Corrosion Products and corroded Canister compartments (EPRI 2000 [DIRS 154149], p. 6-21). This value is appropriate for modeling cases involving advective transport, but overestimates releases of radionuclides for the expected large fraction of the repository that has no seepage flux, where the only water present is adsorbed water. The in-package diffusion submodel specifically applies to those regions and provides a more realistic estimate of saturation as a function of relative humidity.

The EPRI model uses a fixed value for effective diffusion coefficient of 4.645×10^{-4} m^2 yr^{-1} in both the Corrosion Products and corroded Canister compartments (EPRI 2000 [DIRS 154149], p. 6-22). This converts to 1.472×10^{-7} cm^2 s^{-1} or to 1.472×10^{-11} m^2 s^{-1}. For diffusion through a fully degraded waste package (Equation 6.3.4.3.5-5), this corresponds to a relative humidity of 97.9 percent. Thus, when the humidity is high, the EPRI model and the in-package diffusion submodel agree well. In contrast, the in-package diffusion submodel provides humidity-dependent diffusion coefficient values.

The EPRI model also specifies fixed diffusive lengths, which are defined as the distance from the center of the compartment to the interface of the two contacting compartments. For the Corrosion Products compartment, the diffusion length is 0.046 m; for the Canister compartment, the diffusion length is 0.025 m (EPRI 2000 [DIRS 154149], p. 6-22). In a well-degraded waste package, these are reasonable values, comparable to those used in the in-package diffusion submodel. However, the in-package diffusion submodel accounts for the uncertainty in diffusion lengths at all times, and provides special treatment at early times when large masses of corrosion products are not yet formed.

For the conditions assumed in the EPRI model, namely, at later times when the waste package is extensively corroded, the in-package diffusion submodel agrees quite well with the EPRI model. The primary differences are that the in-package diffusion submodel accounts for a wider range of conditions, including times just after breaches first appear in the waste package. In addition, the in-package diffusion submodel accounts explicitly for the relative humidity, which realistically is the only source of water when seepage does not occur. And finally, in contrast to the EPRI model, the in-package diffusion submodel accounts for uncertainty in diffusive path lengths.

Using the self-diffusion coefficient for water as a bounding value for all radionuclides partially compensates for not accounting for the effect of temperature on the diffusion coefficient in the corrosion product domain. See the discussion at the end of Section 6.3.4.3.5.

The compilation below (Table 7.2-1) lists a selection of diffusion coefficients for some trivalent lanthanides and actinides. Table 7.2-1 also includes some anions not listed in most compilations but relevant and/or analogous to those expected for radionuclides released from the waste package. The listing shows that the diffusion coefficients for these species are all smaller than the self-diffusion of water, by factors ranging from 1.6 to 14.7. In the case of uranium, the carbonate complexes of the metal species have even smaller diffusion coefficients. Based on the Stokes-Einstein equation (Bird et al. 1960 [DIRS 103524], p. 514, Equation 16.5-4), the diffusivity of a solute in a liquid is inversely proportional to the radius of the diffusing particles. It is therefore expected that other carbonate and hydroxyl complexes, on the basis of the greater size of the complexes relative to the metal species, will also have smaller diffusion coefficients than the metal species listed in Table 7.2-1.

As an alternative, four diffusion coefficients could be used. One coefficient could be used for each charge (mono-, di-, and tri-valent species) and one for the hydroxyl and carbonate complexes of the actinides and lanthanides. At 25°C, the mono-, di-, and trivalent species have bounding values of 2.2×10^{-5} cm^2 s^{-1}, 1.2×10^{-5} cm^2 s^{-1}, 0.7×10^{-5} cm^2 s^{-1}, respectively, as shown in Figure 7.2-2. Although this alternative model is not used for TSPA, it provides further evidence that the use of the self-diffusion coefficient of water bounds the diffusion coefficients of diffusing radionuclide species in the EBS.

7.2.2.2 Modification for Porosity and Saturation

Validation of the dependence of invert diffusion coefficient on porosity and saturation is provided by comparison with measured data obtained independently of the data used for model development. Data used for validation are obtained from diffusivity measurements for crushed tuff using electrical conductivity measurements (CRWMS M&O 2000 [DIRS 156680]) and from direct measurements of diffusivity between machined cubes of tuff (Hu et al. 2001 [DIRS 161623]).

Conca and Wright (1992 [DIRS 100436]) and Conca et al. (1993 [DIRS 170709]) obtained diffusion coefficients from electrical conductivity measurements for various granular materials, including tuff, with volumetric moisture content ranging from 0.5 percent to 66.3 percent. A statistical fit of the data (Conca and Wright 1992 [DIRS 100436], Figure 2; Conca et al. 1993 [DIRS 170709], Figure 2; listed in Table 4.1-17) ranging from 1.5 percent to 66.3 percent volumetric moisture content, based on Archie's law, results in the model used in TSPA (Section 6.3.4.1.1 and Appendix G):

$$\begin{aligned} \theta D_I &= D_0 \phi^{1.863} S_w^{1.863} 10^{ND(\mu=0.033,\sigma=0.218)} \\ &= D_0 \theta^{1.863} 10^{ND(\mu=0.033,\sigma=0.218)} \end{aligned} \qquad \text{(Eq. 7.2.2.2-1)}$$

where $\theta = \phi S_w$ is the volumetric moisture content (fraction: m^3 water m^{-3} rock), and ND represents a normal distribution with a mean, μ, of 0.033 and a standard deviation, σ, of 0.218. The object of this validation is to show that the diffusion coefficient given by Equation 7.2.2.2-1 obtained from the electrical conductivity measurements of Conca and Wright (1992 [DIRS 100436]) and Conca et al. (1993 [DIRS 170709]) tends to overestimate the diffusivity of invert materials.

The diffusion coefficient has also been determined specifically for tuff, also using electrical conductivity measurements (CRWMS M&O 2000 [DIRS 156680], Tables A-1 and A-2). These data are listed in Table 7.2-2 and are plotted in Figure 7.2-3, along with the mean value and plus and minus three standard deviations from Equation 7.2.2.2-1. This plot shows that the fit to the measured diffusion coefficient data (Equation 7.2.2.2-1) overestimates the diffusion coefficient relative to *The Determination of Diffusion Coefficient of Invert Materials* (CRWMS M&O 2000 [DIRS 156680], Tables A-1 and A-2). This plot was created using Microsoft Excel; see Appendix G, Worksheet: Validation, p. VII-10.

The electrical conductivity measurements by Conca and Wright (1992 [DIRS 100436]) and Conca et al. (1993 [DIRS 170709]) use conductivity as an analog for diffusivity. While the analog is known to be valid in fully saturated media, its application to unsaturated media, particularly at low moisture contents, is questionable due to the difficulty in preparing samples and in making reliable electrical contact between the electrical leads and the samples. To avoid these problems, Hu et al. (2001 [DIRS 161623]) measured diffusive tracer concentrations in tuff cubes directly using laser ablation coupled with inductively coupled plasma-mass spectrometry (LA-ICP-MS), rather than relying on electrical analogs.

of a thick water film that behaves like bulk water. These measurements provided a bounding value for the diffusivity of the tracer, comparable to the diffusion coefficient of 1.48×10^{-5} cm^2 s^{-1} (Table 7.2-1) for its analog, TcO_4^-. In other words, in regions on the tuff samples that were saturated or at least had high water saturation, the direct diffusivity measurements agreed with theoretical predictions.

Hu et al. also measured tracer concentrations at greater depths into the cube by using the laser ablation technique to probe into the surface. They found that internal diffusion coefficients, at depths of 60-410 μm, were on the order of 10^{-12} cm^2 s^{-1} (Hu et al. 2001 [DIRS 161623], p. 22). The measured volumetric water content of the tuff matrix was 8.9 percent (Hu et al. 2001 [DIRS 161623], p. 25). The mean diffusion coefficient predicted by the invert diffusion properties submodel (Equation 7.2.2.2-1) would then be 2.6×10^{-7} cm^2 s^{-1}. This is a factor of 10^5 larger than the measurement. Thus, the diffusion coefficient throughout most of a grain of crushed tuff is lower than that predicted by the invert diffusion properties submodel. This provides corroborating evidence that the invert diffusion properties submodel overestimates releases of radionuclides from the EBS. These data also show that the overestimation of diffusivities in the invert diffusion properties submodel may be excessive. However, insufficient data exist to reduce the uncertainty in this model, and, if this additional uncertainty were included in the invert diffusion submodel, estimated releases of radionuclides from the EBS would be reduced and no longer be bounding. Because the model has a low impact on repository performance, the degree of uncertainty in this model is acceptable for TSPA.

The study by Hu et al. (2001 [DIRS 161623]) was primarily a development of the technique for using LA-ICP-MS of microscale profiling of the distribution of diffusing tracers. However, in the process, some preliminary data were obtained that can be used to corroborate the electrical conductivity measurements of Conca and Wright (1992 [DIRS 100436]) and Conca et al. (1993 [DIRS 170709]).

Sections 7.2.1 and 7.2.2 have demonstrated that the component models of the EBS transport model meet Level II validation. Based on the validation results, the EBS transport model is adequate for its intended use.

7.2.3 Results of Independent Model Validation Technical Review of the EBS Flow and Transport Models

An independent model validation technical review of the EBS flow and transport models was conducted, as specified in the TWP (BSC 2005 [DIRS 173617], Section 2.2.3). This model validation approach is justified based on requirements of LP-SIII.10Q-BSC, Section 5.3.2c), where independent technical review is listed as an appropriate method for model validation. The results of the independent model validation technical review of the EBS flow and transport models are presented in a memo, a facsimile of which follows.

7.3 EBS-UZ INTERFACE MODEL

The output of the invert domain feeds into the unsaturated zone through the EBS-UZ interface model. In the *EBS RT Abstraction*, the invert is modeled as a single-continuum porous medium whereas the adjacent UZ is modeled as a dual continuum fracture-matrix medium. The model is described in detail in Section 6.5.3.6.

The mass flux from the invert flows into the top layer of the middle zone in the UZ. The portion of the advective flux from the invert that is attributable to the seepage flux (F_1) flows into the UZ fractures. The imbibition flux into the invert (F_7) flows out of the invert into the UZ matrix. The diffusive flux from the invert can go into both UZ continua based on the concentration gradient and effective diffusion coefficient. The diffusive area remains the same because they are overlapping continua. The advective flux flowing through the UZ fracture cells in the middle zone is given by the greater of the advective flux out of the invert and the steady state UZ fracture flux. The advective flux in the two outer zones is given by the steady state UZ flow in each continuum at the repository horizon; the drift shadow effects are ignored.

For TSPA, a semi-infinite zero concentration boundary condition is used for the EBS-UZ interface. This is approximated by applying an effective zero-concentration boundary at approximately three drift diameters below the invert-UZ boundary into the UZ. By moving the zero concentration boundary some distance below the invert, a more realistic diffusive gradient through the invert is achieved.

The EBS-UZ interface model of the *EBS RT Abstraction* provides input to the unsaturated zone radionuclide transport model in *Particle Tracking Model and Abstraction of Transport Processes* (BSC 2004 [DIRS 170041]). The appropriate level of confidence identified for unsaturated zone radionuclide transport is Level II. Therefore, Level II also represents appropriate level of confidence for the EBS-UZ interface model of the *EBS RT Abstraction*.

Section 7.3.1.1 describes the semi-analytical fracture-matrix partitioning model that is used to validate the EBS-UZ interface model of the *EBS RT Abstraction*. Section 7.3.1.2 compares the two interface models, and Section 7.3.1.3 provides an evaluation of differences between the two models and discussion of the applicability and suitability of the EBS-UZ interface model for TSPA transport modeling.

7.3.1 Validation of EBS-UZ Boundary Condition Implementation in TSPA

In this section, the predictions of the analytical fracture-matrix partitioning model developed in *Drift-Scale Radionuclide Transport* (BSC 2004 [DIRS 170040]) are compared with the fracture-matrix partitioning at the EBS-UZ boundary predicted by the *EBS RT Abstraction* (Section 6.5.3.6). Because the two models are conceptually different, exact agreement in their results is not expected. The objective of the validation is to demonstrate qualitative agreement, i.e., that the trends and general qualitative behavior of the EBS-UZ boundary condition implementation in the *EBS RT Abstraction* are also seen in a model that has been independently developed and uses a completely different solution approach.

7.3.1.2 Comparison of Results from Fracture-Matrix Partitioning Model with Results from the Modified *EBS RT Abstraction*

The two models are compared for the predictions of the fraction of mass of radionuclides released to fractures of the unsaturated zone. The comparison is based on the results of the Fracture-Matrix Partitioning Model reported in Section 6.4.6 of the *Drift-Scale Radionuclide Transport* (BSC 2004 [DIRS 170040]). In that report, calculations are done for the three infiltration rates (lower, mean and upper) of the glacial transition climate. The calculations include parameter uncertainty. The EBS-UZ interface model is modified, as discussed below, to allow comparison of the two models without changing the conceptual design or solution algorithm. GoldSim V8.01 (Golder Associates 2003 [DIRS 166572]) is used for the *EBS RT Abstraction* calculations. The GoldSim run files and the analysis of the results in an Excel spreadsheet are found in DTN: MO0508SPAFRAPM.000. The results of the comparison are shown in Figure 7.3-1.

In order to compare the *EBS RT Abstraction* with the fracture-matrix partitioning model, all sampled and time-varying parameters in the EBS and UZ in the TSPA system model are made consistent with the parameters used in the fracture-matrix partitioning model. Additional modifications made to the *EBS RT Abstraction* are listed below:

1. Delete the upstream waste form and corrosion products domains.

2. Apply uniform concentration at the top of the invert domain (1000 mg/L). For this purpose, the radionuclide chosen is ^{99}Tc, because it has no sorption in the invert and UZ. The inventory for all other radionuclides is set to zero.

3. Set the seepage flux entering the invert domain to zero, so that the only transport mechanism is diffusion.

4. Set the water saturation of invert intragranular continuum to 1.0 (fully saturated) and the water saturation of the intergranular continuum to zero. For the single continuum representation of the invert, the bulk water content is computed.

5. Turn off the imbibition flux entering the invert domain.

6. Change the diffusive property of the invert domain to match Equation E-1 of *Drift-Scale Radionuclide Transport* (BSC 2004 [DIRS 170040]).

7. Change the free water diffusion coefficient (D_0) to a lognormal distribution with the mean of $\log D_0$ of 4.69 and standard deviation of $\log D_0$ of 0.150, where D_0 is in units of $mm^2\ yr^{-1}$ (thus, the value of D_0 corresponding to the mean of $\log D_0$ is $10^{4.69} = 4.90 \times 10^4\ mm^2\ yr^{-1}$, or $1.55 \times 10^{-5}\ cm^2\ s^{-1}$), consistent with the approach adopted in *Drift-Scale Radionuclide Transport* (BSC 2004 [DIRS 170040], p. E-2 of Appendix E).

8. Change the diffusive thickness in the invert to a uniform distribution between 0.675 m and 0.806 m, as shown in *Drift-Scale Radionuclide Transport* (BSC 2004 [DIRS 170040], Appendix G, p. G-8).

9. Set the diffusive outflow area of the UZ matrix cells to zero, consistent with the boundary conditions imposed by the fracture-matrix partitioning model *Drift-Scale Radionuclide Transport* (BSC 2004 [DIRS 170040], Section 6.4.1). As a result, only diffusive transport occurs from invert domain to the UZ matrix continuum, and only advective transport occurs in the UZ matrix continuum.

10. The distance where the flow occurs in the UZ fracture is uniformly sampled between 0 m and the fracture spacing (inverse of fracture frequency). For the UZ matrix, the flow occurs immediately under the invert. Residual saturation is applied to the UZ fracture for the part where there is no flow. For the UZ matrix, the flow occurs immediately under the invert and thus the diffusive thickness of the first layer of the UZ matrix is set to a small value equal to 1×10^{-5} m.

11. Set the diffusive mass transfer term between the UZ matrix and fracture continuum to zero.

12. Ignore the transverse diffusion to the side UZ matrix and fracture cells from the UZ cells in the middle zone (These zones and cells in the EBS-UZ interface model are described in Section 6.5.3.6 and Figure 6.5-4).

13. Instead of setting the thickness of the second UZ layer as twice that of the first layer, the thickness of the second layer is changed to 1 m.

Figure 7.3-1 (shown below) compares the fraction of the radionuclide mass released to the fractures as predicted by the fracture-matrix partitioning model (labeled as "F-M Partitioning Model" in Figure 7.3-1) with the fraction predicted by the EBS-UZ boundary condition implementation for TSPA in the modified *EBS RT Abstraction* (labeled as "EBS RT Model" in Figure 7.3-1). The cumulative distribution function from the *EBS RT Abstraction* (thick red and green curves) is based on 100 realizations, while that for fracture-matrix partitioning model is based on 24 random samples selected for each infiltration case, as discussed in Section 6.4.6 of *Drift-Scale Radionuclide Transport* (BSC 2004 [DIRS 170040]). The 24 samples are the minimum required to ensure sampling of hydrologic parameters from each of the four host rock units (TSw33, TSw34, TSw35, and TSw36). Based on this sample size, it is estimated that for 95 percent confidence limit, the sample mean is within $\pm 0.41\sigma_s$ of the population mean, where σ_s is the sample standard deviation. Increasing the sample size narrows the estimated spread around the true mean and improves the accuracy of estimation. For the 100 realizations performed by the modified *EBS RT Abstraction*, the estimate of the sample mean for 95 percent confidence limit is within $\pm 0.2\sigma_s$ of the population mean. The uncertain parameters for the 100 realizations are sampled using the Latin Hypercube Sampling methodology employed by GoldSim.

The results for the fracture-matrix partitioning model for the three infiltration cases have been combined (weighted by the probability of each infiltration case) into a single curve (thick blue curve – "Combined Infiltration") for comparison with the EBS-UZ boundary condition implementation for TSPA *EBS RT Abstraction*. The thick red curve shows the results for the modified *EBS RT Abstraction* using the single continuum representation of the invert, which is the base case model used in TSPA. (Though not pertinent to model validation, the modified *EBS RT Abstraction* was also run using the dual continuum representation of the invert, an alternative conceptual model; results are shown as the thick green curve. These thick red and green curves virtually overlap showing little effect on the mass fraction released to fractures.)

In general, the modified *EBS RT Abstraction* predicts approximately the same mass fraction released to fractures compared to the fracture-matrix partitioning model. The difference is due to the fact that the two models are conceptually different with regard to the placement of fracture and matrix medium underneath the invert and in computing the flux out of the invert. The fracture-matrix partitioning model solves the transport equation semi-analytically, whereas the modified *EBS RT Abstraction* model uses a finite difference approach. Because of these differences, a perfect match between the two models is not expected. Nevertheless, the comparison shows a similar qualitative and quantitative behavior between the two models.

The modified *EBS RT Abstraction* and the fracture-matrix partitioning model (combined infiltration curve) agree within a factor about of three. The uncertainty in the three infiltration curves, shown as error bars in Figures 6-26b and 6-28 of *Drift-Scale Radionuclide Transport* (BSC 2004 [DIRS 170040]), is bounded by the "Upper Error Margin" and "Lower Error Margin" curves in Figure 7.3-1. The thick red (or green) curve falls within the "error margins" of the individual infiltration case curves, indicating a close match between the modified *EBS RT Abstraction* and the fracture-matrix partitioning model.

Although conceptual differences exist between the fracture-matrix partitioning model and the EBS-UZ interface model in the *EBS RT Abstraction,* with appropriate modifications to bring them into closer conceptual alignment, the two models display similar qualitative and quantitative behavior. The similarity in the results gives confidence that the EBS-UZ interface model is valid for use in TSPA.

7.3.1.3 Applicability of EBS-UZ Interface Model in TSPA in Comparison with Fracture-Matrix Partitioning Model

The EBS-UZ interface model of the *EBS RT Abstraction* is more suitable for TSPA compared to the fracture-matrix partitioning model for the following reasons:

- The fracture-matrix partitioning model assumes steady state mass transport and is solved with a semi-analytic solution to the Laplace equation, assuming a constant concentration boundary at the top of the invert and a variable flux boundary at the bottom. This approach is restrictive compared to the *EBS RT Abstraction*, wherein the radionuclide concentrations will be varying with time. Thus, important transient effects related to fuel degradation, thermal-hydrology, in-drift chemistry, and seepage are captured in the *EBS RT Abstraction*, but may not be captured adequately in the fracture-matrix partitioning model.

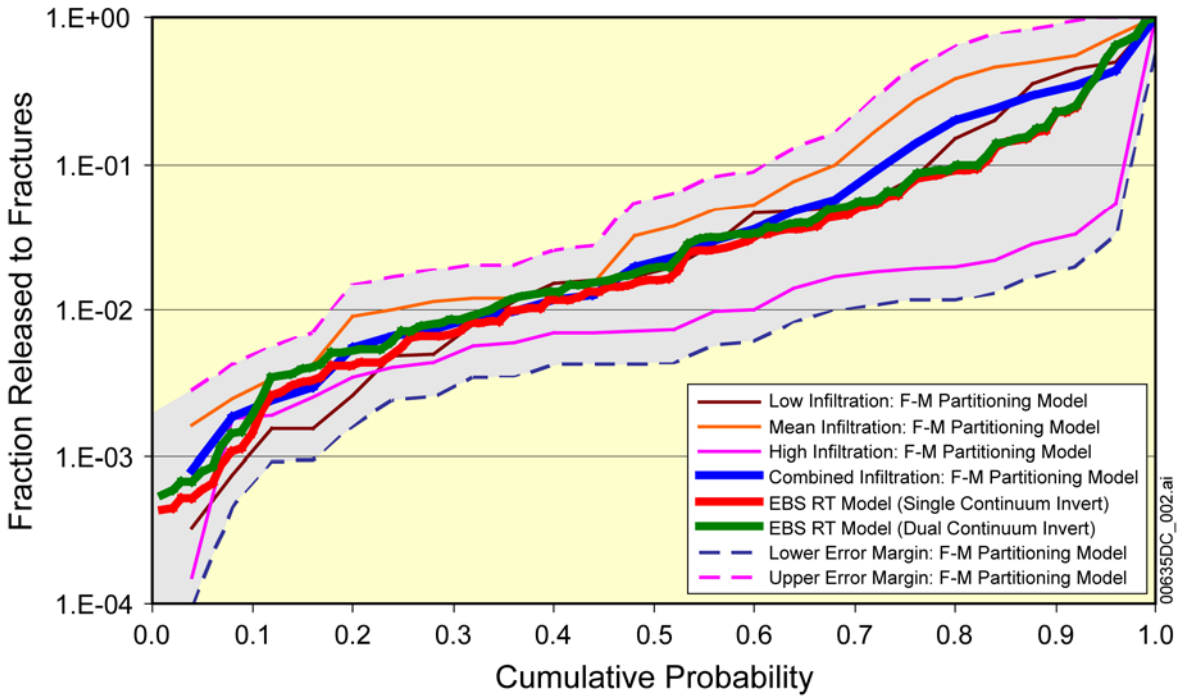

Fracture-Matrix Partitioning Model Error Margins: BSC 2004 [DIRS 170040], Figures 6-26b and 6-28b.

Output DTN: MO0508SPAFRAPM.000.

Figure 7.3-1. Fracture-Matrix Partitioning for No Seepage Case

- The *EBS RT Abstraction* is a finite difference type model that treats the EBS processes and the near-field UZ processes as a coupled system. The upstream boundary condition is provided by a specified mass flux based on the degradation rate of the waste form and the radionuclide solubility limits, while the downstream boundary is provided by assuming a zero concentration boundary at some distance (~3 drift diameters) from the invert in the UZ. Consequently, the mass flux of radionuclides from the waste package to the invert and from the invert to the UZ is based on solving the coupled system of differential equations with realistic boundary conditions. Since the mass flux from the invert to the UZ is based on the EBS-UZ boundary condition implementation for TSPA in the *EBS RT Abstraction*, to be consistent, the mass flux partitioning into the far-field UZ transport model (FEHM) should also be based on the *EBS RT Abstraction*, rather than on the fracture-matrix partitioning model.

- The fracture-matrix partitioning model assumes a discrete fracture network with no coupling between the fracture and matrix domains. In contrast, the EBS-UZ boundary condition implementation for TSPA in the *EBS RT Abstraction* treats the UZ as a dual continuum (overlapping UZ fracture and matrix continua), with diffusive mass transfer capability between the two continua. This dual continuum modeling approach is consistent with the various process-level UZ flow and transport models created for the YMP.

- The imbibition flux from the surrounding host rock into the intragranular continuum is modeled in the *EBS RT Abstraction*, whereas its contribution in the fracture-matrix

partitioning model is ignored. This flux could potentially carry some radionuclide mass into the UZ matrix that could lower the partitioning to the fracture continuum, which is realistic. The fracture-matrix partitioning model may overestimate the fraction released to the fractures where imbibition flux is significant.

- In the regions of the repository where water seeps through the drift, the fracture-matrix partitioning model arbitrarily proposes putting all the mass from the invert into the UZ fracture. This is a bounding approach and ignores the matrix pathway, which occupies most of the area under the invert. The EBS-UZ boundary condition implementation for TSPA in the *EBS RT Abstraction*, however, applies a more realistic approach, computing the fracture-matrix partitioning based on the appropriate set of boundary conditions in drifts with seepage and including transport in the UZ matrix, as discussed in the second bullet above. Sections 6.5.3.5 and 6.5.3.6 discuss how the advective flux from the invert is apportioned between fractures and matrix in the UZ.

The above comparisons of the results of the two models and their comparative suitability for TSPA have demonstrated that the EBS-UZ interface model meets Level II validation criteria. Based on the validation results, the EBS-UZ interface model is suitable for its intended use.

7.3.2 Results of Independent Model Validation Technical Review of the EBS-UZ Interface Model

An independent model validation technical review of the EBS-UZ interface model was conducted, as specified in the TWP (BSC 2005 [DIRS 173617], Section 2.2.3). This model validation approach is justified based on requirements of LP-SIII.10Q-BSC, Section 5.3.2 c), where independent technical review is listed as an appropriate method for model validation. The results of the independent model validation technical review of the EBS-UZ interface model are presented in a memo (Baker and Grisak 2004 [DIRS 170953]), a verbatim copy of which follows.

MEMO

Date: July 27, 2004

To: James Schreiber and Cliff Howard, Yucca Mountain Project

Cc:

From: Noreen A. Baker, Gerald E. Grisak, INTERA Inc., Austin, Texas

RE: **Independent Model Validation Technical Review of the EBS-UZ Interface Sub-Model of the Radionuclide Transport Abstraction Model for the Yucca Mountain Project**

---

8. CONCLUSIONS

This abstraction defines the conceptual model used to determine the rate of release of radionuclides from the EBS to the unsaturated zone in the TSPA given the assumptions listed in Section 5. The *EBS RT Abstraction* includes algorithms used in the TSPA for computing the flow of water and the transport of radionuclides through the EBS and specifies how parameters used in the model are calculated or from what other models they are obtained. This model is reasonably bounding because it overestimates flow through the drip shield and into the waste package and transport out of the EBS. At the same time, wherever possible, it is realistic, not just bounding, within the appropriate range of uncertainty for TSPA calculations.

8.1 CONCEPTUAL MODEL SUMMARY

This section summarizes the conceptual model for transport of radionuclides from the EBS as modeled in TSPA. Radionuclide transport out of the waste form and waste package, through the invert, and into the unsaturated zone is dependent on a complex series of events in the repository. After the waste packages are emplaced, radioactive decay of the waste will heat the drifts and locally perturb the normal percolation of water through the mountain. As the drifts cool, some of the water percolating through the mountain may drip into the drifts and subsequently contact some of the drip shields. Over time, the drip shield, waste package, and other components of the EBS are expected to degrade, leading to contact between the water and the waste form, resulting in the mobilization and transport of radionuclides through the EBS to the unsaturated zone. The primary transport medium through the EBS is anticipated to be water. Either a thin film of water or moving water is necessary for radionuclides to be transported out of the waste package and through the invert to the unsaturated zone.

A number of key factors will affect the mobilization and transport of radionuclides through the EBS, including barrier effectiveness and transport behavior:

- Performance of the drip shields
- Performance of the waste packages
- Protection provided by cladding
- Waste form degradation rates
- Entry and movement of water through waste packages
- Solubilities of radionuclides
- Transport of radionuclides through and out of the waste packages
- Transport of radionuclides through the invert below the waste packages
- Colloidal transport of radionuclides.

Once the drip shield is breached, water may contact the waste packages. Once a waste package is breached, water may enter the package as water vapor or as drips. If the cladding around spent fuel rods or the canister around a vitrified waste form is also breached, radionuclides may start to dissolve in the water. The concentration of each radionuclide mobilized from the waste form cannot exceed the radionuclide solubility limit, unless suspended colloids are included. Colloids are important for two reasons: they may potentially increase the release of radionuclides from the waste package, and they may potentially increase the transport velocity of radionuclides.

Table 8.1-1. Summary of EBS Flow Abstraction (Continued)

Flow Pathway, Pathway Flux	Flow Parameters	Data Sources and Notes
8. Flux from the invert into to the unsaturated zone, F_8	$F_8 = F_6 + F_7$ $= F_1 + F_7$	Total dripping flux portion (F_1) of advective flux from the invert flows into the UZ fractures, imbibition flux (F_7) flows into the UZ matrix.

Output DTN: SN0410T0507703.018.

WP = waste package.

In the transport abstraction, the EBS is modeled as consisting of three domains. The first domain is the source (i.e., SNF or HLW). The second domain consists of corrosion products from the degradation of steel waste package internal components. The third domain is the invert. The physical and chemical properties and conditions are uniform throughout each domain, as though the contents of the domain were thoroughly and continuously stirred.

Parameters that define the size of the two waste package domains, specifically the volumes and diffusive path lengths, are summarized in Table 8.2-1. Parameter values that are provided by other models are identified there. The path length for diffusion through the invert is set to the average thickness of the invert, 0.597 m.

The mass of corrosion products is a function of time and depends on the corrosion rates of carbon steel and stainless steel, which are uncertain parameters with values that are sampled in TSPA. In a seep environment, the corrosion products are fully saturated with water. In a no-seep environment for CSNF, the water saturation is based on the amount of water adsorbed onto iron oxide surfaces, which is a function of the relative humidity. The RH is an input to the transport model that depends on time and location in the repository. Calculation of corrosion products mass and saturation is discussed in Section 6.5.3.2.

The diffusion coefficient in the corrosion products is based on the self-diffusion coefficient of water at 25°C as a bounding value for all radionuclides, modified for the porosity and time-dependent water saturation.

The diffusion coefficient in the invert is also based on the self-diffusion coefficient of water at 25°C as a bounding value for all radionuclides. The effects of porosity and time-dependent saturation in the invert are incorporated, based on experimental data. The effect of temperature is also incorporated into the abstraction for the diffusion coefficient. The diffusion coefficient for colloids is assumed to be $1/100^{th}$ of the diffusion coefficient for a dissolved species (Section 6.3.4.4).

Sorption of radionuclides may occur on corrosion products in the waste package and on crushed tuff in the invert. Values for sorption distribution coefficients on corrosion products and on crushed tuff for all radionuclides of interest are determined in Section 6.3.4.2. K_d values for sorption on corrosion products are set to zero for all radionuclides as a bounding approach; i.e., no credit is taken for retardation due to reversibly sorbed radionuclides on stationary corrosion products.

are not included in DTN: SN0410T0507703.018, as well as the zero K_d values specified for corrosion products. DTN: SN0508T0503305.003 contains sorption data for goethite and HFO that are summarized in Table 6.3-6.

In addition, three preliminary output DTNs were created prior to final approval of this report: DTNs: SN0403T0507703.015, SN0409T0507703.017, and SN0503T0503305.001. DTNs: SN0410T0507703.018 and MO0506SPAINPAR.000 consist of the tables found in Sections 8.1 and 8.2 of the *EBS RT Abstraction*. Differences between the preliminary and final DTNs are described in Appendices I and J. Both of the preliminary DTNs: SN0403T0507703.015 and SN0409T0507703.017 have been superseded by the final output DTN: SN0410T0507703.018. These two preliminary output DTNs are discussed in Appendix I solely to provide transparency and traceability for TSPA applications that were initially developed based on the preliminary DTNs. These two DTNs are not intended for any other application. Preliminary DTN: SN0503T0503305.001 is used in TSPA and is not intended for any other application.

Table 8.2-1. Parameters for EBS Transport Abstraction

Waste Type	Transport Properties	Seep Case	No-Seep Case
Waste Form Domain (Fuel Rods, HLW, DSNF)			
CSNF	Rind volume and water volume	Waste form domain consists of fuel rods. • Rind volume provided by *Cladding Degradation Summary for LA* (BSC 2005 [DIRS 172895]) • S_w = water saturation in rind = 1.0	• Same as Seep Case
	Advection and Diffusion	Advective flux = volumetric flow rate through the WP Diffusive area of Waste Form Domain: • Total exposed surface area of all failed (axially split) fuel rods, limited to the total surface area of the waste package. • Provided by *Cladding Degradation Summary for LA* (BSC 2005 [DIRS 172895]) Diffusion path length: • Thickness of rind; function of time. • Provided by *Cladding Degradation Summary for LA* (BSC 2005 [DIRS 172895]) Diffusion coefficient in Waste Form Domain, D_{WF}: • $\phi S_w D_{WF} = \phi^{1.3} S_w^2 D_0$ • ϕ = porosity of rind (BSC 2005 [DIRS 172895]) • S_w = water saturation in rind = 1.0 • D_0 = free water diffusion coefficient (D_{WF} is an effective value defined in the same manner as D_s in Equation 6.3.4.3.5-2.)	• No advective flux • Diffusive properties same as Seep Case

As a bounding approach, no credit is taken for retardation due to reversibly sorbed radionuclides on waste package corrosion products. Thus, sorption distribution coefficients are set to zero for all radionuclides (Table 8.2-3; output DTN: MO0506SPAINPAR.000). Nonzero K_d values, an alternative conceptual model described in Section 6.6.6, are given in DTN: SN0410T0507703.018.

The ranges and distributions of radionuclide sorption distribution coefficients for sorption on devitrified unsaturated zone tuff given in Table 4.1-15 (DTN: LA0408AM831341.001 [DIRS 171584]) are assigned to K_d values on crushed tuff in the invert. Correlations for sampling sorption distribution coefficient probability distributions for devitrified UZ tuff given in Table 4.1-16 (DTN: LA0311AM831341.001 [DIRS 167015]) are assigned to invert crushed tuff.

Sorption distribution coefficient (K_d) values and interval probabilities used for reversible radionuclide sorption on colloids in TSPA calculations are provided by DTN: SN0306T0504103.006 [DIRS 164131], Table 1.

Parameter ranges and distributions for irreversible sorption of plutonium and americium onto stationary waste package corrosion products are given in Table 6.3-6 and summarized in output DTN: SN0508T0503305.003.

Table 8.2-2 summarizes various sampled parameters to be used in the EBS radionuclide transport abstraction, with the range and distribution of each parameter provided. This table is itself a summary of Table 6.5-6, which, along with the rest of Section 6.5.2, gives further details about each parameter and the location in this document where the parameter is developed. A summary of fixed, single-value parameters to be used in the EBS radionuclide transport abstraction is given in Table 8.2-3 (output DTNs: SN0410T0507703.018 and MO0506SPAINPAR.000). Equations used to compute various parameters in the EBS radionuclide transport abstraction are shown in Table 8.2-4.

Acceptance Criterion 5–Model Abstraction Output Is Supported by Objective Comparisons.

(1) The models implemented in this total system performance assessment abstraction provide results consistent with output from detailed process-level models and/or empirical observations (laboratory and field testings and/or natural analogs).

Response: The models implemented in this total system performance assessment abstraction provide results consistent with output from detailed process-level models and/or empirical observations (laboratory testings), as described in Sections 6.3, 6.5, and 7. Section 7 provides comparisons of models developed in this model report with other models and experimental results.

(3) DOE adopts well-documented procedures that have been accepted by the scientific community to construct and test the numerical models, used to simulate coupled thermal-hydrologic-chemical effects on radionuclide release. For example, DOE demonstrates that the numerical models used for high-level radioactive waste degradation and dissolution, and radionuclide release from the engineered barrier system, are adequate representations; include consideration of uncertainties; and are not likely to underestimate radiological exposures to the reasonably maximally exposed individual and releases of radionuclides into the accessible environment.

Response: The EBS radionuclide transport abstraction uses well-documented procedures in Section 6.5 that have been accepted by the scientific community to construct and test the numerical models used to simulate radionuclide release. The abstraction demonstrates that the numerical models used for radionuclide release from the EBS include consideration of uncertainties and are not likely to underestimate radiological exposures to the reasonably maximally exposed individual and releases of radionuclides into the accessible environment.

8.4 RESTRICTIONS FOR SUBSEQUENT USE

This abstraction was developed specifically for application in TSPA. Assumptions and approximations are made in order to integrate with and be consistent with other models and abstractions incorporated in TSPA. Therefore, individual submodels should not be used independently outside of the TSPA framework. This abstraction must be reevaluated if any models that feed into it are modified.

Use of the three preliminary output DTNs: SN0403T0507703.015, SN0409T0507703.017, and SN0503T0503305.001 is restricted to providing traceability in TSPA. For any other application, the final output DTNs: SN0410T0507703.018, MO0506SPAINPAR.000, and SN0508T0503305.003 are to be used. Differences between the preliminary DTNs: SN0403T0507703.015 and SN0409T0507703.017 are described in Appendix I. This appendix also compares the second preliminary DTN: SN0409T0507703.017 with the corresponding final DTN: SN0410T0507703.018. Differences between the two related DTNs: SN0503T0503305.001 and SN0508T0503305.003 are described in Appendix J.

The discretization of the balance Equation B-35 for irreversible Pu mass on the colloids yields

$$c_{Irrv\_Pu\_FeO\_c}^{n+1} = \frac{c_{Irrv\_Pu\_FeO\_c}^{n} + \overline{R}_1^{n+1}\Delta t c_{Pu\_aq}^{n+1}}{1+(\overline{U}^{n+1} + \overline{D}_{right\_col} + \lambda)\Delta t} \qquad \text{(Eq. B-53)}$$

and for irreversible Pu mass on the corrosion products, Equation B-36 yields

$$c_{Irrv\_Pu\_FeO\_CP}^{n+1} = \frac{c_{Irrv\_Pu\_FeO\_CP}^{n} + \overline{R}_2^{n+1}\Delta t c_{Pu\_aq}^{n+1}}{1+\lambda\Delta t}. \qquad \text{(Eq. B-54)}$$

SAMPLE CALCULATION WITH REPRESENTATIVE PARAMETERS

A sample calculation is performed to demonstrate the solution technique and illustrate the types of behavior that might be expected in this model. Parameter values used in this sample calculation are given in Table B-1. Let the solubility, flow velocity, and irreversible reaction parameters, which are actually time-dependent, be constant over time.

For this set of parameters, the irreversible reactive rates, advective rate, diffusive rates, decay rate and the dimensionless colloids and corrosion product partition coefficients are:

$$\begin{aligned}
\overline{R}_1 &= 0.02000\ \text{yr}^{-1} \\
\overline{R}_2 &= 786\ \text{yr}^{-1} \\
\overline{U} &= 0.04367\ \text{yr}^{-1} \\
\overline{D}_{left_aq} &= 0.09127\ \text{yr}^{-1} \\
\overline{D}_{right_aq} &= 2.229\times10^{-3}\ \text{yr}^{-1} \\
\overline{D}_{right_col} &= 2.229\times10^{-5}\ \text{yr}^{-1} \\
\lambda &= 2.875\times10^{-5}\ \text{yr}^{-1} \\
\overline{K}_{d_FeO_c} &= 0.20 \\
\overline{K}_{d_FeO_CP} &= 1.965\times10^{4} \\
\overline{K}_{d_WF_c} &= 0.60 \\
\overline{K}_{d_GW_c} &= 0.020.
\end{aligned}$$

The simulation for the mixing cell (Cell 2) concentrations over a 1000-year time interval is shown in Figure B-2. The dominant rate constant, by several orders of magnitude, is the irreversible rate constant of the corrosion products, $\overline{R}_2 = 786\ \text{yr}^{-1}$. This is a result of the large mass of corrosion products and results in a relative large concentration of irreversibly sorbed Pu on the corrosion products, $c_{Irrv\_Pu\_FeO\_CP}$. For this simulation, the amount of corrosion product mass is representative of the total mass of corrosion products in a waste package, and all the corrosion products are available at initial time. In the TSPA abstraction model, the corrosion

BOUNDARY FLUXES

Now consider the two boundary flux conditions given in Equations B-1 and B-2. The left or upstream boundary flux accounts for advection/diffusion of Pu mass in solution (Pu_aq) and Pu mass sorbed to waste form colloids. In this section of the analysis, upstream diffusion of colloids is ignored, although the TSPA implementation does account for upstream colloid diffusion. The mass flux rates (kg yr^{-1}) at the upstream (left) boundary for the n^{th} time step are:

Advective_Pu_aq (kg yr^{-1}) $= \overline{U} V_{water} c_s$

Diffusive_Pu_aq (kg yr^{-1}) $= \overline{D}_{left\_aq} V_{water} (c_s - c^n_{Pu\_aq})$

Advective_Pu_WF_c (kg yr^{-1}) $= \overline{U} V_{water} \overline{K}_{d\_WF\_c} c_s$

Diffusive_Pu_WF_c (kg yr^{-1}) $= \overline{D}_{left\_col} V_{water} \overline{K}_{d\_WF\_c} (c_s - c^n_{Pu\_aq})$.

The right or downstream boundary flux has contributions from advection/diffusion of Pu in solution and colloid together with advection/diffusion of Irrv_Pu on colloids. There is no advective or diffusive flux associated with the immobile corrosion products. The mass flux rates (kg yr^{-1}) at the right boundary assuming zero downstream concentrations are:

Advective_Pu_aq (kg yr^{-1}) $= \overline{U} V_{water} c^n_{Pu\_aq}$

Diffusive_Pu_aq (kg yr^{-1}) $= \overline{D}_{right\_aq} V_{water} c^n_{Pu\_aq}$

Advective_Pu_FeO_c (kg yr^{-1}) $= \overline{U} V_{water} \overline{K}_{d\_FeO\_c} c^n_{Pu\_aq}$

Diffusive_Pu_FeO_c (kg yr^{-1}) $= \overline{D}_{right\_col} V_{water} \overline{K}_{d\_FeO\_c} c^n_{Pu\_aq}$

Advective_Irrv_Pu_FeO_c (kg yr^{-1}) $= \overline{U} V_{water} c^n_{Irrv\_Pu\_FeO\_c}$

Diffusive_Irrv_Pu_FeO_c (kg yr^{-1}) $= \overline{D}_{right\_col} V_{water} c^n_{Irrv\_Pu\_FeO\_c}$

Advective_Pu_WF_c (kg yr^{-1}) $= \overline{U} V_{water} \overline{K}_{d\_WF\_c} c^n_{Pu\_aq}$

Diffusive_Pu_WF_c (kg yr^{-1}) $= \overline{D}_{right\_col} V_{water} \overline{K}_{d\_WF\_c} c^n_{Pu\_aq}$

Advective_Pu_GW_c (kg yr^{-1}) $= \overline{U} V_{water} \overline{K}_{d\_GW\_c} c^n_{Pu\_aq}$

Diffusive_Pu_GW_c (kg yr^{-1}) $= \overline{D}_{right\_col} V_{water} \overline{K}_{d\_GW\_c} c^n_{Pu\_aq}$.

The total flux at the left boundary (upstream) at the n^{th} time step, $F^n_{left\_bddy\_total}$, is

$$F^n_{left\_bddy\_total} = \overline{U} V_{water} c_s + \overline{D}_{left\_aq} V_{water} (c_s - c^n_{Pu\_aq})$$

$$+ \overline{U} V_{water} \overline{K}_{d\_WF\_c} c_s + \overline{D}_{left\_col} V_{water} \overline{K}_{d\_WF\_c} (c_s - c^n_{Pu\_aq}).$$

COMPARISON OF OUTPUT DTNs

The output from this report consists of three preliminary output DTNs: SN0403T0507703.015, SN0409T0507703.017 and SN0503T0503305.001, and three final output DTNs: SN0410T0507703.018, SN0508T0503305.003, and MO0506SPAINPAR.000. In this appendix, the differences between two preliminary output DTNs (SN0403T0507703.015 and SN0409T0507703.017) are discussed. In addition, the final output DTN: SN0410T0507703.018 is compared with the second preliminary DTN: SN0409T0507703.017. These comparisons provide traceability for TSPA applications that were initially developed based on the preliminary output DTNs. Appendix J contains the comparison between DTNs: SN0503T0503305.001 and SN0508T0503305.003.

The output in the three DTNs discussed in this appendix consists of tables from Section 8 (Conclusions) of the *EBS RT Abstraction*. Each of these tables is compared in this appendix. Numerous editorial revisions were made in converting the first preliminary version of the DTN to the second preliminary version; because these editorial revisions have no impact on TSPA results, they are not discussed in this appendix.

TABLE 57 (DTN: SN0403T0507703.015) VS. TABLE 8.1-1 (DTN: SN0409T0507703.017)

Table 57 (Summary of EBS Flow Abstraction) in DTN: SN0403T0507703.015 corresponds to Table 8.1-1 in DTN: SN0409T0507703.017. The key differences in this table between the two DTN versions are the expressions for the flux through the drip shield, F_2, and the flux into the waste package, F_4. In preliminary DTN: SN0403T0507703.015, F_2 is expressed as:

$$F_2 = F_1 L_{DS\_Patch} f'_{DS} / (2L_{DS}). \quad \text{(Eq. I-1)}$$

The parameters are defined in the Table 57 in DTN: SN0403T0507703.015. This equation is technically correct, but it is expressed more completely in DTN: SN0409T0507703.017 as:

$$F_2 = \min[F_1 N_{bDS} L_{DS\_Patch} f'_{DS} / (2L_{DS}), F_1]. \quad \text{(Eq. I-2)}$$

The parameters are defined in the Table 8.1-1 in DTN: SN0409T0507703.017. Equation I-2 replicates Equation 6.5.1.1.2-37 in the *EBS RT Abstraction*. Equations I-1 and I-2 give the same result when the number of corrosion patches in the drip shield, N_{bDS}, is one, which is the case in the WAPDEG model of drip shield failure (BSC 2004 [DIRS 169996], Section 6.3). The min function in Equation I-2 provides a numerical check to prevent an unrealistic result of $F_2 > F_1$ from being obtained if the parameter values used in the equation were to give that result.

The same discussion applies to the flux into the waste package. In DTN: SN0403T0507703.015, F_4, is expressed as:

$$F_4 = F_2 L_{WP\_Patch} f'_{WP} / (2L_{WP}). \quad \text{(Eq. I-3)}$$

The parameters are defined in the Table 57 in DTN: SN0403T0507703.015.

This equation is technically correct, but it is expressed more completely in DTN: SN0409T0507703.017 as:

$$F_4 = \min[F_2 N_{bWP} L_{WP\_Patch} f'_{WP} / (2L_{WP}), F_2]. \quad \text{(Eq. I-4)}$$

The parameters are defined in the Table 8-1 in DTN: SN0409T0507703.017. Equation I-4 replicates Equation 6.5.1.1.3-1 in the *EBS RT Abstraction*. The difference between Equations I-3 and I-4 is the definition of L_{WP_Patch}. In Equation I-3, L_{WP_Patch}, is the length of *all* corrosion patches in the waste package, whereas in Equation I-4, L_{WP_Patch} is the length of *each* corrosion patch; thus, the product $N_{bWP}L_{WP\_Patch}$ in Equation I-4 is equal to L_{WP_Patch} in Equation I-3. The min function in Equation I-4 provides a numerical check to prevent an unrealistic result of $F_4 > F_2$ from being obtained if the parameter values used in the equation were to give that result.

In the Flow Parameter column for Flow Pathway 8 in Table 57 in DTN: SN0403T0507703.015, a flux F_9 is erroneously included in the equation and is deleted in the final DTN. Since this flux does not exist, its inclusion in the preliminary DTN has no impact on the TSPA calculation.

The references and comments in the Data Sources & Notes column in Table 8.1-1 in DTN: SN0409T0507703.017 are updated from Table 57 in DTN: SN0403T0507703.015; these updates have no impact on TSPA calculations.

TABLE 58 (DTN: SN0403T0507703.015) VS. TABLE 8.1-2 (DTN: SN0409T0507703.017)

In DTN: SN0409T0507703.017, the cross-sectional area for radionuclide transport is clarified in Table 8.1-2, with references to sections in the report. In DTN: SN0403T0507703.015, the same parameter is referred to as the flow cross-sectional area in Table 58 and described in vague terms that prompted a revised description in the final DTN. References are updated in DTN: SN0409T0507703.017, Table 8.1-2. None of these changes has any impact on TSPA calculations.

TABLE 59 (DTN: SN0403T0507703.015) VS. TABLE 8.2-1 (DTN: SN0409T0507703.017)

In Table 57 in DTN: SN0403T0507703.015, the lower end of the range on sampled parameter Diff_Path_Length_CP_CDSP is erroneously shown as 0.02 m; this error is also found in Table 63 in DTN: SN0403T0507703.015. Because the correct value, 0.025 m, is included in the database used for TSPA, this error has no impact on TSPA. In the corresponding table in DTN: SN0409T0507703.017, Table 8.2-1, the range for this parameter is not shown, since it is given correctly in Table 8.2-3.

References to parameter sources and sections in the *EBS RT Abstraction* are updated in DTN: SN0409T0507703.017. These changes have no impact on TSPA calculations.

TABLE 60 (DTN: SN0403T0507703.015) VS. TABLE 8.2-2 (DTN: SN0409T0507703.017)

Table 8.2-2 in DTN: SN0409T0507703.017 (K_d values for corrosion products) is identical to Table 60 in DTN: SN0403T0507703.015. Therefore, there is no impact on TSPA calculations.

TABLES 61 & 62 (DTN: SN0403T0507703.015) VS. TEXT (DTN: SN0409T0507703.017)

Tables 61 and 62 in DTN: SN0403T0507703.015 (K_d values and correlations for the invert) are replaced in DTN: SN0409T0507703.017 with text clarifying that TSPA is to use UZ K_d values for the invert. This change has no impact on TSPA calculations.

TABLE 63 (DTN: SN0403T0507703.015) VS. TABLE 8.2-3 (DTN: SN0409T0507703.017)

In Table 63 in DTN: SN0403T0507703.015, sampled parameter Diff_Path_Length_CP_CDSP is erroneously shown as having a lower end of the range of 0.02 m. Because the correct value, 0.025 m, is included in the database used for TSPA, this error has no impact on TSPA. The correct range is shown in Table 8.2-3 in DTN: SN0409T0507703.017. References are updated in Table 8.2-3 in DTN: SN0409T0507703.017. These changes have no impact on TSPA calculations.

TABLE 64 (DTN: SN0403T0507703.015) VS. TABLE 8.2-4 (DTN: SN0409T0507703.017)

References are updated in Table 8.2-4 in DTN: SN0409T0507703.017. Three parameters were added to this table to provide a source for the values used in TSPA: DS_Total_Length (5805 mm), Invert_Viscosity_Ref_Temp (298.15 K), and Interface_Scale_Factor (1×10^{-6}). These changes have no impact on TSPA calculations. No other changes were made in converting Table 64 to Table 8.2-4.

TABLE 65 (DTN: SN0403T0507703.015) VS. TABLE 8.2-5 (DTN: SN0409T0507703.017)

The following changes were made to convert Table 65 to Table 8.2-5. References to the equations in the *EBS RT Abstraction* were added to the Input Description column. In the Parameter Description for Equation 8-1, clarification of the definition of *ND*, the truncated normal distribution, was added. In Equation 8-2, the range of validity was added to the definition of temperature. In Equation 8-3, the definition of θ_m was changed from fraction to percent, and the equation was modified accordingly by changing the term $0.138\theta_m$ to $0.00138\theta_m$. Equation 8-7 was completely revised in order to clarify the calculation of corrosion product mass as computed in TSPA over each time interval, from t_0, when breach occurs, to t_{f1} and t_{f2}, the lifetimes of each type of steel. These changes have no impact on TSPA calculations.

TABLE 66 (DTN: SN0403T0507703.015) VS. TABLE 8.2-6 (DTN: SN0409T0507703.017)

Table 8.2-6 DTN: SN0409T0507703.017 (Invert Diffusion Coefficient Alternative conceptual Model Parameters) is identical to Table 66 in DTN: SN0403T0507703.015. Therefore, there is no impact on TSPA calculations.

TABLE 67 (DTN: SN0403T0507703.015) VS. TABLE 8.2-7 (DTN: SN0409T0507703.017)

Equation 8-8 was reformulated in the *EBS RT Abstraction* and revised accordingly in Table 8.2-7. Because this is an alternative conceptual model, this change has no impact on TSPA calculations. Equation 8-9, the definitions of θ_{intra} and θ_{min} were changed from fractions to percent. This change has no impact on the results.

TABLE 8.1-1 (DTN: SN0410T0507703.018)VS. TABLE 8.1-1 (DTN: SN0409T0507703.017)

The differences in this table (Summary of EBS Flow Abstraction) between the two DTN versions are the expressions for the flux through the drip shield, F_2, and the flux into the waste package, F_4. In DTN: SN0409T0507703.017, F_2 is expressed as:

$$F_2 = \min\left[F_1 N_{bDS} L_{DS\_Patch} f'_{DS} / (2L_{DS}), F_1\right]. \quad \text{(Eq. I-5)}$$

The parameters are defined in Table 8.1-1 in both DTNs. Because L_{DS_Patch} is defined as the axial *half*-length of each corrosion patch, the factor of 2 should not appear in the denominator. This equation is presented correctly in DTN: SN0410T0507703.018 as:

$$F_2 = \min\left[F_1 N_{bDS} L_{DS\_Patch} f'_{DS} / L_{DS}, F_1\right]. \quad \text{(Eq. I-6)}$$

Similarly, in DTN: SN0409T0507703.017, F_4 is expressed in Table 8.1-1 as:

$$F_4 = \min\left[F_2 N_{bWP} L_{WP\_Patch} f'_{WP} / (2L_{WP}), F_2\right]. \quad \text{(Eq. I-7)}$$

This equation is presented correctly in Table 8.1-1 in DTN: SN0410T0507703.018 as:

$$F_4 = \min\left[F_2 N_{bWP} L_{WP\_Patch} f'_{WP} / L_{WP}, F_2\right]. \quad \text{(Eq. I-8)}$$

These differences have no impact because the correct equations (Equations I-6 and I-8) have been implemented in the TSPA.

TABLE 8.2-4 (DTN: SN0410T0507703.018)VS. TABLE 8.2-5 (DTN: SN0409T0507703.017)

The differences in this table (Calculated Model Inputs Used in the EBS Radionuclide Transport Abstraction) between the two DTN versions include Equation 8-5 for the effective water saturation of corrosion products. In DTN: SN0409T0507703.017, this equation is:

$$S_{we,CP} = 1.312 \times 10^{-6} \bar{s}_{CP} \left(-\ln RH\right)^{-1/2.45}. \quad \text{(Eq. I-9)}$$

This equation, developed in an earlier draft of Section 6.5.1.2.1.4.2 as Equation 6.5.1.2.1-27, is incorrect. The correct equation (as shown in Section 6.3.4.3.5, Equation 6.3.4.3.5-5 of this report), is given in DTN: SN0410T0507703.018 as:

$$S_{we,CP} = 3.28 \times 10^{-6} \bar{s}_{CP} \left(-\ln RH\right)^{-1/2.45}. \quad \text{(Eq. I-10)}$$

APPENDIX J

SORPTION DATA USED IN TSPA

SORPTION DATA USED IN TSPA

The data used in TSPA for the irreversible sorption submodel is contained in a preliminary output DTN: SN0503T0503305.001. Four of the data points in the preliminary DTN have been found to be incorrect. The correct data values are listed in Table 4.1-10, and included in the discrete distributions presented in Table 6.3-6. The data values and discrete distributions are also included in final output DTN: SN0508T0503305.003. The erroneous data and the sorption parameter distributions that are used in TSPA are described in this appendix. In some instances, it refers to DTN: SN0503T0503305.001 as the "uncorrected data set" and to DTN: SN0508T0503305.003 as the "corrected data set" as a way of differentiating which data set has the correct values.

The first erroneous data value in preliminary DTN: SN0503T0503305.001 is a sorption site density for goethite of 1.00 sites nm^{-2} attributed to Kooner (1993 [DIRS 173819]). This value is not given in Kooner (1993 [DIRS 173819]) and has been deleted from the discrete distribution for goethite site density shown in Table 6.3-6. This deletion has two effects. First, the lower end of the distribution increases from 1.00 sites nm^{-2} to 1.02 sites nm^{-2}. Since the upper end of the distribution is 8.38 sites nm^{-2}, this change results in a reduction of the range of less than 0.3 percent and is expected to have negligible impact on dose calculations in TSPA. The second effect is to increase the probability of each entry in the distribution, since there are now 56 points instead of 57. Therefore, each data point now has a probability of 1/56 = 0.01786 instead of 1/57 = 0.01754. This change in the probability of each entry in the distribution should also have a negligible effect on TSPA dose calculations.

The second data error in preliminary DTN: SN0503T0503305.001 is a total sorption site density for goethite of 5.92 sites nm^{-2}. The correct value, as given by Hiemstra and Van Riemsdijk (1996 [DIRS 173023], p. 498), is 6.15 sites nm^{-2} (DTN: SN0508T0503305.003).

The third data error in preliminary DTN: SN0503T0503305.001 is a sorption site density for goethite of 8.83 sites nm^{-2}. The correct value, as given by Robertson and Leckie (1997 [DIRS 173763], Table 4), is 8.38 sites nm^{-2} (DTN: SN0508T0503305.003).

These second and third data values have a minor impact on the discrete distribution for goethite site density in preliminary DTN: SN0503T0503305.001, shown in Table J-1, that is sampled in TSPA. Comparing this with the correct distribution in Table 6.3-6 shows a negligible difference (see Figure J-1, where the cumulative distribution for goethite site density used in TSPA, computed in Table J-2, is compared in with the distribution developed in the *EBS RT Abstraction*). The maximum value in the range of site densities is larger in Table J-1 due to the erroneous data point 8.83 sites nm^{-2}. This point expands the range by about 3%, from a range of 1.02 to 8.59 sites/nm^2 to a range of 1.02 to 8.83 sites nm^{-2}. The value being used in TSPA (8.83) is about 5% greater than the correct value. Since it represents one of 57 data points in the distribution, the probability that it will be sampled is low (1/57 = 0.01754). Therefore, this error is expected to have negligible impact on dose calculations in TSPA. The second error, where the value used in TSPA is 5.92 sites nm^{-2} and the correct value is 6.15 sites nm^{-2}, will also have a negligible effect. The value used in TSPA is smaller than the correct value by about 4%, and thus partially offsets the error in the maximum site density. The correct value and the erroneous value occupy the same position in the distribution, so this error does not alter the shape or range

of the distribution. The net effect of these two small errors on dose calculations in TSPA should be negligible.

The fourth data error in preliminary DTN: SN0503T0503305.001 is in a value for the percentage of high-affinity sorption sites for goethite. Instead of the correct value of 2.7 sites nm^{-2} (Hiemstra and Van Riemsdijk 1996 [DIRS 173023], p. 498), an incorrect value of 2.47 sites nm^{-2} was used. This value is used to obtain a value for the percentage of high-affinity sorption sites for goethite in Table 6.3-4b. The incorrect site density value resulted in a value for the percentage of high-affinity sorption sites for goethite of 41.67 percent, whereas the correct value is 43.90 percent (see Table 6.3-4b). The effect of this error on dose calculations in TSPA should be negligible, as indicated by Figure J-2, where the cumulative distribution for the percentage of high-affinity sorption sites for goethite used in TSPA, computed in Table J-2, is compared in with the distribution developed in the *EBS RT Abstraction*.

Table J-1 shows discrete probabilities for various values of several parameters. The sum of these parameters is 1.0, and the cumulative sum at any parameter value is the cumulative (probability) distribution function, CDF.

One additional deviation from the discrete distributions shown in Table 6.3-6 as shown in preliminary DTN: SN0503T0503305.001 involves the number of digits of precision used for the parameters. As discussed in Section 6.3.4.2.3.2, specific surface areas and site density data are accurate to at most three significant digits due to the difficulty in measuring these parameters and variability in samples. The high-affinity site percentages are even less precise. The parameters comprising the discrete distributions in Table 6.3-6 are presented to three significant digits. However, in the Excel file contained in preliminary DTN: SN0503T0503305.001, the data are available to 15 digits of precision. These are shown rounded to 9 digits in Table J-1 (goethite high-affinity site percentages are shown to 11 digits). The differences in precision between the data in Table 6.3-6 and the parameters used in preliminary DTN: SN0503T0503305.001 will have a negligible effect on dose calculations and are discussed here solely to provide full traceability of the data.

Table J-1. Sample Ranges and Distributions Used for Irreversible Sorption on Stationary Corrosion Products from the Uncorrected Data Set

Input Name	Input Description	Range	Distribution
Relative_Abundance_Goethite_a	Fraction of total iron oxide that is goethite	0.45 – 0.8	Uniform
Goethite_SA_a	Goethite surface area; discrete distribution	Specific Surface Area (m^2 g^{-1})	Probability Level
		14.7	0.018867925
		20.0	0.056603774
		21.0	0.037735849
		21.4	0.018867925
		27.7	0.018867925
		28.5	0.037735849
		30.8	0.018867925
		32.0	0.037735849
		33.0	0.056603774
		35.0	0.018867925
		37.0	0.018867925
		38.0	0.018867925
		39.9	0.018867925
		43.0	0.018867925

Table J-1. Sample Ranges and Distributions Used for Irreversible Sorption on Stationary Corrosion Products from the Uncorrected Data Set (Continued)

Input Name	Input Description	Range	Distribution
Goethite_SA_a (continued)		45.0	0.037735849
		47.5	0.018867925
		49.0	0.075471698
		50.0	0.018867925
		52.0	0.037735849
		54.0	0.018867925
		55.0	0.056603774
		55.4	0.018867925
		64.3	0.018867925
		66.0	0.037735849
		70.0	0.037735849
		80.0	0.037735849
		80.5	0.018867925
		81.0	0.075471698
		85.0	0.018867925
		86.0	0.018867925
		105.0	0.037735849
		110.0	0.018867925
HFO_SA_a	HFO (hydrous ferric oxide) surface area; discrete distribution	Specific Surface Area ($m^2\ g^{-1}$)	Probability Level
		600.0	1.000
Goethite_Site_Density_a	Goethite site density; discrete distribution	Density (sites nm^{-2})	Probability Level
		1.00000000	0.01754386
		1.01513714	0.01754386
		1.21013524	0.01754386
		1.32484000	0.03508772
		1.46000000	0.01754386
		1.50000000	0.01754386
		1.65500000	0.01754386
		1.68000000	0.03508772
		1.70000000	0.01754386
		1.80000000	0.01754386
		1.87000000	0.01754386
		1.92704000	0.01754386
		1.94573646	0.01754386
		1.97220500	0.01754386
		2.20000000	0.01754386
		2.30000000	0.07017544
		2.31000000	0.01754386
		2.31903106	0.01754386
		2.55000000	0.01754386
		2.60000000	0.03508772
		2.70000000	0.01754386
		2.88600000	0.01754386
		2.90000000	0.03508772
		3.00000000	0.01754386
		3.12251852	0.01754386
		3.13144000	0.01754386
		3.30000000	0.03508772
		3.40000000	0.01754386
		4.00000000	0.01754386
		4.20000000	0.01754386

Table J-1. Sample Ranges and Distributions Used for Irreversible Sorption on Stationary Corrosion Products from the Uncorrected Data Set (Continued)

Input Name	Input Description	Range	Distribution
Goethite_Site_Density_a (continued)		4.60000000	0.01754386
		4.84195023	0.01754386
		4.90000000	0.01754386
		5.00000000	0.01754386
		5.52819600	0.01754386
		5.92000000	0.01754386
		6.30000000	0.01754386
		6.31000000	0.03508772
		6.60000000	0.01754386
		7.00000000	0.05263158
		7.20000000	0.01754386
		7.40000000	0.01754386
		8.00000000	0.01754386
		8.16000000	0.01754386
		8.58737200	0.01754386
		8.83000000	0.01754386
HFO_Site_Density_a	HFO (hydrous ferric oxide) site density; discrete distribution	Density (sites nm^{-2})	Probability Level
		0.56480960	0.05263158
		1.12961921	0.10526316
		1.46850497	0.05263158
		1.58146689	0.05263158
		1.69442881	0.10526316
		1.80739073	0.05263158
		2.03331458	0.10526316
		2.25923842	0.26315789
		2.59812418	0.05263158
		2.71108610	0.05263158
		4.00000000	0.05263158
		5.64809604	0.05263158
HFO_Strong_Sites_a	Percentage of high affinity HFO (hydrous ferric oxide) sites; discrete distribution	Percentage	Probability Level
		0.20000000	0.01262626
		0.40000000	0.01010101
		0.41666667	0.01262626
		0.43478261	0.01262626
		0.50000000	0.06313131
		0.55555556	0.02525253
		0.60000000	0.00757576
		0.62500000	0.01262626
		0.66666667	0.02525253
		0.71428571	0.01262626
		0.76923077	0.01262626
		0.83333333	0.01010101
		0.86956522	0.01010101
		1.00000000	0.09343434
		1.11111111	0.02020202
		1.25000000	0.01767677
		1.30434783	0.00757576
		1.33333333	0.02020202

Table J-1. Sample Ranges and Distributions Used for Irreversible Sorption on Stationary Corrosion Products from the Uncorrected Data Set (Continued)

Input Name	Input Description	Range	Distribution
HFO_Strong_Sites_a (continued)		1.40000000	0.00252525
		1.42857143	0.01010101
		1.50000000	0.03787879
		1.53846154	0.01010101
		1.66666667	0.01515152
		1.87500000	0.00757576
		2.00000000	0.05303030
		2.08333333	0.01767677
		2.14285714	0.00757576
		2.17391304	0.01767677
		2.30769231	0.00757576
		2.50000000	0.08838384
		2.77777778	0.03535354
		2.91666667	0.00252525
		3.00000000	0.01515152
		3.04347826	0.00252525
		3.12500000	0.01767677
		3.33333333	0.03535354
		3.50000000	0.01262626
		3.57142857	0.01767677
		3.84615385	0.01767677
		3.88888889	0.00505051
		4.00000000	0.01010101
		4.16666667	0.00505051
		4.34782609	0.00505051
		4.37500000	0.00252525
		4.66666667	0.00505051
		5.00000000	0.06313131
		5.38461538	0.00252525
		5.55555556	0.01010101
		6.00000000	0.00757576
		6.25000000	0.00505051
		6.66666667	0.01010101
		7.00000000	0.00505051
		7.14285714	0.00505051
		7.69230769	0.00505051
		10.00000000	0.02777778
		14.00000000	0.00252525
		20.00000000	0.00505051
Goethite_Strong_Sites_a	Percentage of high affinity goethite sites; discrete distribution	Percentage	Probability Level
		8.835904628	0.1
		11.450381679	0.1
		12.357581069	0.1
		22.709163347	0.1
		23.059866962	0.1

Table J-1. Sample Ranges and Distributions Used for Irreversible Sorption on Stationary Corrosion Products from the Uncorrected Data Set (Continued)

Input Name	Input Description	Range	Distribution
Goethite_Strong_Sites_a (continued)		24.657534247	0.1
		26.829268293	0.1
		41.666666667	0.1
		49.664429530	0.1
		73.913043478	0.1

Source: Preliminary DTN: SN0503T0503305.001.

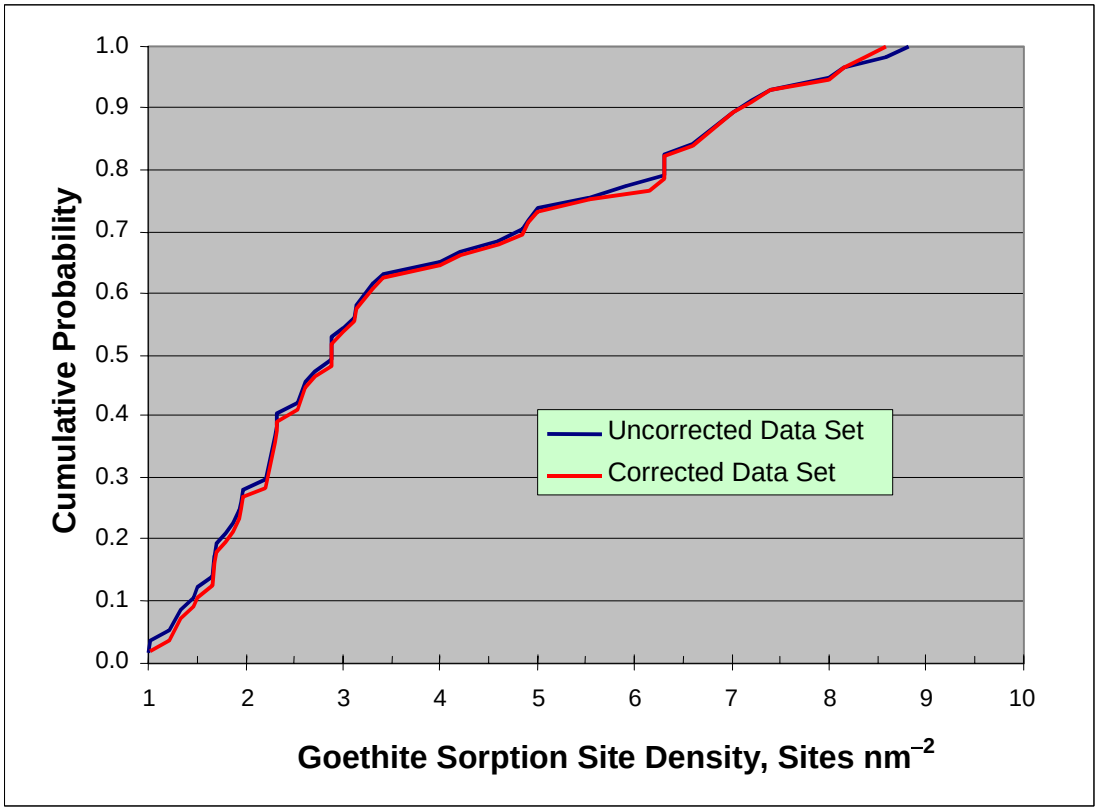

Sources: Uncorrected data set: Table J-2.
Corrected data set: Output DTN: SN0508T0503305.003.

Figure J-1. Comparison of Cumulative Probabilities in Goethite Sorption Site Density Discrete Distributions from the Uncorrected and Corrected Data Sets

Table J-2. Cumulative Probability Distributions for Goethite Site Density and Percentage of High-Affinity Goethite Sites from the Uncorrected Data Set

Input Description	Values	Probability Level	Cumulative Probability
Goethite site density (sites nm^{-2})	1.00000000	0.01754386	0.01754386
	1.01513714	0.01754386	0.03508772
	1.21013524	0.01754386	0.05263158
	1.32484000	0.03508772	0.08771930
	1.46000000	0.01754386	0.10526316
	1.50000000	0.01754386	0.12280702
	1.65500000	0.01754386	0.14035088
	1.68000000	0.03508772	0.17543860
	1.70000000	0.01754386	0.19298246
	1.80000000	0.01754386	0.21052632
	1.87000000	0.01754386	0.22807018
	1.92704000	0.01754386	0.24561404
	1.94573646	0.01754386	0.26315790
	1.97220500	0.01754386	0.28070176
	2.20000000	0.01754386	0.29824562
	2.30000000	0.07017544	0.36842106
	2.31000000	0.01754386	0.38596492
	2.31903106	0.01754386	0.40350878
	2.55000000	0.01754386	0.42105264
	2.60000000	0.03508772	0.45614036
	2.70000000	0.01754386	0.47368422
	2.88600000	0.01754386	0.49122808
	2.90000000	0.03508772	0.52631580
	3.00000000	0.01754386	0.54385966
	3.12251852	0.01754386	0.56140352
	3.13144000	0.01754386	0.57894738
	3.30000000	0.03508772	0.61403510
	3.40000000	0.01754386	0.63157896
	4.00000000	0.01754386	0.64912282
	4.20000000	0.01754386	0.66666668
	4.60000000	0.01754386	0.68421054
	4.84195023	0.01754386	0.70175440
	4.90000000	0.01754386	0.71929826
	5.00000000	0.01754386	0.73684212
	5.52819600	0.01754386	0.75438598
	5.92000000	0.01754386	0.77192984
	6.30000000	0.01754386	0.78947370
	6.31000000	0.03508772	0.82456142
	6.60000000	0.01754386	0.84210528
	7.00000000	0.05263158	0.89473686

Table J-2. Cumulative Probability Distributions for Goethite Site Density and Percentage of High-Affinity Goethite Sites from the Uncorrected Data Set (Continued)

Input Description	Values	Probability Level	Cumulative Probability
Goethite site density (sites nm^{-2}) (continued)	7.20000000	0.01754386	0.91228072
	7.40000000	0.01754386	0.92982458
	8.00000000	0.01754386	0.94736844
	8.16000000	0.01754386	0.96491230
	8.58737200	0.01754386	0.98245616
	8.83000000	0.01754386	1.00000002
Percentage of high-affinity goethite sites	8.835904628	0.1	0.1
	11.450381679	0.1	0.2
	12.357581069	0.1	0.3
	22.709163347	0.1	0.4
	23.059866962	0.1	0.5
	24.657534247	0.1	0.6
	26.829268293	0.1	0.7
	41.666666667	0.1	0.8
	49.664429530	0.1	0.9
	73.913043478	0.1	1

Source (Values and Probability Levels): Preliminary DTN: SN0503T0503305.001.

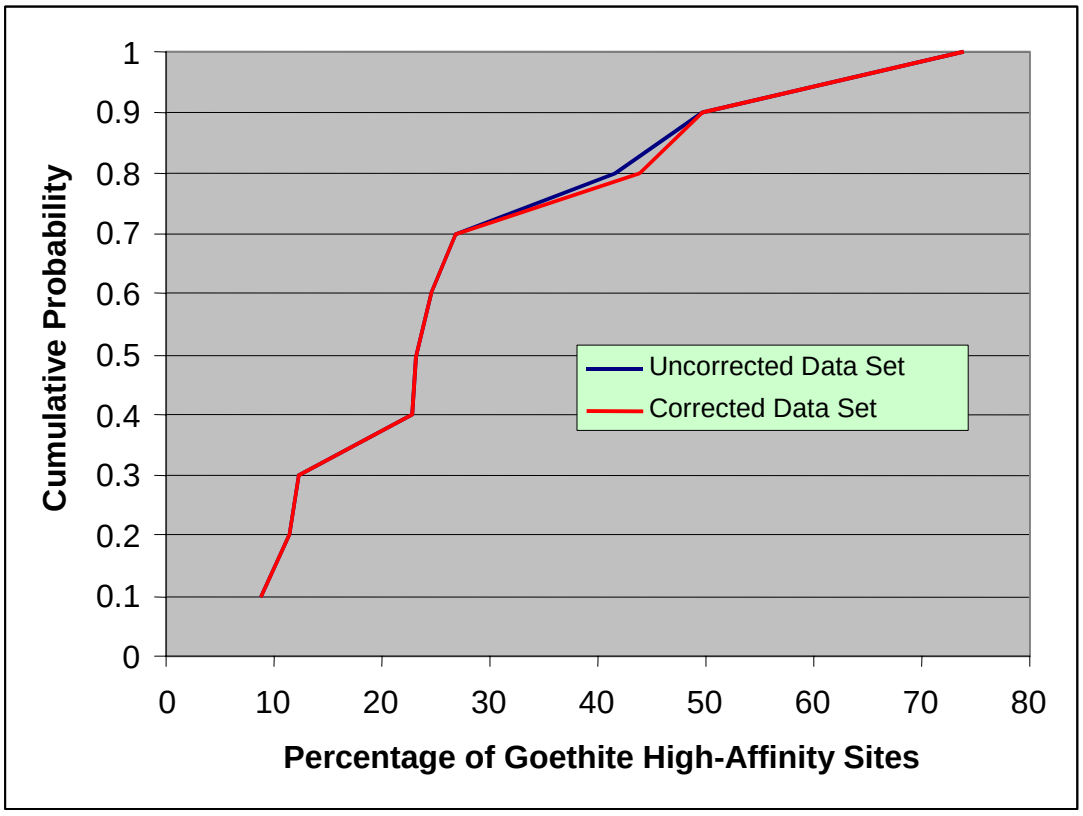

Sources: Uncorrected Data Set: Table J-2.
Corrected Data Set: Output DTN: SN0508T0503305.003.

Figure J-2. Comparison of Cumulative Probabilities in Goethite Percentage of High-Affinity Sites Discrete Distributions from the Uncorrected and Corrected Data Sets